DYNAMIC MODELING AND STABILITY ANALYSIS OF MOBILE MANIPULATORS WITH APPLICATION TO HEAVY DUTY HYDRAULIC MACHINES

BY

ROSHDY FOAAD A. ABO-SHANAB

A Thesis
Submitted to the Faculty of Graduate Studies
In Partial Fulfillment of the Requirements for the Degree of

DOCTOR OF PHILOSOPHY

Department of Mechanical and Industrial Engineering
The University of Manitoba
Winnipeg, Manitoba
Canada

THE UNIVERSITY OF MANITOBA

FACULTY OF GRADUATE STUDIES

*****

COPYRIGHT PERMISSION

Dynamic Modeling and Stability Analysis of Mobile Manipulators with Application to Heavy Duty Hydraulic Machines

BY

Roshdy Foaad A. Abo-Shanab

A Thesis/Practicum submitted to the Faculty of Graduate Studies of The University of

Manitoba in partial fulfillment of the requirement of the degree

Of

DOCTOR OF PHILOSOPHY

Abstract

This thesis describes the development of a complete model to study the tip-over stability of mobile manipulators. The model takes into account the detailed dynamics of the manipulator's base, which can rock back and forth during the movement of the manipulator. It also takes into account the flexibility and the friction of the contact between the base and the ground. The model is used to investigate the effects of different factors, such as the variation of stiffness and damping of the flexible contacts between the base and the ground, compliance at the manipulator joints, and friction between the base and the ground, on the stability of a Caterpillar excavator-based log-loader.

First, the method of virtual links (VL) is employed to model non-fixed base robots or manipulators with multi-degree of freedom joints. It is shown that using the VL method, all the previous dynamic models and simplifications made to develop the equations of motion for manipulators with fixed bases and single degree of freedom at each joint, can readily be applied for manipulators with non-fixed bases and/or multi-degree of freedom at some joints. The method also allows calculating the reaction forces/torques at any chosen manipulator joint directly.

Next, a dynamic model for a general planar mobile manipulator, which assumes rigid contacts between the base and the ground, is developed. The model takes into account the impact with the ground. Both aspects of the impact, i.e., changes in the generalized states of the system and creation of impulsive forces, are included in the model. The combined vehicle suspension and ground-tire compliance and the friction between the wheels and the ground are then included in the model. The simulation results show that the flexibility of the contact reduces the manipulator's tip-over stability (i.e., increases the magnitude of

tip-over rotation of the base) and should be included in the dynamic model in order to accurately investigate the stability of mobile manipulators. It is also shown that the changes of the frictional properties between the wheels and the ground affect the machine stability.

Finally, a complete model of the dynamics of general 3D motion of mobile manipulators is developed. When applying the model to simulate the general three-dimensional motion of the Caterpillar log-loader, it is shown that the flexibility of the contact between the base and the ground reduces the machine stability, whereas the flexibility at the manipulator joints due to the hydraulic compliance improves the stability. The effects of the speed of the swing, and the simultaneous or sequential movements of the manipulator links on the tip-over stability are also investigated.

The results of this work, which will serve as a good guide to the tip-over analysis of manipulators mounted on mobile platforms, clearly show the effect of the manipulator movement on overturning of such machines. Also, it is shown that by proper manipulation of the linkages, some tip-over situations can be recovered. This is significant, since with the introduction of computer control, safety, productivity, and lifetime of mobile manipulators can be improved by automatic prediction, prevention, and recovering from tip-over.

To my family

Acknowledgements

I would like to thank all of those who supported me throughout the course of this thesis. First of all, I would like to express my sincere thanks and appreciation to my supervisor, Dr. Nariman Sepehri for guidance, stimulating suggestions, and encouragement that helped me in all the times of research and writing of this thesis.

My appreciation goes to the members of my advisory committee who monitored my work and provided me with valuable comments in the earlier versions of this thesis: Dr. Subramaniam Balakrishnan, Dr. Steve Onyshko, and Dr. Christine Wu. Particularly, I would like to thank Dr. Wu for her valuable discussion on the theoretical aspects of Chapters 3 and 4 of this thesis. Thanks also to the external examiner of the thesis examination committee: Dr. Shahram Payandeh, Simon Fraser University, British Columbia.

I thank my family for providing me with love, encouragement, and support that helped me throughout this study.

Finally, I would like to acknowledge the support of the Natural Sciences and Engineering Research Council (NSERC) of Canada, the Institute of Robotics and Intelligent Systems (IRIS), Precarn Associates Inc., and the fellowship awarded by the University of Manitoba.

Table of Contents

List of Figures

List of Tables

Nomenclature

$\mathbf{q}$, $\dot{\mathbf{q}}$, $\ddot{\mathbf{q}}$	vectors of the joint variables, velocities and accelerations
$\mathbf{T}_i$	homogeneous transformation matrix from coordinate frame *i* to the reference coordinate frame
$\mathbf{z}_i$	*z-axis* of coordinate frame *i*
$\mathbf{p}_i$	position vector of the origin of coordinate frame *i*
$\mathbf{I}_i^i$	3×3 inertial matrix of link *i* about its mass center in coordinate frame *i*
$\mathbf{r}_i^i$	position vector of mass center of link *i* in coordinate frame *i*
$\mathbf{g}$	gravitational acceleration vector in base coordinate frame
$\mathbf{x}_b$, $\dot{\mathbf{x}}_b$	instantaneous position and velocity vectors of a robotic point coming in contact with environment
$\mathbf{J}$	Jacobean matrix
a_i, a_o, a_e	inlet, outlet and exit areas, respectively
P_i, P_o	input and output pressures, respectively
P_s, P_e	supply and tank pressures, respectively
X	actuator displacement
β	effective bulk modulus
m_i	mass of link *i*
k	stiffness coefficient
c	damping coefficient
D_m	volumetric displacement of the hydraulic motor
x_{sp}	servovalve spool displacement
μ_s	static friction coefficient
μ_c	dynamic friction coefficient
σ_o	normalized lumped stiffness

σ_1	normalized lumped damping
σ_2	normalized viscous relative damping
z	bristle deflection

Superscripts

n	normal force
f	frictional force

Subscripts

f	front wheel
r	rear wheel
fr, fl, rr, lr	front right wheel, front left wheel, rear right wheel, and rear left wheel, respectively
frx, fry	x and y components of the friction force at the front right wheel, respectively
flx, fly	x and y components of the friction force at the front left wheel, respectively
rrx, rry	x and y components of the friction force at the rear right wheel, respectively
rlx, rly	x and y components of the friction force at the rear left wheel, respectively

Chapter 1

Introduction

1.1 Preliminary Remarks

The development of automated systems for the operation of manipulator-like mobile machines, for example excavator-based log-loaders (see Figure 1.1), has recently received particular attention (Sepehri and Lawrence, 2000). Current research effort also includes developing means for converting existing log-loaders, which can be considered as mobile manipulators, into teleoperated systems (Sepehri et al., 1994). One issue is the proper monitoring and prevention of tip-over in the operation of such machines. Presently, the operators must face the difficult task of maintaining the stability of the machines particularly when handling heavy loads. Although sensor systems are available for some mobile manipulators, such as cranes, that detect whether a static load exceeds the safe operating load, there is no mechanism available that includes dynamic situations. Therefore, the operator must remain alert at all times to accomplish the work efficiently

and, at the same time protect his/her safety and that of others. In spite of much research in this area, the machine stability has not been fully explored and there are many issues that need to be further investigated. Factors that might affect the stability of mobile manipulators, such as the flexibility of the contact between the base and the ground, the compliance at the manipulator joints, and the friction between the base and the ground have not been addressed in any of the previous work in this area. Also, understanding the details of the base movement during the tipping over can help to define an accurate measure of stability and therefore potentially help to prevent and/or recover from the tipping over.

Unlike conventional industrial manipulators mounted on a stationary base, a mobile manipulator does not have a base fixed in an inertial frame. So, most of the existing formulations that are used for deriving the equations of motion of fixed base

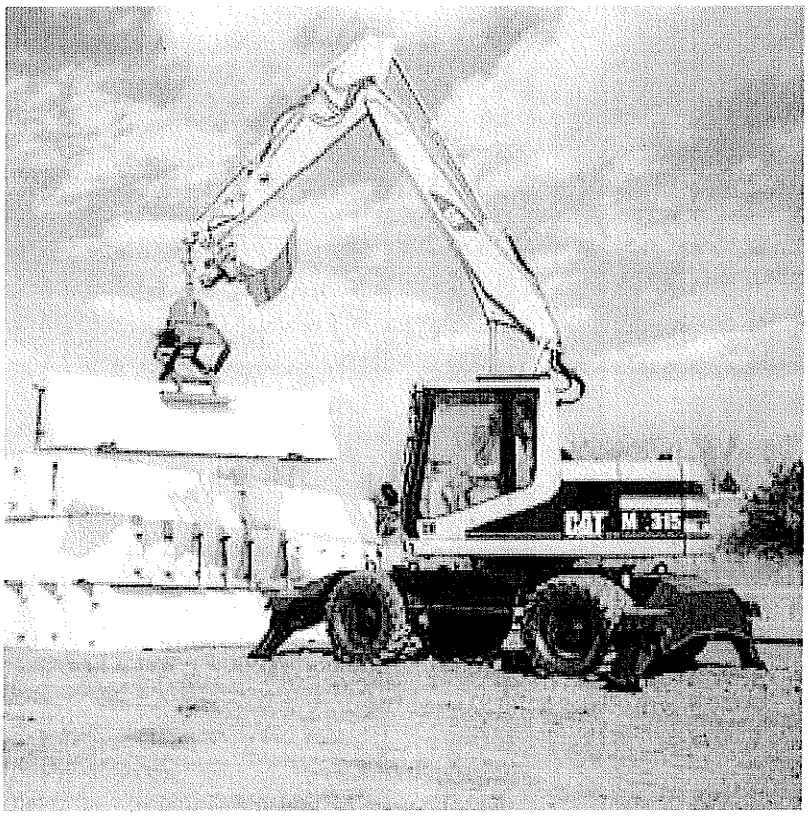

Figure 1.1. Typical mobile manipulator; a Caterpillar excavator-based log-loader.

manipulators cannot be used to model the dynamics of mobile manipulators. One has to start from 'first principles*' to derive the dynamic equations of a mobile manipulator, which makes the derivation of the equations of motion tedious and error prone especially for general three-dimensional manipulator motion. Secondly, all manipulator links, including the base and the suspension, interact with each other dynamically. This coupling will degrade system performance, resulting in problems such as excessive end-effector errors, oscillations, and potential instability. It is therefore desirable to have a systematic method for dynamic modeling of mobile manipulators and a comprehensive model that can be used for simulation and stability analysis of mobile manipulators. This model should include the various aspects of these manipulators such as the movement of the base that can rock back and forth, the combined vehicle suspension and tire-ground compliance, and the friction between the tires and the ground.

Early work on stability of mobile vehicles was concerned only with the static stability and gait generation of slow moving legged machines (see Messuri and Klein, 1985 and the references listed therein). The most comprehensive one belongs to Messuri and Klein (1985) who introduced a measure of stability termed "energy stability margin". This method could deal only with cases in which the only destabilizing load is due to the gravitational force. In a moving base manipulator, however, a large portion of destabilizing forces and moments could be due to the inertial or external loads arising from maneuvering the end-effector. Nagy et al. (1994) extended the energy stability method to take into account the effect of known walker terrain compliance on the

* The term "first principles" means that the derivation of the equations of motion starts by defining the kinetic and potential energies for each link of the mobile manipulator including the base. Lagrange's equations are then used to derive the equations of motion.

stability of the walker. The method is still confined to the stability analysis of vehicles that are subject to only weight forces. The inclusion of external forces and inertial loads is important in the stability analysis of mobile manipulators.

Dubowsky and Vance (1989) proposed a time optimal motion planning strategy for manipulators that are mounted on mobile platforms. The goal was to allow the manipulators to perform tasks quickly but without generating substantial dynamic forces and moments that cause the system to overturn. The method, however, did not attempt to study the tip-over case or to develop a measure of stability. Sugano et al. (1993) and Huang et al. (1995; 1997; 1998) employed the ZMP (Zero Moment Point) concept to construct a quantitative criterion for manipulators mounted on a vehicle. In their work, the manipulator, including the vehicle and the payload, was considered to be a system of particles moving on only rigid horizontal floors. ZMP concept is a moment-based approach and therefore does not include the effect of the walking height in the stability analysis. Papadopoulos and Rey (1996; 1997; 2000) proposed a Force-Angle measure of the tip-over stability margin. The Force-Angle stability measure has a simple graphical interpretation and is easy to compute. Force-Angle method, however, does not give any information about the state of base, i.e., whether the base is going to tip over completely or just rock back and forth. Iagnemma et al. (2000) introduced the kinematic reconfiguration method to enhance the system's tip-over stability. The method, however, is based on the Force-Angle measure and is applied to a quasi-static system, i.e., it does not include the dynamic effects. Recently, Ghasempoor and Sepehri (1998) extended the energy stability method of Messuri and Klein (1985) to quantitatively reflect the effect of forces and moments arising from the manipulation of the implement. The significance of

this extension is that it can be used as an off-line tool to provide the designer with an inexpensive and fast method that helps to maintain the stability of mobile manipulators. The extension, however, does not consider the dynamic situation i.e., tipping over of the entire machine during an unstable stance. Moreover, depending upon the subsequent states of the end-effector motion, the entire machine may rock back and forth, a phenomenon that cannot be characterized by any of the previously developed methods. Much research is needed in this area, particularly to develop a model that can simulate the tip-over motion of the manipulator base.

1.2 Objectives and Scope of this Thesis

The objectives of this thesis are to: (*i*) develop a simulation model of tip-over motion of mobile manipulators, and (*ii*) study tip-over mechanisms, and understand various dynamic situations that promote vehicle instability. Towards this goal, first, an appropriate model is developed that contains enough features to yield the information about the stability of mobile manipulators. Secondly, a comprehensive investigation of the effects of different factors that may play a role in the tipping over of mobile manipulators is conducted. These factors include: (*i*) the variation of stiffness and damping of the flexibility of the contact between the base and the ground, (*ii*) the compliance at the manipulator joints, (*iii*) the friction between the base and the ground, and (*iv*) the effect of various manipulator motions.

The application of this study is directed at industrial mobile machines that carry human-operated hydraulic manipulators. The development here is therefore used to study the stability of a Caterpillar excavator-based log-loader (see Figure 1.1). These machines incorporate many aspects of typical robotic systems and are the basis for most heavy-duty

hydraulic machines. The previous simulation of these machines (Vaha and Skibniewski 1993; and Sepehri et al. 1994; 1996) did not incorporate the tipping over scenario. The model developed in this thesis incorporates the dynamics of the rocking base for such machines. Both rigid as well as flexible contact, including suspension and ground-tire interaction, are considered for modeling the interaction between the base and the ground.

The organisation of this thesis is as follows. In Chapter 2, a background on previous work on the dynamics simulation and stability analysis of mobile manipulators is presented. The novel method of virtual links (VL) is developed in Chapter 3. The applications of this method for modeling non-fixed base manipulators or manipulators with joints having multi-degree of freedoms are introduced. In Chapter 4, modeling the machine stability assuming rigid contact between the base and the ground is presented. The model includes the dynamics of the manipulator linkages and the impact between the base and the ground during the rocking motion. Chapter 5 presents modeling and simulation issues considering the combined vehicle suspension and ground-tire compliance. The effects of the variations of the parameters pertaining to the flexibilty of the contact on the machine stability are discussed. Chapter 6 is devoted to include the effect of the friction between the base of the mobile manipulator and the ground and to investigate the effect of the variations of the frictional properties on the stability. The development of the general three-dimensional simulation model is presented in Chapter 7. The developed model is applied to a typical Caterpillar excavator-based log-loader. Simulations are then performed to evaluate the effect of different factors influencing the machine stability. Conclusions are presented in Chapter 8.

Chapter 2

Background

The previous studies on modeling and simulation of non-fixed base manipulators are described first. Potentials and limitations of these studies are outlined. Next, the problem of stability* analysis of mobile machines is discussed. In most of the previous works, a mobile manipulator is considered unstable once it starts to rotate about an edge of potential overturning. None of these studies considered the case in which the manipulator's base just rocks back and forth without complete overturning.

2.1 Dynamic Modeling of Non-Fixed Base Manipulators

Although most industrial manipulators have a base fixed in an inertial frame, there are many manipulators that are mounted on non-fixed bases such as free flying-satellites, submarines, and vehicles. For these manipulators, there is a dynamic coupling between

* In this thesis, the stability of a mobile manipulator is defined as the ability of the manipulator to do its job without complete overturning, i.e., the manipulator is allowed to rock back and forth.

the base and the manipulator. The calculation of the arm motion, assuming a fixed base, will result in a position error of the end-effector (Hootsmans 1992). A significant amount of work has been done in space robotics, which considers the dynamic interaction between a manipulator and its spacecraft. For example, see the work by Dubowsky and Papadopoulos (1993); Vafa and Dubowsky (1987); or Carter and Cherchas (1998). Some of the analytical approaches and models developed in these studies are also useful in studying the dynamics of the ground-based mobile manipulators. However, earth-based systems present special dynamics problems not found in space systems. First, gravity can seriously degrade the manipulator performance causing base motions, which could result in large errors at the manipulator end-effector. Gravity could even cause a mobile system to tip over. Secondly, the suspensions and tire compliance of ground-based vehicles could cause resonance, which would seriously degrade and destabilize the manipulator (Hootsmans 1992).

Research on ground-based manipulators that includes the dynamic coupling between the vehicle and the manipulator is limited and most of these studies are fairly recent. Li and Frank (1986) presented a preliminary work on stability of moving base robots. The objective was to include the stability criteria in the solution of the inverse kinematics problem. Simple formulation that can be used only to determine the onset of the instability for a two-link mobile manipulator was presented; no dynamic simulations were performed.

Dubowsky and Tanner (1987) considered a planar three-link mobile manipulator. The vehicle was assumed to be far more massive than the manipulator system and, therefore, the motion of the manipulator was assumed not to affect the vehicle. They showed that

using a feed forward compensation method, based on measured base motions, end-effector errors could be reduced to within required tolerances for the mobile manipulator task. The assumption of a vehicle, which is much more massive than the manipulator and its payload, though appropriate for some applications such as in a military tank, is not valid for many other mobile manipulator systems.

Dubowsky et al. (1991) presented a method for dynamic modeling of mobile manipulators with flexible links, vehicle, and suspension. They showed that the dynamic interactions between a manipulator and its mobile vehicle could result in large end-effector errors and simple gravity compensators based on rigid link and without suspension model cannot effectively reduce these errors.

Hootsmans (1992) applied Newton-Euler formulation to derive the dynamic equations of a planar mobile manipulator. He showed that using a conventional controller that neglects the dynamic interactions between the manipulator and its base leads to a poor performance. A control approach was then developed to compensate for these interactions and it was shown to provide good trajectory control.

Akpan and Kujath (1998) studied the sensitivity of a planar mobile manipulator response to system parameters, such as stiffness, damping and surface roughness. They concluded that, to minimize the amplitude of the stochastic vibration on the manipulator tip due to the movement of the base on rough surfaces, the lower links of the manipulator should be longer than the upper links and the vehicle suspension stiffness should be higher than the links' stiffness. The vehicle suspension damping alone is not sufficient to reduce the stochastic vibrations, the links of the manipulator have to be also damped.

Yu and Chen (2002) introduced a general approach to derive the dynamic equations of mobile manipulators. Terms representing the dynamic interactions between the manipulator and the mobile platform were introduced. However, it was assumed that the motion of the platform is confined to planar motion with no translations along the vertical axis and that there is no slipping between the wheels and the floor. These assumptions make the approach limited and less practical.

2.2 Stability of Mobile Manipulators

Initial work on stability of mobile manipulators was concerned only with the static stability as applied to slow moving walking machines. McGhee and Frank (1968) defined the static stability of an ideal legged locomotion machine. An ideal legged locomotion machine is a rigid body attached to a specific number of massless legs. Following their definition, the magnitude of the static stability margin (SSM) is equal to the shortest distance from the vertical projection of the center of gravity (CG) to any point on the boundary of the support pattern. The support pattern associated with any phase of a given gait of an ideal legged machine is the convex hull (minimum area convex polygon) that contains all of the leg contact points. As an example, the static stability measures, S_f and S_r, for a body on horizontal plane are shown in Figure 2.1. McGhee and Iswandhi (1979) extended SSM to an uneven terrain by redefining the support pattern as the minimum

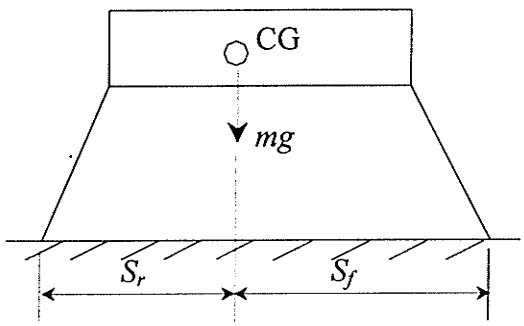

Figure 2.1. Static stability measures for a body on a horizontal plane.

area convex polygon of the point set in the horizontal plane which contains the vertical projections of the feet of all the supporting legs. The longitudinal stability margin (LSM) was defined as the shortest distance from the projection of the CG to the front or the rear boundary of the support pattern as measured in the direction of travel. Figure 2.2 shows the static stability measures, S_f and S_r, for a body on an inclined plane. Mahalingham and Whittaker (1989) defined a conservative support polygon (CSP) to take into account the possibility of support failure of a single leg. The CSP is determined as follows. If there are n ground-contacting feet whose projections form the support polygon, then n subsets of the support polygon can be formed as follows. Each subset is the convex hull of the projections onto a horizontal plane of one of the n possible combinations of (n-1) of the feet that form the support polygon. The intersection of these n subsets forms the CSP. Figure 2.3 shows the CSP for a walker machine with five ground-contacting feet. The CSP becomes a point for walker machines with fewer than five ground-contacting feet. Thus, the use of CSP is restricted to machines with five or more legs. The conservative stability margin (CSM) is then defined as the shortest distance between the projected CG location and the edges of the conservative support polygon. The SSM, LSM, and CSM

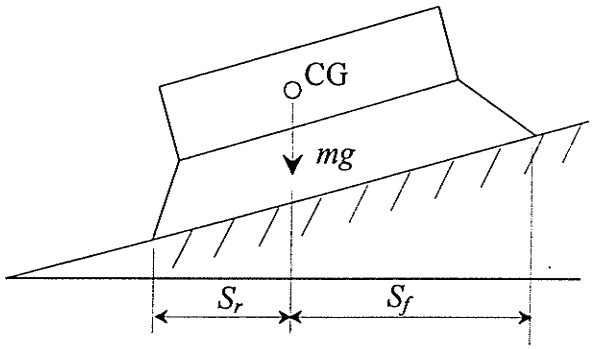

Figure 2.2. Static stability measures for a body on an inclined plane.

methods consider only the projections of the ground-contacting feet and the center of gravity onto a horizontal plane. However, the height of the center of gravity and the differences in the terrain elevations of ground-contacting feet have a significant impact on the machine stability (Nagy et al. 1994). Messuri and Klein (1985) showed that, for a leveled body on an inclined plane (see Figure 2.4), the SSM for the front side (S_f) is equal to SSM for the rear side (S_r). However, by intuition one can see that the vehicle is more likely to tip "downhill" rather than "uphill". Messuri and Klein concluded that static stability margins do not provide a sufficient measure for the amount of stability when the terrain is not a horizontal plane. In order to take into account the effects of the uneven terrain, they introduced a different measure of stability called energy stability margin (ESM). The following definitions form a basis for determining the ESM.

Definition 1: The support boundary associated with a given support state consists of the line segments, which connect the tips of the support feet. The support boundary is a three-dimensional curve as opposed to the two-dimensional support pattern.

Definition 2: The energy stability level (ESL) associated with a particular edge of a support boundary is equal to the work required to rotate the CG of the body about that

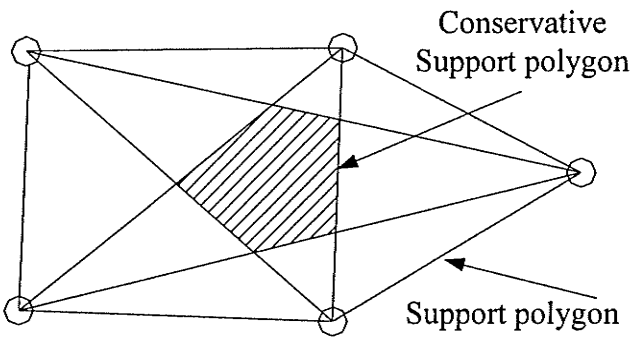

Figure 2.3. Support polygons for five ground-contacting feet.

edge, to the position where the vertical projection of the body center of gravity lies along that edge of the support boundary.

Definition 3: The ESM for an arbitrary support boundary is equal to the minimum ESL associated with each edge of the support boundary.

Calculating the energy stability level for the body shown in Figure 2.4, the ESL for the front edge is mgh_f, which is greater than the ESL for the rear edge mgh_r (m is the mass of the body and g represents the acceleration due to the gravity). The ESM produces a qualitative idea of the amount of impact energy the vehicle could withstand and also considers the effect of the walking height (Garcia et al. 2002). However, the ESM still considers neither the effect of compliant terrain nor the stabilizing effect of non-supporting legs.

Nagy et al. (1994) introduced the compliant stance stability margin (CSSM) as an extension of the ESM to consider foot sinkage on compliant terrain. It was shown that the terrain compliance can significantly affect the magnitude of a stability measure. Not taking the terrain compliance into account may result in a significant overestimate of the

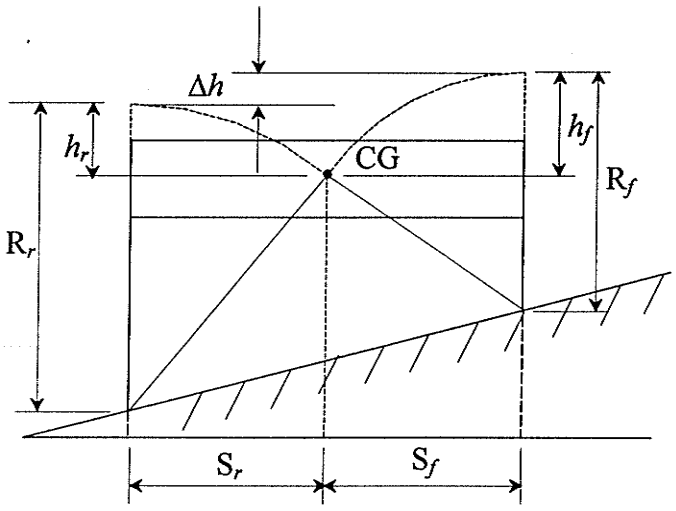

Figure 2.4. Leveled body on an inclined plane.

stability of the machine. Nagy's approach is still confined to the stability analysis of vehicles that are subject only to weight forces.

Ghasempoor and Sepehri (1998) extended the ESM to quantitatively reflect the effect of the forces and moments arising from the manipulation of the implement. The extended ESM is determined by the following definitions:

Definition 4: With reference to Figure 2.5, the equilibrium plane associated with a particular edge of a support boundary is a plane containing the edge with an angle with respect to the vertical plane, such that if the body rotates around the edge until the center of gravity is placed in this plane, the net moment due to all forces and moments around the edge becomes minimum in the absolute sense.

Definition 5: The energy stability level associated with a particular edge of the support boundary, at any stance, is equal to the work done when the vehicle body (which is subject to gravitational loads as well as external and inertial forces and moments) is hypothetically rotated around the edge until the center of gravity reaches the equilibrium

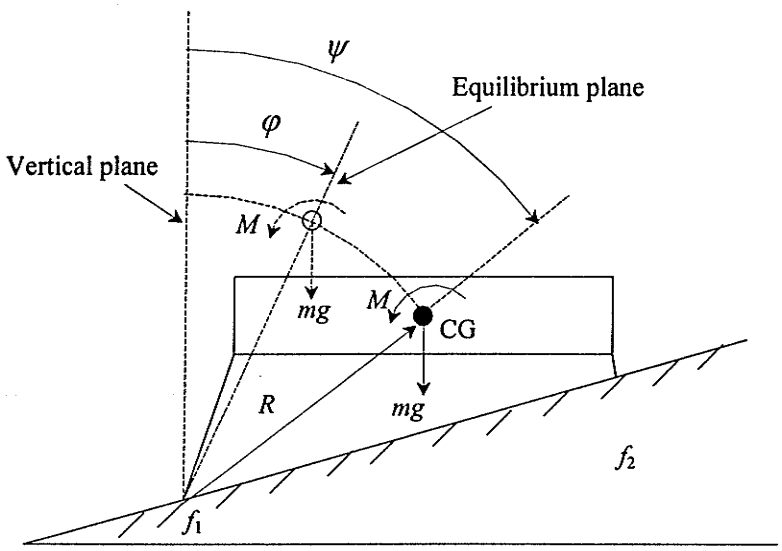

Figure 2.5. Concept of Equilibrium plane.

plane. This work is equivalent to the instantaneous maximum impact energy that can be sustained by the vehicle, without reaching the unstable configuration.

Figure 2.5 also shows the application of these definitions for a vehicle over an inclined plane. The vehicle is subject to a destabilizing moment, M, in addition to its own weight. Angle φ, which defines the orientation of the equilibrium plane with respect to the vertical plane, is obtained by equating the summation of all moments around edge f_1 to zero.

$$M - mgR\sin\varphi = 0 \tag{2.1}$$

then,

$$\varphi = \sin^{-1}\frac{M}{mgR} \tag{2.2}$$

The energy stability level for edge f_1, is calculated as follows:

$$ESL_1 = mgR(\cos\varphi - \cos\psi) - M(\psi - \varphi) \tag{2.3}$$

where mg is the gravitational load and M is the external moment.

The extension of ESM, however, does not take into account the dynamics of the platform and also assumes constant magnitude and direction of the external forces and moments throughout the tip-over motion.

Sugano et al. (1993) employed the Zero Moment Point (ZMP) concept to construct a quantitative stability criterion for mobile manipulators. ZMP is defined as the point on the floor where the resultant moment of the gravity, inertial force, and external forces is zero. If the ZMP is within the support polygon, the mobile manipulator is stable. The stability degree (α) was defined as a quantitative measure of a stable extent for a mobile

manipulator according to the relationship between the ZMP position and the stable region. With reference to Figure 2.6, the stability degree can then be written as follows:

$$\alpha = \frac{d}{r_o} \tag{2.4}$$

$$d = \min\{d(ZMP)\} \tag{2.5}$$

where $d(ZMP)$ is a set of the distances from ZMP to the boundary of the stable region. r_o is the maximum of the stable distance (shown in Figure 2.6).

The ZMP concept has been used in the design of biped walking robots (Soe and Yoon, 1994), motion planning of mobile manipulators (Qiang et al., 1998), and stability control of mobile manipulators (Qiang et al., 1994). The concept, however, is a moment-based approach and therefore does not include the effect of the walking height in the stability analysis.

Papadopoulos and Rey (1996; 1997; 2000) introduced the Force-Angle stability measure. The Force-Angle stability criterion determines the angle (θ_i) between the resultant force acting on the CG of the system, $\mathbf{f}_r$, and the normal from the CG to the axis of tipping over, $\mathbf{l}_i$ (see Figure 2.7). When the angle (θ_i) equals zero, the system becomes on the verge of stability and the tipping over is in progress if it is less than zero. The stability

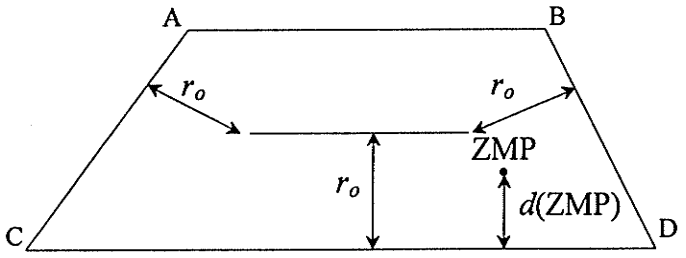

Figure 2.6. Stable region and stability degree (A, B, C, and D are the contact points between the manipulator and the ground and represent the stable region).

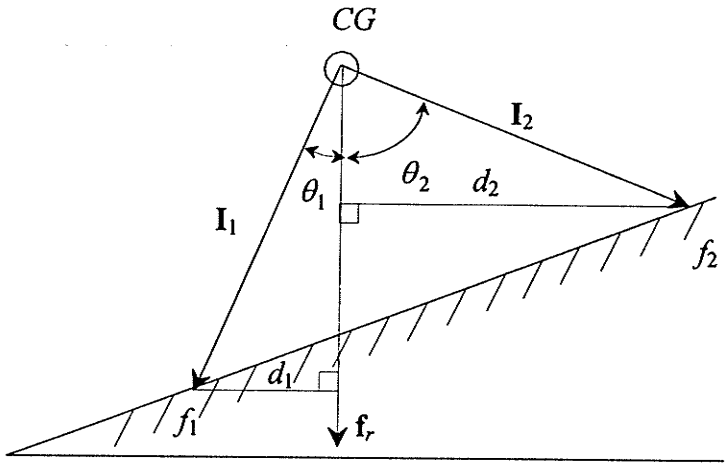

Figure 2.7. Planar Force-Angle measure.

margin is then calculated as follows:

$$\beta = \min\{\theta_i \cdot \|d_i\| \cdot \|\mathbf{f}_r\|\} \tag{2.6}$$

The Force-Angle measure, however, does not give any information about the state of the base, i.e., whether the base overturns completely or just rocks back and forth. Using this method, Iagnemma et al. (2000) introduced a kinematic reconfiguration method to enhance system's tip-over stability. The method is based on designing the machine with the ability to reconfigure its structure to improve the stability. The method was built on the Force-angle measure and was intended for quasi-static systems.

2.3 Description of a Caterpillar Excavator-Based Log-Loader

The Caterpillar excavator-based log-loader, shown in Figure 2.8, was used for all the simulation tasks in this thesis. The machine was considered as a mobile three-degree of freedom manipulator with an additional moveable implement. The implement is a grapple for holding and handling objects such as trees. The whole machine can move forward or backward. The upper structure of the machine rotates by a 'swing' hydraulic motor through a gear train. 'Boom' and 'stick' are the two other links, which together with the

'swing', serve to position the implement. Boom and stick are operated through hydraulic cylinders. The cylinders and the swing motor are activated by means of pressure and flow through the main valves. Modulation of the oil flow in the main valves is controlled by the pilot oil pressure through manually operated control valves.

Figure 2.9 shows a schematic diagram of the hydraulic actuator system used in the machine under investigation. The hydraulic cylinder is connected to an open-center valve through flexible hoses. The valve monitors the flow to and from the cylinder. This system works with a constant flow pump system. With reference to Figure 2.9, when the spool of the open-center valve is in neutral position, the flow passes through the valve and returns to the tank. As the spool moves to the left or to the right, the flow is distributed to the load and the tank, depending on the orifice arrangement and the load. Assuming that the losses due to leakage flow and internal friction are negligible, the equations governing the flow distribution can be written as follows (Merritt, 1967):

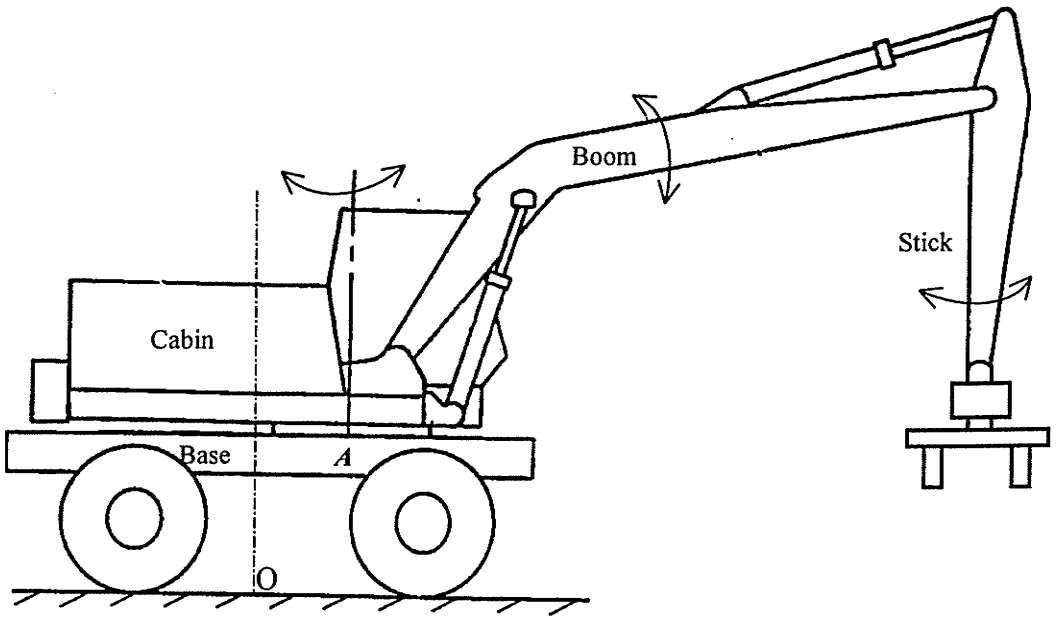

Figure 2.8. Typical excavator-based log-loader.

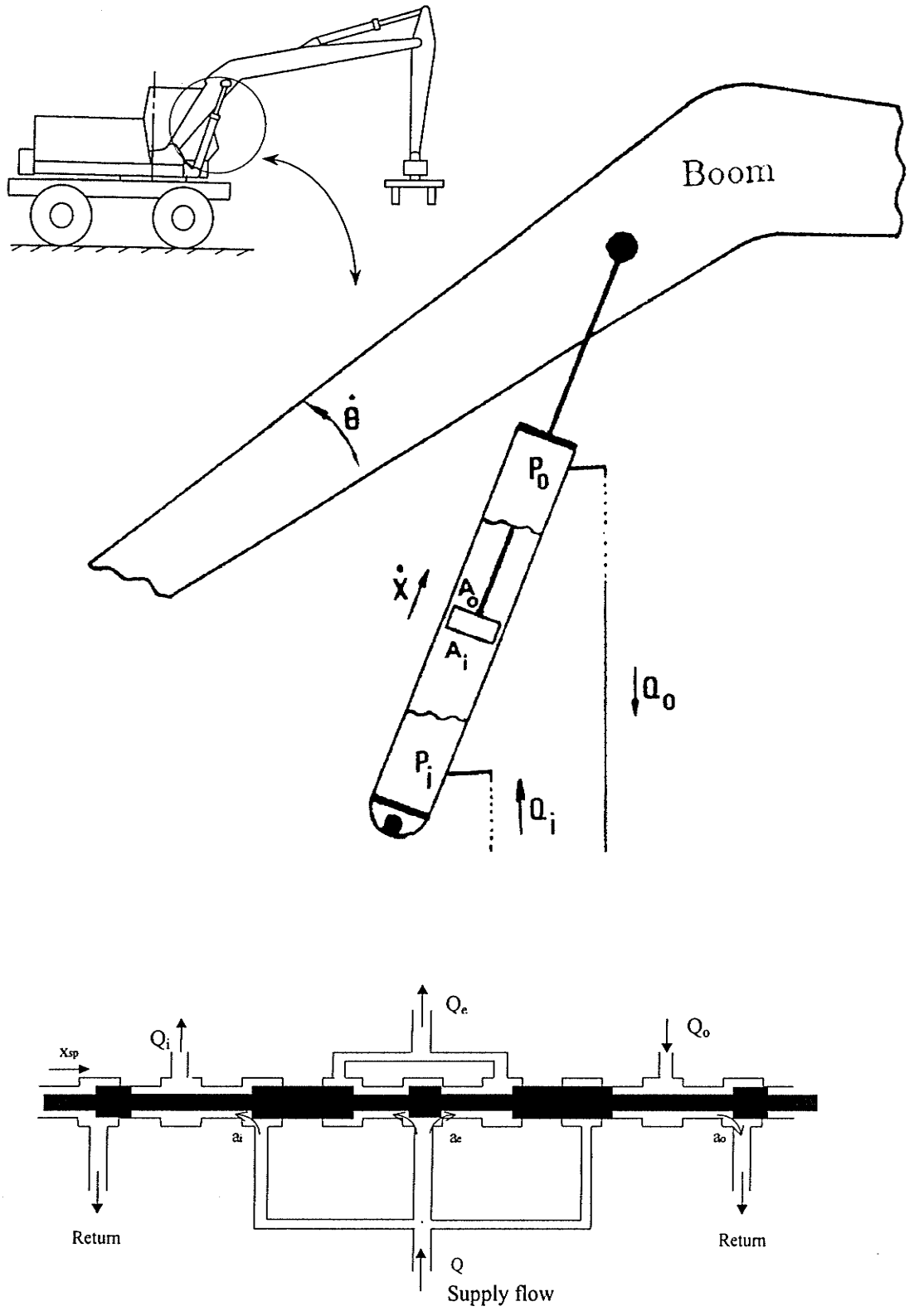

Figure 2.9. Schematic diagram of the hydraulic actuator with open center valve.

$$Q_i = ka_i\sqrt{P_s - P_i} \tag{2.7}$$

$$Q_o = ka_o\sqrt{P_o - P_e} \tag{2.8}$$

$$Q_e = Q - Q_i = ka_e\sqrt{P_s - P_e} \tag{2.9}$$

where Q_i , Q_o, and Q_e are the inlet, outlet, and exit flows to and from the cylinder, respectively and Q is the supply flow. a_i, a_o and a_e are the inlet, outlet and exit areas, respectively. k is the orifice coefficient. The rate of change of the inlet pressure $\dot{P}_i$ and the outlet pressure $\dot{P}_o$ are:

$$\dot{P}_i = \frac{\beta}{V_i(X)}\left(Q_i - A_i\dot{X}\right) \tag{2.10}$$

$$\dot{P}_o = \frac{\beta}{V_o(X)}\left(A_o\dot{X} - Q_o\right) \tag{2.11}$$

where X is actuator displacement, $\dot{X}$ is the actuator velocity, β is the effective bulk modulus, and A_i and A_o are the effective piston areas. $V_i(X)$ and $V_o(X)$ are the volumes of the fluid trapped at the sides of the actuator. They are expressed as

$$V_i(X) = \overline{V}_i + X\,A_i \tag{2.12}$$

$$V_o(X) = \overline{V}_o - X\,A_o \tag{2.13}$$

$\overline{V}_i$ and $\overline{V}_o$ are volumes of the initial fluid trapped at the sides of the actuator. The output force from the actuator, F, is

$$F = P_iA_i - P_oA_o \tag{2.14}$$

Finally, the torque generated by the hydraulic cylinder is:

$$\tau = F\frac{dX}{d\theta} \tag{2.15}$$

where $\frac{dX}{d\theta}$ represents the nonlinear relationship between the actuator linear velocity, $\dot{X}$, and the corresponding link rotational velocity, $\dot{\theta}$.

For the swing hydraulic motor:

$$\tau = n\,D_m(\Delta P) \tag{2.16}$$

where ΔP is the pressure difference across the motor lines, D_m is the volumetric displacement of the motor, and n is the gear reduction from motor to the output shaft.

The relationship between the spool displacement, x_{sp}, and the input voltage, u, to the servovalve can be expressed by the following first-order differential equation:

$$u = (\frac{\tau_c}{k_{sp}})\frac{dx_{sp}}{dt} + (\frac{1}{k_{sp}})x_{sp} \tag{2.17}$$

where τ_c and k_{sp} are gains describing the valve dynamics.

Chapter 3

Method of Virtual Links

3.1 Introduction

There exist many mechanisms that have multi-degree of freedom joints or non-fixed bases. All the previous work arrived at the equations of motion for such systems using first principles. These methods are tedious and error prone. On the other hand, in the past three decades, many studies were done to simplify the derivation of the dynamic equations for fixed base serial link manipulators with single degree of freedom joints. These studies contain systematic and simple formulations such as Lagrange-Euler (Fu et al., 1987), recursive Lagrangian (Hollarbach, 1980), or Generalized D'Alembert principle (Sallam et al., 1998), which can be applied only to fixed base manipulators with a single degree of freedom at each joint. No one, to the best of the author's knowledge, used these formulations to derive the dynamic equations for manipulators having multi-degrees of freedom joints or non-fixed bases.

In this chapter, a novel method is developed which transfers a robotic manipulator with multi-degree of freedom joints or non-fixed bases into an equivalent fixed base manipulator with single degree of freedom at each joint. This process allows using the existing formulations to derive the dynamic equations for manipulators mounted on non-fixed bases or for those with multi-degree of freedom joints. The approach taken is to first add virtual links to the original system. Next, the augmented state space is formed by the states describing the original system plus the virtual links. The equations of motion, describing the expanded system, are then derived in the reduced state space. Finally, the equations of motion for the original multi-link system are obtained by setting all the kinematic and dynamic parameters pertaining to the virtual links to zero.

The proposed method also facilitates direct calculation of the reaction forces/torques at any chosen manipulator joint. Currently, there are two techniques to calculate these forces. The first one uses Lagrange multipliers, but it results in a set of differential algebraic equations (DAEs). Solving systems of DAEs is more complicated than solving systems of ordinary differential equations (ODEs) and increases the computational load. The second technique uses Newton's method. Using this method, the problem of having systems of DAEs is avoided. However, to calculate the reaction forces at a certain joint, the reaction forces at all the distal joints must be calculated backward starting from the end-effector. The proposed approach allows the reaction forces at any chosen manipulator joint to be directly determined without solving the system's DAEs. This means that the proposed method has the advantages of both methods described above while avoiding their disadvantages.

Two application areas are described to substantiate the method outlined above:

1- Modeling multi-degree of freedom joints.

2- Calculation of constraint forces at manipulator joints.

The application of the method to the development of models for non-fixed base manipulators will be discussed in following chapters.

3.2 Modeling of Links with Multi-degree of Freedom Joints*

A serial n-link manipulator with $(n+m)$ degree of freedom is considered. This means that some of the manipulator joints have more than one degree of freedom. To model this manipulator, m virtual links are added in such a way that every joint has only one degree of freedom. The original n-link system now becomes an $(n+m)$-link system. Vector $\mathbf{q} = \{q_1, q_2, \ldots\ldots, q_{n+m}\}^T$ denotes the generalized coordinates and $\tau = \{\tau_1, \tau_2, \ldots, \tau_{n+m}\}^T$ is the generalized force vector of the new system. The dynamic equations are then derived using the existing formulations for dynamic modeling of fixed-base serial link manipulators with single degree of freedom at each joint. The final equations will take the following general form:

$$\widetilde{\mathbf{M}}(\mathbf{q})\ddot{\mathbf{q}} + \widetilde{\mathbf{C}}(\mathbf{q}, \dot{\mathbf{q}}) + \widetilde{\mathbf{G}}(\mathbf{q}) = \tau \qquad (3.1)$$

where $\widetilde{\mathbf{M}}(\mathbf{q})$ is the symmetric, positive definite inertial acceleration-related matrix, $\widetilde{\mathbf{C}}(\mathbf{q}, \dot{\mathbf{q}})$ is the vector of centripetal and Coriolis torques and $\widetilde{\mathbf{G}}(\mathbf{q})$ is the vector of gravitational torques. To obtain the final equations for the original system, all the kinematic and dynamic parameters of the virtual links are set to zero. Final equations for the original multi-link system are shown below:

---

* A version of this section has been presented at the *ASME Design Engineering Technical Conferences*, paper # DETC2002/MECH-34225, Montreal, Canada, 2002, "On Dynamic Modeling of Robot Manipulators: the Method of Virtual Links," R.F. Abo-Shanab, N. Sepehri, and Q. Wu.

$$\mathbf{M}(\mathbf{q})\ddot{\mathbf{q}} + \mathbf{C}(\mathbf{q},\dot{\mathbf{q}}) + \mathbf{G}(\mathbf{q}) = \tau \tag{3.2}$$

Note that $\mathbf{M}(\mathbf{q}), \mathbf{C}(\mathbf{q},\dot{\mathbf{q}})$, and $\mathbf{G}(\mathbf{q})$ in Equation (3.2) are similar to $\tilde{\mathbf{M}}(\mathbf{q}), \tilde{\mathbf{C}}(\mathbf{q},\dot{\mathbf{q}})$, and $\tilde{\mathbf{G}}(\mathbf{q})$ in Equation (3.1) but are simpler, since the virtual link parameters are set to zero. Also, it should be noted that one could set the virtual link parameters to zero from the beginning if the final form of Lagrange-Euler (LE) method is used to derive the equations of motion.

Example: Modeling a Spherical Joint

Consider a rigid body with three degrees of freedom shown in Figure 3.1. The inertial reference frame is labeled {xyz} while $\{x_b y_b z_b\}$ represents the three-dimensional space spanned by the body's principal axes. The Euler angles θ_1, θ_2, and θ_3 are generated by successive rotations of the rigid body about its body axes z_b, y_{b1}, and z_{b2}, respectively (see Figure 3.2). Any Euler angles set can be used based upon the configuration of interest and to avoid

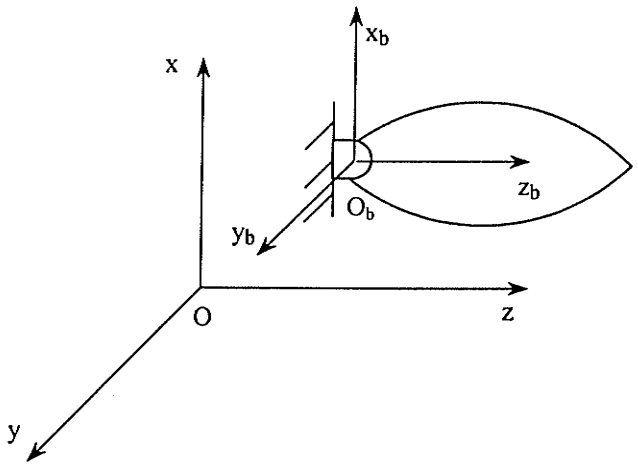

Figure 3.1. Rigid body with spherical joint.

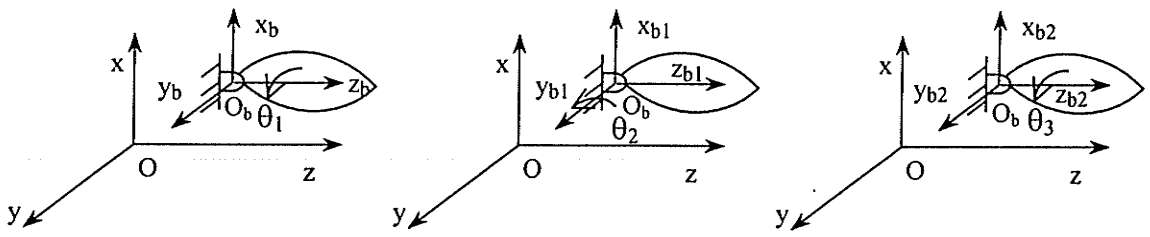

Figure 3.2. Euler angles.

singular points at this configuration.

To obtain the equations of motion for this rigid body, two virtual links are added as shown in Figure 3.3. Then, Denavit-Hartenberg (DH) coordinate systems are assigned as in Figure 3.4.

Here, the formulation described by Sallam et al. (1998) is used to obtain the equations of motions. Let $\mathbf{A}_i$ be the 4×4 homogeneous transformation matrix from coordinate system i to $(i-1)$, then:

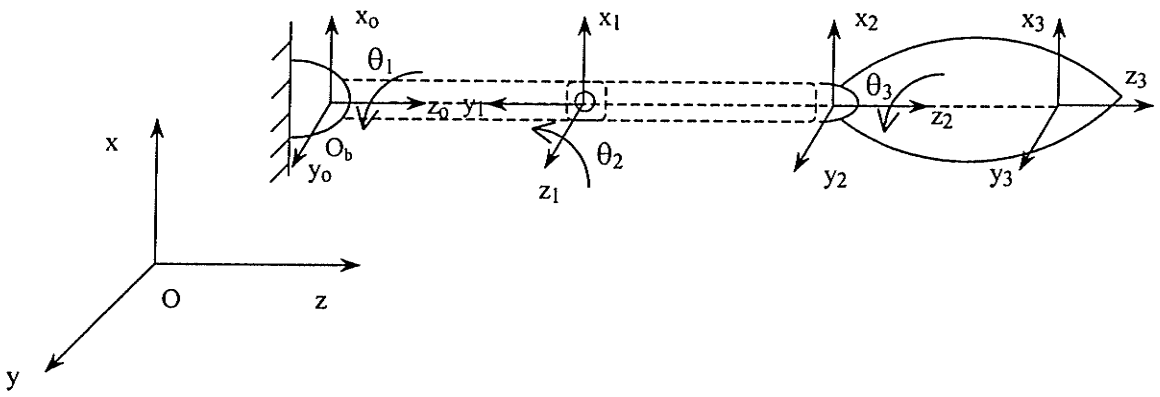

Figure 3.3. Euler angles representation using virtual links.

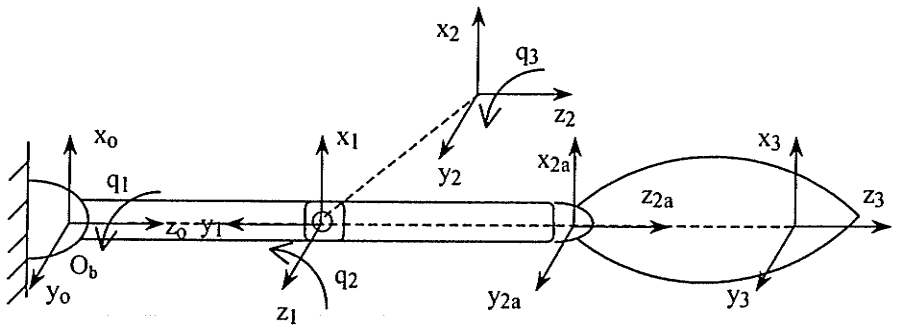

Figure 3.4. DH coordinate systems.

$$\mathbf{A}_i = \begin{bmatrix} \cos\theta_i & -\cos\alpha_i \sin\theta_i & \sin\alpha_i \sin\theta_i & a_i \cos\theta_i \\ \sin\theta_i & -\cos\alpha_i \cos\theta_i & \sin\alpha_i \cos\theta_i & a_i \sin\theta_i \\ 0 & \sin\alpha_i & \cos\alpha_i & d_i \\ 0 & 0 & 0 & 1 \end{bmatrix}$$

$\theta_i, \alpha_i, a_i,$ and d_i are the links and joints parameters and are shown in Table 3.1.

Table 3.1. Link and joint parameters

Link	θ_i	α_i	a_i	d_i
1	q_1	-π/2	0	d_1
2	q_2	π/2	0	0
2a	0	0	0	d_2
3	q_3	0	0	d_3

Let $\mathbf{T}_i$ be the homogeneous transformation matrix from coordinate system i to the inertial coordinate system, then:

$$\mathbf{T}_i = \mathbf{A}_1 \mathbf{A}_2 .... \mathbf{A}_i$$

The equations of motion are obtained from the following Lagrange-Euler based formulation:

$$\tilde{\mathbf{M}}(\mathbf{q})\ddot{\mathbf{q}} + \tilde{\mathbf{C}}(\mathbf{q}, \dot{\mathbf{q}}) + \tilde{\mathbf{G}}(\mathbf{q}) = \tau$$

The elements of the inertial acceleration-related matrix $\tilde{\mathbf{M}}(\mathbf{q})$ are:

$$\tilde{M}_{ij} = Trace\left\{ \Delta_i \left[\sum_{p=j}^{n} \mathbf{T}_p \mathbf{I}_p \mathbf{T}_p^T \right] \Delta_j^T \right\} \qquad (j \geq i) \qquad (3.3)$$

$$\tilde{M}_{ji} = \tilde{M}_{ij}$$

and

$$\mathbf{I}_p = \begin{bmatrix} \mathbf{I}_p^p + m_p \mathbf{r}_p^p \mathbf{r}_p^{pT} & m_p \mathbf{r}_p^p \\ m_p \mathbf{r}_p^{pT} & m_p \end{bmatrix}$$

$\mathbf{I}_p^p$ is a 3×3 inertial matrix of link p about its center of mass with respect to its own coordinate frame. $\mathbf{r}_p^p$ is the position vector of mass center of link p expressed in the coordinate system p and m_p is the mass of link p. Δ_i is a differential operator and is defined as:

$$\mathbf{\Delta}_i = \begin{bmatrix} \lambda_i \hat{\mathbf{z}}_{i-1} & (\lambda_i \hat{\mathbf{p}}_{i-1} + \varphi_i \mathbf{E}) \mathbf{z}_{i-1} \\ \mathbf{0} & 0 \end{bmatrix} \tag{3.4}$$

where

$\mathbf{z}_i$ is the z-*axis* of the coordinate frame *i*. $\mathbf{p}_i$ is the position vector of the origin of the coordinate frame *i*. $\lambda_i = 1$ for revolute (rotating) joints and $\lambda_i = 0$ for prismatic (sliding) joints. $\varphi_i = 1 - \lambda_i$ and $\mathbf{E}$ is a 3×3 unity matrix.

For any 3×1 vector $\mathbf{u} = \{u_x, u_y, u_z\}^T$, we define a 3×3 skew symmetric matrix $\hat{\mathbf{u}}$ as

$$\hat{\mathbf{u}} = \begin{bmatrix} 0 & -u_z & u_y \\ u_z & 0 & -u_x \\ -u_y & u_x & 0 \end{bmatrix}$$

Finally,

$$\widetilde{C}_i(\mathbf{q}, \dot{\mathbf{q}}) = \sum_{j=1}^{n} \sum_{k=1}^{n} C_{ijk} \dot{q}_j \dot{q}_k \tag{3.5}$$

$$\widetilde{C}_{ijk} = Tr\left\{ \Delta_i \left[\sum_{p=k}^{n} \mathbf{T}_p \mathbf{I}_p \mathbf{T}_p^T \right] \mathbf{\Delta}_k^T \mathbf{\Delta}_j \right\} \qquad (i < k, j \le k) \tag{3.6}$$

$$\widetilde{C}_{ikj} = \widetilde{C}_{ijk}$$

$$\widetilde{C}_{ijk} = -\widetilde{C}_{kji} \qquad (j \le i,k)$$

$$\widetilde{G}_i(\mathbf{q}) = -\mathbf{g}^T \Delta_i \left[\sum_{p=i}^{n} m_p \mathbf{T}_p \left(\mathbf{r}_p^p ; 1 \right) \right] \tag{3.7}$$

where $\mathbf{r}_i^i$ is a 3×1 position vector of mass center of link i with respect to its own coordinate frame, $\mathbf{g} = \{-g, 0, 0, 0\}^T$ where $g = 9.81\, m/s^2$, and m_i is the mass of link i. The dynamic and kinematic parameters of the links are chosen as follows:

$$\mathbf{I}_1^1 = \begin{bmatrix} I_1 & 0 & 0 \\ 0 & I_1 & 0 \\ 0 & 0 & I_{1zz} \end{bmatrix}, \quad \mathbf{I}_2^2 = \begin{bmatrix} I_2 & 0 & 0 \\ 0 & I_2 & 0 \\ 0 & 0 & I_{2zz} \end{bmatrix}, \quad \mathbf{I}_3^3 = \begin{bmatrix} I_3 & 0 & 0 \\ 0 & I_3 & 0 \\ 0 & 0 & I_{3zz} \end{bmatrix}, \quad \mathbf{r}_1^1 = \{0, 0, z_1\}^T$$

$\mathbf{r}_2^2 = \{0, 0, z_1\}^T$, and $\mathbf{r}_3^3 = \{0, 0, z_3\}^T$.

The complete equations of motion for the three-link system are:

$$\begin{aligned} \tau_1 = {} & \left[I_1 + m_1 z_1^2 + \left(I_2 + m_2 z_2^2 + I_3 + m_3 (d_3 + z_3)^2 \right)(1 - C_2^2) + (I_{2zz} + I_{3zz}) C_2^2 \right] \ddot{q}_1 \\ & + I_{3zz} C_2 \ddot{q}_3 + 2 S_2 C_2 \dot{q}_1 \dot{q}_2 \left[-I_{3zz} + I_3 + m_3 (d_3 + z_3)^2 \right] - I_{3zz} S_2 \dot{q}_2 \dot{q}_3 \\ & - m_1 g C_1 z_1 - m_2 g S_1 S_2 z_2 - m_3 g S_1 S_2 (d_3 + z_3) \end{aligned}$$

$$\begin{aligned} \tau_2 = {} & \left[I_2 + m_2 z_2^2 + I_3 + m_3 (d_3 + z_3)^2 \right] \ddot{q}_2 \\ & - \dot{q}_1^2 S_2 C_2 \left[I_2 + I_{2zz} + I_3 - I_{3zz} + m_3 (d_3 + z_3)^2 \right] + \dot{q}_1 \dot{q}_3 I_{3zz} S_2 + m_3 g C_1 C_2 (d_3 + z_3) \end{aligned}$$

$$\tau_3 = I_{3zz} C_2 \ddot{q}_1 + I_{3zz} \ddot{q}_3 - I_{3zz} \dot{q}_1 \dot{q}_2 S_2$$

where $C_i = \cos(q_i)$ and $S_i = \sin(q_i)$.

Setting the kinematic and dynamic parameters of the virtual links (the first two links) to zero, i.e., $\mathbf{I}_1^1 = \mathbf{I}_2^2 = \begin{bmatrix} 0 & 0 & 0 \\ 0 & 0 & 0 \\ 0 & 0 & 0 \end{bmatrix}$, $m_1 = m_2 = 0$, $\mathbf{r}_1^1 = \mathbf{r}_2^2 = \{0, 0, 0\}^T$, and $d_1 = d_2 = 0$, we obtain the required equations. Thus, the final equations are:

$$\begin{aligned}\tau_1 &= \left[\left(I_3 + m_3(d_3 + z_3)^2\right)(1 - C_2^2) + I_{3zz}C_2^2\right]\ddot{q}_1 + I_{3zz}C_2\ddot{q}_3 \\ &\quad + 2S_2C_2\dot{q}_1\dot{q}_2\left[-I_{3zz} + I_3 + m_3(d_3 + z_3)^2\right] - I_{3zz}S_2\dot{q}_2\dot{q}_3 - m_3gS_1S_2(d_3 + z_3)\end{aligned}$$

$$\begin{aligned}\tau_2 &= \left[I_3 + m_3(d_3 + z_3)^2\right]\ddot{q}_2 + \dot{q}_1^2S_2C_2\left[(I_{3zz} - I_3) - m_3(d_3 + z_3)^2\right] \\ &\quad + \dot{q}_1\dot{q}_3I_{3zz}S_2 + m_3gC_1C_2(d_3 + z_3)\end{aligned}$$

$$\tau_3 = I_{3zz}C_2\ddot{q}_1 + I_{3zz}\ddot{q}_3 - I_{3zz}\dot{q}_1\dot{q}_2S_2$$

To explain the advantages of using the method of virtual links, the conventional method (using the first principles) is then used to derive the dynamic equations. First the components of the angular velocity ω of the rigid body are determined:

$$\begin{aligned}\omega_x &= -S_2C_3\dot{q}_1 + S_3\dot{q}_2 \\ \omega_y &= S_2S_3\dot{q}_1 + C_3\dot{q}_2 \\ \omega_z &= C_2\dot{q}_1 + \dot{q}_3\end{aligned} \tag{3.8}$$

The kinetic energy (KE) and potential energy (PE) are calculated:

$$KE = \frac{1}{2}\omega^T\mathbf{I}_o\omega$$

Where $\mathbf{I}_o$ is the mass moment of inertia of the rigid body about axes parallel to the body axes and passing through O_b.

$$\mathbf{I}_o = \begin{bmatrix} I_3 + m_3(d_3 + z_3)^2 & 0 & 0 \\ 0 & I_3 + m_3(d_3 + z_3)^2 & 0 \\ 0 & 0 & I_{3zz} \end{bmatrix}$$

$$PE = -m\,\mathbf{g}^{T\,R}\mathbf{P}_c$$

where ${}^{R}\mathbf{P}_c$ is the center of gravity of the rigid body defined in the inertial axes. The Lagrangian function (L) is

$$L = KE - PE$$

Applying the Lagrange's equation

$$\frac{d}{dt}\left[\frac{\partial L}{\partial \dot{q}_i}\right] - \frac{\partial L}{\partial q_i} = \tau_i \tag{3.9}$$

The final equations are:

$$\begin{aligned}\tau_1 = {} & \left[\left(I_3 + m_3(d_3 + z_3)^2\right)(1 - C_2^2) + I_{3zz}C_2^2\right]\ddot{q}_1 + I_{3zz}C_2\ddot{q}_3 \\ & + 2S_2C_2\dot{q}_1\dot{q}_2\left[-I_{3zz} + I_3 + m_3\left(d_3 + z_3\right)^2\right] - I_{3zz}S_2\dot{q}_2\dot{q}_3 - m_3gS_1S_2(d_3 + z_3)\end{aligned}$$

$$\begin{aligned}\tau_2 = {} & \left[I_3 + m_3(d_3 + z_3)^2\right]\ddot{q}_2 + \dot{q}_1^2S_2C_2\left[(I_{3zz} - I_3) - m_3(d_3 + z_3)^2\right] \\ & + \dot{q}_1\dot{q}_3I_{3zz}S_2 + m_3gC_1C_2(d_3 + z_3)\end{aligned}$$

$$\tau_3 = I_{3zz}C_2\ddot{q}_1 + I_{3zz}\ddot{q}_3 - I_{3zz}\dot{q}_1\dot{q}_2S_2$$

The above equations of motion are similar to those obtained in the previous section using the method of virtual links. However, the method of virtual links is more straightforward since it transforms a link with a multi-degree of freedom joint into links with single degree of freedom joints. Furthermore, the terms of the equations of motion can be obtained using Equations (3.3), (3.6), and (3.7) either symbolically or numerically. On

the other hand the terms of the equations of motion, with the conventional method, have to be determined symbolically using Equation (3.9). For multi-body systems, in which the symbolic form of the dynamic equations are lengthy (Zomaya, 1992), this task becomes tedious and error prone.

3.3 Calculation of Constraint Forces/Torques*

3.3.1 Introduction

There has been an increasing interest in formulation of the dynamic equations for interconnected large multi-body systems with constraints. Interest has arisen almost simultaneously in three areas: robotics, biomechanics, and space vehicle dynamics. In each area, the goal is to find an efficient procedure for obtaining and solving the governing equations of motion. There are two distinct ways for deriving the equations of motion for multi-body systems with constraints. The first approach is to formulate the equations of motion in the reduced state space with minimal dimension to adequately describe the phenomena studied. The approach is advantageous in that the general form of the dynamic equations and various computer software for automatic generation of the equations of motion are available to the users. Automatic derivation of dynamic equations using computers is highly desirable because manual symbolic derivation of equations of motion for multi-body systems is tedious and time-consuming. Furthermore, using this approach, the equations of motion can be described by a set of ordinary differential equations (ODEs).

---

* A version of this section has been published in the *Proceedings of the American Control Conference*, Arlington, VA, pp. 3565-3569, 2001, "On Derivation of Constrained Multiple Rigid Body Dynamic Equations," R.F. Abo-Shanab, Q. Wu, and N. Sepehri.

The second approach is to derive the equations of motion in the non-reduced state space, in which constrained forces/torques are introduced and the equations of motion as well as the constraint equations are solved simultaneously to determine the kinematic variables and the constraint forces/torques. Direct determination of constraint forces/torques makes this approach more attractive; however, it results in a set of differential algebraic equations (DAEs).

There exist many systematic numerical methods to solve ODEs. However, systems of DAEs cannot be solved by conventional numerical methods that are used for ODEs. Methods for solving DAEs can be divided into two groups. The first group employs integration algorithms for a specific class of DAEs (Gear, 1971; Blajer, 1992; Shampine et al., 1999). The second group is built upon the idea of feedback control theory and employs modified differential equations that implicitly account for constraint to replace the algebraic equations (Baumgarte, 1972). The major drawback of both groups of methods of solving DAEs, is that all generalized coordinates must be integrated simultaneously although some of them are dependent. Consequently, the error resulting from the numerical integration techniques leads to the violation of constraint equations (especially using methods from the second group). A number of methods have been developed to stabilize the constraints (Baumgarte, 1983; Park and Chiou, 1988; Bayo et al., 1988; Rosen and Edelstein, 1997). It has been documented that it is desirable to first integrate the independent coordinates. This ensures that the solution of the remaining equations to calculate the constraint forces and/or torques has error control on constraint violations. Within this context, some algorithms have been developed to partition the

dependent and independent generalized coordinates (Wehage and Haug, 1982; Mani et al., 1985).

Here, an alternative method of derivation of equations of motion for interconnected multi-body systems is suggested using the concept of augmented state-space and virtual links. At each joint for which it is desired to calculate the constraint forces, a number of virtual links, equals to the number of the reaction forces and moments to be determined, is added. The augmented state space is formed by the states describing the original system and the addition of virtual links. The equations of motion for the expanded multi-body systems are then derived using the first method, in the augmented state space. Following that, the virtual links are removed by setting all kinematic and dynamic parameters and the states associated with them, to zero. This results in a set of equations containing constraint forces and generalized coordinates. The equations containing the generalized coordinates are independent from the constraint forces and can be solved first. The remaining equations are solved next, using the obtained values from the first set of equations, to determine the constraint forces. Thus, the proposed method (*i*) reduces the state space and speeds up the computations, (*ii*) determines the constraint forces directly, and (*iii*) avoids constraint violations since only the generalized coordinates (i.e., independent coordinates) are integrated.

3.3.2 Description of the Method

Consider an *n*-link spatial system. Vector $\mathbf{q} = \{q_1, q_2, ...q_n\}^T$ denotes the generalized coordinates, and $\tau = \{\tau_1, \tau_2, ...\tau_n\}^T$ describes the corresponding generalized forces. In order to determine the constraint forces/torques $\tau_v = \{\tau_{v1}, \tau_{v2}, ..., \tau_{vm}\}$ at a given joint *i*, *m* virtual links are added along the directions of the constraint forces/torques (note that

$m \leq 5$; knowing that all the manipulator joints have at least one degree of freedom, there are at most five constraint forces and torques at each joint). The original n-link system now becomes an $(n+m)$-link system. The new generalized vector, for the expanded dynamic system, is $\tilde{\mathbf{q}} = \{q_1, q_2, ..., q_n, q_{v1}, q_{v2}, ..., q_{vm}\}^T$ where $q_{v1}, q_{v2}, ..., q_{vm}$ are the linear/angular displacements of the virtual links $V_1, V_2, ..., V_m$, respectively. The generalized forces are $\tilde{\tau} = \{\tau_1, \tau_2, ...\tau_n, \tau_{v1}, \tau_{v2}, ..., \tau_{vm}\}^T$ with $\tau_v = \{\tau_{v1}, \tau_{v2}, ..., \tau_{vm}\}^T$ corresponding to $\mathbf{q}_v = \{q_{v1}, q_{v2}, ..., q_{vm}\}^T$. The augmented state space is formed by the state $\tilde{\mathbf{q}}$. The dynamic equations are then derived using existing formulation for serial link fixed base manipulators, in the augmented state space:

$$\tilde{\mathbf{M}}(\tilde{\mathbf{q}})\ddot{\tilde{\mathbf{q}}} + \tilde{\mathbf{C}}(\tilde{\mathbf{q}}, \dot{\tilde{\mathbf{q}}})\dot{\tilde{\mathbf{q}}} + \tilde{\mathbf{G}}(\tilde{\mathbf{q}}) = \tilde{\tau} \tag{3.10}$$

where $\tilde{\mathbf{M}}(\tilde{\mathbf{q}})$ is the symmetric, positive definite inertial acceleration-related matrix, $\tilde{\mathbf{C}}(\tilde{\mathbf{q}}, \dot{\tilde{\mathbf{q}}})\dot{\tilde{\mathbf{q}}}$ is the vector of centripetal and Coriolis forces/torques and $\tilde{\mathbf{G}}(\tilde{\mathbf{q}})$ is the vector of gravitational torques. Equation (3.10) can be rewritten as

$$\begin{bmatrix} \tilde{\mathbf{M}}^{(1)}_{n\times n}(\tilde{\mathbf{q}}) & \tilde{\mathbf{M}}^{(2)}_{n\times m}(\tilde{\mathbf{q}}) \\ \tilde{\mathbf{M}}^{(3)}_{m\times n}(\tilde{\mathbf{q}}) & \tilde{\mathbf{M}}^{(4)}_{m\times m}(\tilde{\mathbf{q}}) \end{bmatrix} \begin{Bmatrix} \ddot{\mathbf{q}} \\ \ddot{\mathbf{q}}_v \end{Bmatrix} + \begin{bmatrix} \tilde{C}^{(1)}_{n\times n}(\tilde{\mathbf{q}}, \dot{\tilde{\mathbf{q}}}) & \tilde{C}^{(2)}_{n\times m}(\tilde{\mathbf{q}}, \dot{\tilde{\mathbf{q}}}) \\ \tilde{C}^{(3)}_{m\times n}(\tilde{\mathbf{q}}, \dot{\tilde{\mathbf{q}}}) & \tilde{C}^{(4)}_{m\times m}(\tilde{\mathbf{q}}, \dot{\tilde{\mathbf{q}}}) \end{bmatrix} \begin{Bmatrix} \dot{\mathbf{q}} \\ \dot{\mathbf{q}}_v \end{Bmatrix} + \begin{Bmatrix} \tilde{\mathbf{G}}(\tilde{\mathbf{q}}) \\ \tilde{\mathbf{G}}_v(\tilde{\mathbf{q}}) \end{Bmatrix} = \begin{Bmatrix} \tau \\ \tau_v \end{Bmatrix} \tag{3.11}$$

To obtain the final equations for the original multi-link system, the following constraints must be satisfied:

$$\begin{aligned} q_{v1} &= q_{v2} = ... = q_{vm} = 0 \\ \dot{q}_{v1} &= \dot{q}_{v2} = ... = \dot{q}_{vm} = 0 \\ \ddot{q}_{v1} &= \ddot{q}_{v2} = ... = \ddot{q}_{vm} = 0 \end{aligned} \tag{3.12}$$

Substituting (3.12) into (3.11) and setting all kinematic and dynamic parameters associated with the virtual links to zero, final equations of motion for the original multi-link system will be:

$$\mathbf{M}^{(1)}_{n\times n}(\mathbf{q})\ddot{\mathbf{q}} + \mathbf{C}^{(1)}_{n\times n}(\mathbf{q},\dot{\mathbf{q}})\dot{\mathbf{q}} + \mathbf{G}(\mathbf{q}) = \tau \tag{3.13}$$

$$\mathbf{M}^{(3)}_{m\times n}(\mathbf{q})\ddot{\mathbf{q}} + \mathbf{C}^{(3)}_{m\times n}(\mathbf{q},\dot{\mathbf{q}})\dot{\mathbf{q}} + \mathbf{G}_v(\mathbf{q}) = \tau_v \tag{3.14}$$

First, variables $\mathbf{q}, \dot{\mathbf{q}}$ and $\ddot{\mathbf{q}}$ are obtained from Equation (3.13). They are then substituted into Equation (3.14) to solve for constraint forces/torques, τ_v.

Remarks:

(1) From the above derivation, it is seen that in the augmented state space, the equations of motion shown in (3.10) are in the reduced state space form. Thus, we can take advantage of the previous work on automatic generation of the equations of motion and methods to solve them.

(2) The constraint forces are solved directly from Equation (3.14). Equation (3.13) describes the motion of the original multi-link system without the addition of the virtual links. Thus, the violations of the constraint are avoided (Mani et al., 1985). This is the major advantage of the proposed method over the conventional method.

(3) The presented method is also different from the conventional method for determining the joint forces which first solves for generalized coordinates and then determines the joint forces by using Newton-Euler equations, recursively. Using this recursive formulation, if the reaction force at the base is of interest, one has to calculate all the reaction forces and torques starting from the distal link. In the proposed method, the equations for joint forces (3.14) are derived simultaneously with the equations of motion (3.13) and the required forces are calculated directly.

3.3.3 Demonstrative Example

A three-link system, taken from the study by Hemami (1982), is used to demonstrate the proposed method. With reference to Figure 3.5, the constraint forces at joint A are to be determined. Using the proposed method, two virtual links are inserted at joint A as link AC and link CA_1, (see in Figure 3.6). The generalized coordinate vector is then $\tilde{\mathbf{q}} = \{\theta_1, x, y, \theta_2, \theta_3\}^T$. The generalized force vector $\tilde{\tau} = \{\tau_1, F_x, F_y, \tau_3, \tau_4\}^T$ contains the constraint forces F_x and F_y. In the augmented state space, the equations of motion can be derived using standard Lagrangian Mechanics and are shown as follows:

$$\begin{aligned} T_1 = {} & \left(m_2 l_1^2 + I_1 + m_1 d_1^2 + m_3 l_1^2 + m_{v1} l_1^2 + m_{v2} l_1^2 + I_{v1} + I_{v2}\right)\ddot{\theta}_1 + \left(m_2 l_1 d_2 + m_3 l_1 l_2\right)\cos\left(\theta_2 - \theta_1\right)\ddot{\theta}_2 \\ & + m_3 l_1 d_3 \cos\left(\theta_3 - \theta_1\right)\ddot{\theta}_3 + \left(m_{v1} + m_{v2} + m_3 + m_2\right) l_1 \cos\theta_1 \ddot{x} + \left(m_{v2} + m_3 + m_2\right) l_1 \sin\theta_1 \ddot{y} \\ & + \left(m_2 + m_3\right) l_1 d_2 \sin\left(\theta_2 - \theta_1\right)\dot{\theta}_2^2 + m_3 l_1 d_3 \sin\left(\theta_3 - \theta_1\right)\dot{\theta}_3^2 \\ & + \left(m_1 d_1 + m_{v1} l_1 + m_{v2} l_1 + m_2 l_1 + m_3 l_1\right) g \sin\theta_1 \end{aligned} \tag{3.15a}$$

$$\begin{aligned} T_2 = {} & \left(m_2 l_1 d_2 \cos\left(\theta_2 - \theta_1\right) + m_3 l_1 l_2 \cos\left(\theta_2 - \theta_1\right)\right)\ddot{\theta}_1 + \left(m_3 l_2^2 + m_2 d_2^2 + I_2\right)\ddot{\theta}_2 \\ & + m_3 l_2 d_3 \cos\left(\theta_3 - \theta_2\right)\ddot{\theta}_3 + \left(m_3 l_2 + m_2 d_2\right)\cos\theta_2 \ddot{x} + \left(m_3 l_2 + m_2 d_2\right)\sin\theta_2 \ddot{y} \\ & + \left(m_3 l_2 l_1 + m_2 d_2 l_1\right)\sin\left(\theta_2 - \theta_1\right)\dot{\theta}_1^2 - m_3 l_1 d_3 \sin\left(\theta_3 - \theta_2\right)\dot{\theta}_3^2 + \left(m_2 d_2 - m_2 l_3\right)\sin\theta_2 \, g \end{aligned} \tag{3.15b}$$

$$\begin{aligned} T_3 = {} & m_3 l_1 d_3 \cos\left(\theta_3 - \theta_1\right)\ddot{\theta}_1 + m_3 l_2 d_3 \cos\left(\theta_3 - \theta_2\right)\ddot{\theta}_2 + \left(m_3 d_3^2 + I_3\right)\ddot{\theta}_3 + m_3 d_3 \cos\theta_3 \ddot{x} \\ & + m_3 d_3 \sin\theta_3 \ddot{y} + m_3 l_1 d_3 \sin\left(\theta_3 - \theta_1\right)\dot{\theta}_1^2 - m_3 l_1 d_3 \sin\left(\theta_3 - \theta_2\right)\dot{\theta}_2^2 + m_3 d_3 g \sin\theta_3 \end{aligned} \tag{3.15c}$$

$$\begin{aligned} F_x = {} & \left(m_{v1} + m_{v2} + m_3 + m_2\right) l_1 \cos\theta_1 \ddot{\theta}_1 + \left(m_2 d_2 + m_3 l_2\right)\cos\theta_2 \ddot{\theta}_2 + m_3 d_3 \cos\theta_3 \ddot{\theta}_3 \\ & + \left(m_{v1} + m_{v2} + m_3 + m_2\right)\ddot{x} - \left(m_2 + m_3\right) l_1 \sin\theta_1 \dot{\theta}_1^2 - \left(m_2 d_2 + m_3 l_2\right)\sin\theta_2 \dot{\theta}_2^2 \\ & - m_3 d_3 \sin\theta_3 \dot{\theta}_3^2 - \left(m_{v1} + m_{v2}\right) l_1 \sin\theta_1 \dot{\theta}_1^2 \end{aligned} \tag{3.15d}$$

$$\begin{aligned} F_y = {} & \left(m_{v1} + m_{v2} m_2 + m_3\right) l_1 \sin\theta \ddot{\theta}_1 + \left(m_2 d_2 + m_3 l_2\right)\sin\theta_2 \ddot{\theta}_2 + m_3 d_3 \sin\theta_3 \ddot{\theta}_3 \\ & + \left(m_{v2} + m_2 + m_3\right)\left(g + \ddot{y}\right) + \left(m_2 + m_3\right) l_1 \cos\theta_1 \dot{\theta}_1^2 + \left(m_2 d_2 + m_3 l_2\right)\cos\theta_2 \dot{\theta}_2^2 \\ & + m_3 d_3 \cos\theta_3 \dot{\theta}_3^2 + m_{v2} l_1 \cos\theta_1 \dot{\theta}_1^2 \end{aligned} \tag{3.15e}$$

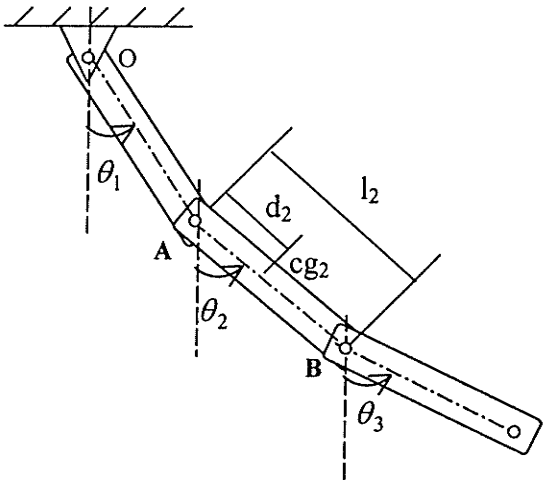

Figure 3.5. Three-link system.

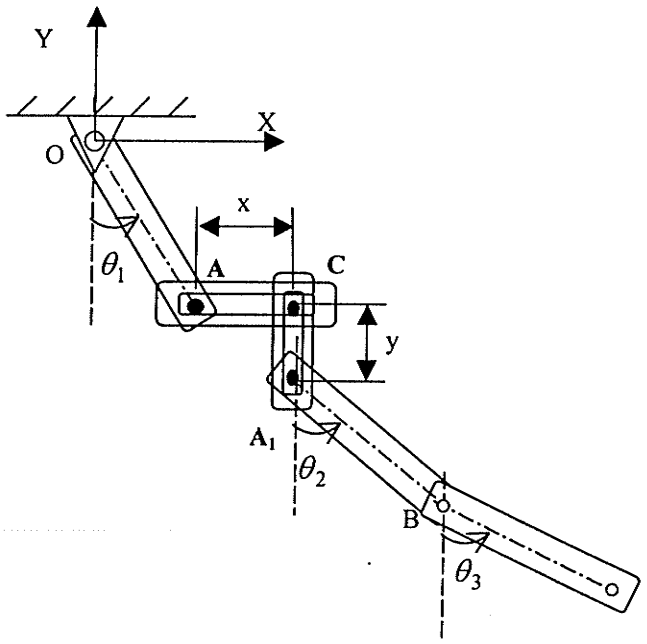

Figure 3.6. Three-link system with the addition of virtual links.

To determine the constraint forces F_x and F_y, we now impose the following constraint equations:

$$\left.\begin{aligned} x = y = 0 \\ \dot{x} = \dot{y} = 0 \\ \ddot{x} = \ddot{y} = 0 \end{aligned}\right\} \tag{3.16}$$

Substituting (3.10) into (3.9) and setting all the kinematic and dynamic parameters associated with the virtual links, AC and CA_1, to zero (for this example $m_{v1} = m_{v2} = 0$ and $I_{v1} = I_{v2} = 0$), we have:

$$\begin{aligned} T_1 = {} & \left(m_2 l_1^2 + I_1 + m_1 d_1^2 + m_3 l_1^2\right)\ddot{\theta}_1 + \left(m_2 l_1 d_2 + m_3 l_1 l_2\right)\cos\left(\theta_2 - \theta_1\right)\ddot{\theta}_2 \\ & + m_3 l_1 d_3 \cos(\theta_3 - \theta_1)\ddot{\theta}_3 + \left(m_2 + m_3\right) l_1 d_2 \sin(\theta_2 - \theta_1)\dot{\theta}_2^2 \\ & + m_3 l_1 d_3 \sin\left(\theta_3 - \theta_1\right)\dot{\theta}_3^2 + \left(m_1 d_1 + m_2 l_1 + m_3 l_1\right)\sin\theta_1 \, g \end{aligned} \tag{3.17a}$$

$$\begin{aligned} T_2 = {} & \left(m_2 l_1 d_2 + m_3 l_1 l_2\right)\cos\left(\theta_2 - \theta_1\right)\ddot{\theta}_1 + \left(m_3 l_2^2 + m_2 d_2^2 + I_2\right)\ddot{\theta}_2 \\ & + m_3 l_2 d_3 \cos\left(\theta_3 - \theta_2\right)\ddot{\theta}_3 + \left(m_3 l_2 l_1 + m_2 d_2 l_1\right)\sin\left(\theta_2 - \theta_1\right)\dot{\theta}_1^2 \\ & - m_3 l_1 d_3 \sin\left(\theta_3 - \theta_2\right)\dot{\theta}_3^2 + \left(m_2 d_2 - m_2 l_3\right)\sin\theta_2 \, \mathrm{g} \end{aligned} \tag{3.17b}$$

$$\begin{aligned} T_3 = {} & m_3 l_1 d_3 \cos\left(\theta_3 - \theta_1\right)\ddot{\theta}_1 + m_3 l_2 d_3 \cos(\theta_3 - \theta_2)\ddot{\theta}_2 + \left(m_3 d_3^2 + I_3\right)\ddot{\theta}_3 \\ & + m_3 l_1 d_3 \sin(\theta_3 - \theta_1)\dot{\theta}_1^2 - m_3 l_1 d_3 \sin(\theta_3 - \theta_2)\dot{\theta}_2^2 + m_3 d_3 g \sin\theta_3 \end{aligned} \tag{3.17c}$$

$$\begin{aligned} F_x = {} & \left(m_3 + m_2\right) l_1 \cos\theta_1 \, \ddot{\theta}_1 + \left(m_2 d_2 + m_3 l_2\right)\cos\theta_2 \ddot{\theta}_2 + m_3 d_3 \cos\theta_3 \ddot{\theta}_3 \\ & - \left(m_2 + m_3\right) l_1 \sin\theta_1 \dot{\theta}_1^2 - \left(m_2 d_2 + m_3 l_2\right)\sin\theta_2 \dot{\theta}_2^2 - m_3 d_3 \sin\theta_3 \dot{\theta}_3^2 \end{aligned} \tag{3.18a}$$

$$\begin{aligned} F_y = {} & \left(m_2 + m_3\right) l_1 \sin\theta \, \ddot{\theta}_1 + \left(m_2 d_2 + m_3 l_2\right)\sin\theta_2 \ddot{\theta}_2 + m_3 d_3 \sin\theta_3 \ddot{\theta}_3 + \left(m_2 + m_3\right) g \\ & + \left(m_2 + m_3\right) l_1 \cos\theta_1 \dot{\theta}_1^2 + \left(m_2 d_2 + m_3 l_2\right)\cos\theta_2 \dot{\theta}_2^2 + m_3 d_3 \cos\theta_3 \dot{\theta}_3^2 \end{aligned} \tag{3.18b}$$

As is seen, set of Equations (3.18) that contains the constraint forces is decoupled from the rest of the Equations (3.17). Thus, Equations (3.17) are solved first for θ_i (i=1,2,3) and their derivatives. The constraint forces are then calculated using (3.18). By

integrating (3.17) only, the violations of constraints are avoided, yet the constraint forces can be determined explicitly.

To signify the developed method, this example is solved again using the conventional method. The Lagrange's equations for mechanical systems with constraints can be written as (Meirovitch, 1970):

$$\frac{d}{dt}\left(\frac{\partial L}{\partial \dot{\theta}_i}\right)-\frac{\partial L}{\partial \theta_i}-\sum_{k=1}^{m} A_{i,k}\zeta_k = \tau_i \qquad i=1...n \tag{3.19}$$

$$h_k(\mathbf{q}) = 0 \qquad k=1...m \tag{3.20}$$

where L is the Lagrangian function, τ_i is the generalized applied force, q_i are the generalized coordinate components, m is the number of constraint equations, $A_{i,k}$ is the i^{th} gradient of the k^{th} constraint equation, and ζ_i is the Lagrange multipliers. Equation (3.20) represents the constraints. For this example, we have

$$\begin{aligned} h_1(\theta_1,\theta_2) &= x_{cg2} - l_1\sin\theta_1 - d_2\sin\theta_2 = 0 \\ h_2(\theta_1,\theta_2) &= y_{cg2} + l_1\cos\theta_1 + d_2\cos\theta_2 = 0 \end{aligned} \tag{3.21}$$

where x_{cg2} and y_{cg2} are the coordinates of the mass center of the second link.

Equation (3.19) can be written in the following form:

$$\mathbf{M}(\mathbf{q})\ddot{\mathbf{q}} + \mathbf{N}(\mathbf{q},\dot{\mathbf{q}}) - \mathbf{A}^T\zeta = \tau \tag{3.22}$$

Where $\mathbf{M}(\mathbf{q})$ is the symmetric, positive definite inertial matrix, $\mathbf{N}(\mathbf{q},\dot{\mathbf{q}})$ is the vector of centripetal, Coriolis, and gravitational generalized forces.

$$T_1 = \left(m_1 d_1^2 + I_1\right)\ddot{\theta}_1 + m_1 g d_1 \sin\theta_1 - l_1\zeta_1\cos\theta_1 - l_1\zeta_2\sin\theta_1$$

$$\begin{aligned} T_2 = &\left[I_2 + \left(d_2^2 + l_2^2 - 2\,d_2\,l_2\right)m_3\right]\ddot{\theta}_2 + \left(l_2 - d_2\right)m_3\,d_3\cos\left(\theta_3-\theta_2\right)\ddot{\theta}_3 \\ &+ \left(l_2 - d_2\right)m_3\cos\theta_2\ddot{x}_{c2} + \left(l_2 - d_2\right)m_3\,\sin\theta_2\left(\ddot{y}_{c2} + g\right) \\ &- \left(d_3 - d_2\right)m_3\,d_3\sin\left(\theta_3-\theta_2\right)\dot{\theta}_3^2 - d_2\zeta_1\cos\theta_2 - d_2\zeta_2\sin\theta_2 \end{aligned}$$

$$T_3 = (l_2 - d_2)m_3\, d_3 \cos(\theta_3 - \theta_2)\ddot{\theta}_2 + (m_3 d_3^2 + I_3)\ddot{\theta}_3 + m_3 d_3 \cos\theta_3 \ddot{x}_{c2} + m_3 d_3 \sin\theta_3 (\ddot{y}_{c2} + g) + (l_2 - d_2)m_3\, d_3 \sin(\theta_3 - \theta_2)\dot{\theta}_2^2$$

$$\zeta_1 = -(l_2 - d_2)m_3 \cos\theta_2 \ddot{\theta}_2 - m_3 d_3 \cos\theta_3 \ddot{\theta}_3 - (m_2 + m_3)\ddot{x}_{c2} + (l_2 - d_2)m_3 \sin\theta_2 \dot{\theta}^2 + m_3 d_3 \sin\theta_3 \dot{\theta}_3^2$$

$$\zeta_2 = -(l_2 - d_2)m_3 \sin\theta_2 \ddot{\theta}_2 - m_3 d_3 \sin\theta_3 \ddot{\theta}_3 - (m_2 + m_3)(\ddot{y}_{c2} + g) - (l_2 - d_2)m_3 \cos\theta_2 \dot{\theta}_2^2 - m_3 d_3 \cos\theta_3 \dot{\theta}_3^2$$

Differentiating the constraint equations (3.21) twice with respect to time

$$\mathbf{A}(\mathbf{q})\ddot{\mathbf{q}} + \dot{\mathbf{A}}(\mathbf{q})\dot{\mathbf{q}} = \mathbf{0} \tag{3.23}$$

where $\mathbf{A}(\mathbf{q}) = \dfrac{\partial \boldsymbol{h}}{\partial \mathbf{q}} = \begin{bmatrix} -l_1\cos\theta_1 & -d_2\cos\theta_2 & 0 & 1 & 0 \\ -l_1\sin\theta_1 & -d_2\sin\theta_2 & 0 & 0 & 1 \end{bmatrix}$

From (3.22) and (3.23)

$$\zeta = \left(\mathbf{A}\mathbf{M}^{-1}\mathbf{A}^{\mathrm{T}}\right)^{-1}\left[\mathbf{A}\mathbf{M}^{-1}(\mathbf{N} - \boldsymbol{\tau}) - \dot{\mathbf{A}}\dot{\mathbf{q}}\right] \tag{3.24}$$

where the elements of the inertial matrix, **M**, are:

$$M_{1,2} = M_{1,3} = M_{1,4} = M_{1,5} = M_{2,1} = M_{3,1} = M_{3,4} = M_{4,1} = M_{4,5} = M_{5,1} = M_{5,4} = 0$$

$$M_{1,1} = m_1 d_1^2 + I_1$$

$$M_{2,2} = I_2 + (d_2^2 + l_2^2 - 2\, d_2\, l_2)m_3$$

$$M_{2,3} = (l_2 - d_2)m_3\, d_3 \cos(\theta_3 - \theta_2)$$

$$M_{2,4} = (l_2 - d_2)m_3 \cos\theta_2$$

$$M_{2,5} = (l_2 - d_2)m_3 \sin\theta_2$$

$$M_{3,2} = (l_2 - d_2)m_3\, d_3 \cos(\theta_3 - \theta_2)$$

$$M_{3,3} = m_3 d_3^2 + I_3$$

$$M_{3,5} = m_3 d_3 \sin\theta_3$$

$$M_{4,2} = (l_2 - d_2)m_3 \cos\theta_2$$

$$M_{4,3} = m_3 d_3 \cos\theta_3$$

$$M_{4,4} = m_2 + m_3$$

$$M_{5,2} = (l_2 - d_2)m_3 \sin\theta_2$$

$$M_{5,3} = m_3 d_3 \sin\theta_3, \; M_{5,5} = m_2 + m_3$$

The elements of the centripetal, Coriolis, and gravitational generalized force vector, $\mathbf{N}(\mathbf{q}, \dot{\mathbf{q}})$, are:

$$N_1 = m_1 g d_1 \sin\theta_1$$

$$N_2 = (l_2 - d_2)m_3 \sin\theta_2 g - (d_3 - d_2)m_3 d_3 \sin(\theta_3 - \theta_2)\dot{\theta}_3^2 d_2$$

$$N_3 = m_3 d_3 \sin\theta_3 g + (l_2 - d_2)m_3 d_3 \sin(\theta_3 - \theta_2)\dot{\theta}_2^2$$

$$N_4 = -(l_2 - d_2)m_3 \sin\theta_2 \dot{\theta}_2^2 - m_3 d_3 \sin\theta_3 \dot{\theta}_3^2$$

$$N_5 = (m_2 + m_3)g + (l_2 - d_2)m_3 \cos\theta_2 \dot{\theta}_2^2 + m_3 d_3 \cos\theta_3 \dot{\theta}_3^2$$

Parameters d_i, l_i and the states θ_i (i=1,2,3) are defined in Figure 3.5. ζ_1 and ζ_2 are Lagrange multipliers. First, ζ_1 and ζ_2 can be calculated using Equation (3.24). Next, Equation (3.22) is solved for the generalized coordinate $\theta_1, \theta_2, \theta_3, x_{cg2}$, and y_{cg2}. It was reported in the literature (Mani et al., 1985) that solving these equations simultaneously causes violation of the constraint equation (3.21).

Chapter 4

Stability Analysis Using Impact Model*

4.1 Outline of the Modeling

In this chapter, a model describing the tip-over dynamics of a mobile manipulator is derived. The movement of the implement is limited to a planar motion. Also, the base and the ground are both considered as rigid bodies and the impact between them is plastic, i.e., the impacting edge will remain on the ground after the first impact and no bouncing occurs. With reference to Figure 4.1, the system to be modeled can be characterized by three distinct phases:

Phase 1: The platform is stable and not moving (see Figure 4.1a). This refers to a case whereby the manipulator movement does not affect the stability and the model consists of only dynamic equations as that of a two-link manipulator.

---

* A version of this chapter has been published in *Robotica*, Vol. 19, pp. 439-449, 2002, "On Dynamic Stability of Manipulators Mounted on Mobile Platforms," R.F. Abo-Shanab and N. Sepehri.

Phase 2: The base is tipping over the rear edge (**Phase 2A**) or the front edge (**Phase 2B**). This situation is schematically shown in Figure 4.1b. This is the case whereby the forces and moments arising from the implement movements can no longer be sustained by the vehicle without overturning. Assuming that the friction between the ground and the machine base is sufficient to allow the rotation only, the machine can be modeled as a three-link manipulator, pivoted on edge **A** (**Phase 2A**) or pivoted on edge **B** (**Phase 2B**).

Phase 3: The base rocks back and forth. For example, with reference to Figure 4.1c, the machine rolls over edge **A** towards a stable position. As the base hits the ground on edge **B**, the system suffers an impulsive force, which causes discontinuities in the joint angular velocities of all links, including the base. The states of the machine and the impulsive forces arising at the stance of impact will determine the subsequent states after the impact.

First the dynamic models for first and second phases are outlined. Then, the dynamic model for the third phase is derived in detail.

4.1.1 Dynamic Model in Case of No Impact (Phases I and II)

As described in the previous section, the first and second phases have no impact with the ground. Thus, the first phase can be modeled as a two-link serial manipulator. The second phase can be modeled as a three-link serial robot manipulator. The dynamic equations describing the above two phases are derived based on Lagrange's equation as follows:

$$\mathbf{M}(\mathbf{q})\ddot{\mathbf{q}} + \mathbf{C}(\mathbf{q},\dot{\mathbf{q}}) + \mathbf{G}(\mathbf{q}) = \tau \qquad (4.1)$$

Different terms of Equation (4.1) have been explained in Section 3.2. The number of links is ($n = 2$) for the first case and ($n = 3$) for the second case.

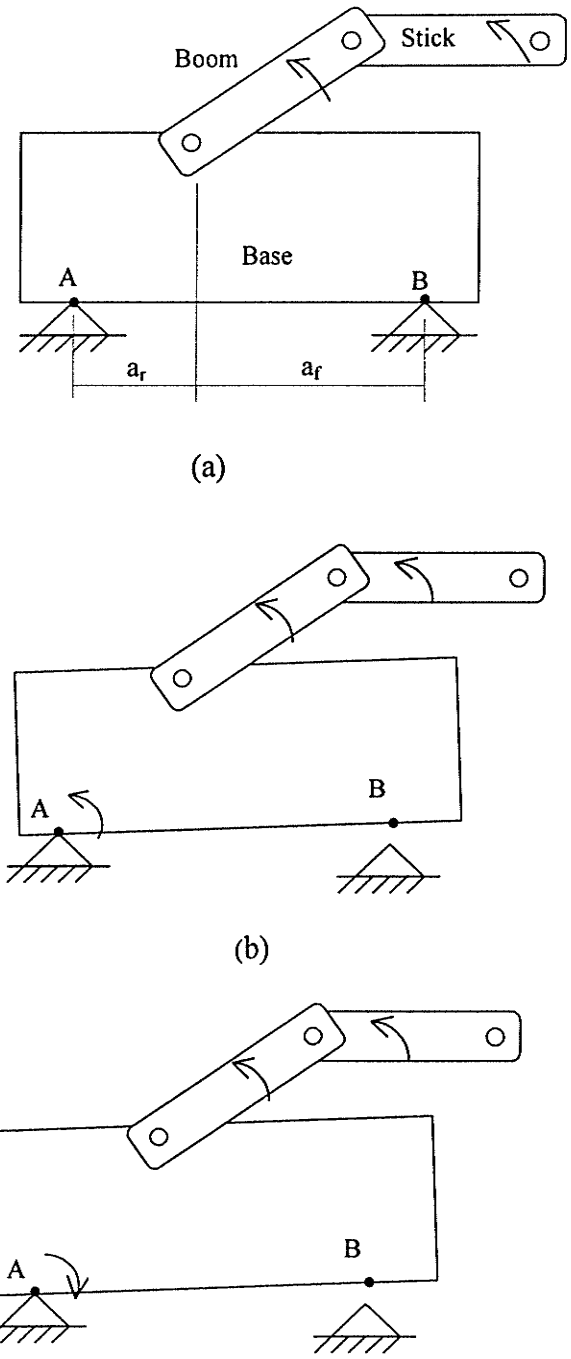

Figure 4.1. Different phases of the base in a mobile manipulator: **(a)** base is stable; **(b)** base is tipping over the rear axis; **(c)** just before the impact with the ground.

4.1.2 Dynamic Model in Case of Impact (Phase III)

Consider the case whereby the base is rotating about edge **A**. Due to the movement of the manipulator, the base may reverse its direction and collide with the ground over edge **B** (see Figure 4.1c). This impact has effects on the velocities and internal forces of the manipulator. First, large impulsive torque develops at each joint. Secondly, the velocities representing joint rates change instantaneously*. Zheng and Hemami (1985) studied the collision of a robot end-effector with the environment. Mathematical models were derived which established quantitative relations between impulsive torques, abrupt changes in velocities, and the severity of the collision. Their method has been adopted here for the problem under investigation. With reference to Figure 4.1c, in order to establish the mathematical model during the period of collision between edge **B** and the ground, edge **A** is considered free to translate in both horizontal and vertical directions (i.e., there is no impulsive force at edge **A**). This means that the dynamic models derived for the cases of no impact cannot be applied to compute the instantaneous changes of the joint angular velocities at the moment when the free end of the base collides with the ground. Therefore, we first derive the dynamic equations for the general case assuming both contact edges are in the air, i.e. non-fixed base robot manipulator. Joint **A** (or **B**), on which the base was originally rotating, is modeled by adding two virtual links. Figure 4.2 shows a schematic diagram of the manipulator including the virtual links. The virtual links have no mass and no inertia. The advantage of this assumption is that the dynamic model can be derived as that of any fixed base manipulator.

* The term 'instantaneously' means that the changes happen in a very short period of time.

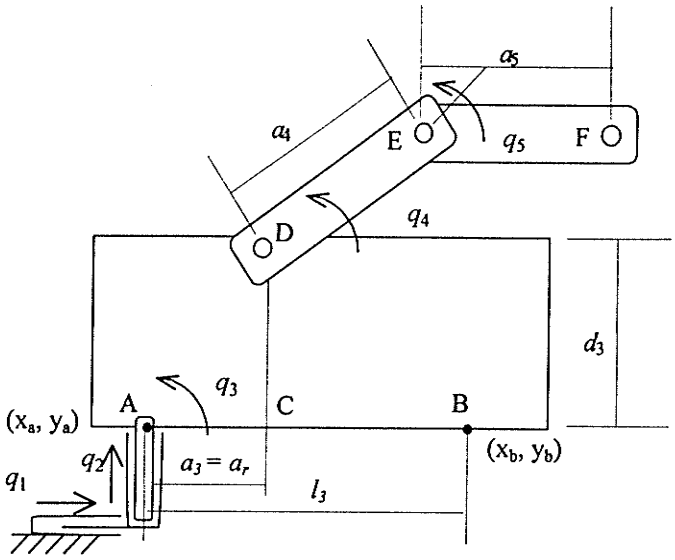

Figure 4.2. Schematic diagram of the manipulator including the virtual links.

In this phase, the first two joints are prismatic and the last three are revolute. The link coordinate systems for this configuration are shown in Figure 4.3. The Denavit-Hartenberg (DH) link coordinate parameters are shown in Table 4.1. Equation (4.1) can be used to derive the dynamic equations for this phase with ($n = 5$).

Table 4.1. Mobile Manipulator Link coordinate parameters

Link	θ_i	d_i	a_i	α_i	Variables
1	$\pi/2$	q_1	0	$\pi/2$	q_1
2	$\pi/2$	q_2	0	$\pi/2$	q_2
3	q_3	0	a_f or a_r	$-\pi/2$	q_3
3a	0	d_3	0	$\pi/2$	-
4	q_4	0	a_4	0	q_4
5	q_5	0	a_5	0	q_5

When the free end of the manipulator base comes in contact with the ground, there will be an instantaneous change in the velocities. Since the other end of the base is free to move, the instantaneous changes of the velocities will also be reflected on the rotation of the base in the form of rotation about the new contact point. The instantaneous change of

the speed for all degrees of freedom, $\Delta\dot{\mathbf{q}}$, upon collision with the ground, is (see the Appendix for detailed derivation):

$$\Delta\dot{\mathbf{q}} = (\mathbf{M}(\mathbf{q}))^{-1}\,\mathbf{J}^T\left(\mathbf{J}\ (\mathbf{M}(\mathbf{q}))^{-1}\,\mathbf{J}^T\right)\Delta\dot{\mathbf{x}}_b \tag{4.2}$$

$\mathbf{M}(\mathbf{q})$ is defined in Section 2.2. $\mathbf{J}$ is the Jacobian matrix defined as:

$$\mathbf{J} = \frac{\partial\,\mathbf{x}_b}{\partial\,\mathbf{q}} \tag{4.3}$$

As seen in Figure 4.2, collision occurs at point $\mathbf{x}_b = [x_b, y_b]^T$, where

$x_b = q_1 + l_1\cos(q_3)$

$y_b = q_2 + l_1\sin(q_3)$

and q_1, q_2, and q_3 are elements of the joint variables vector $\mathbf{q} = [q_1, q_2, q_3, q_4, q_5]^T$

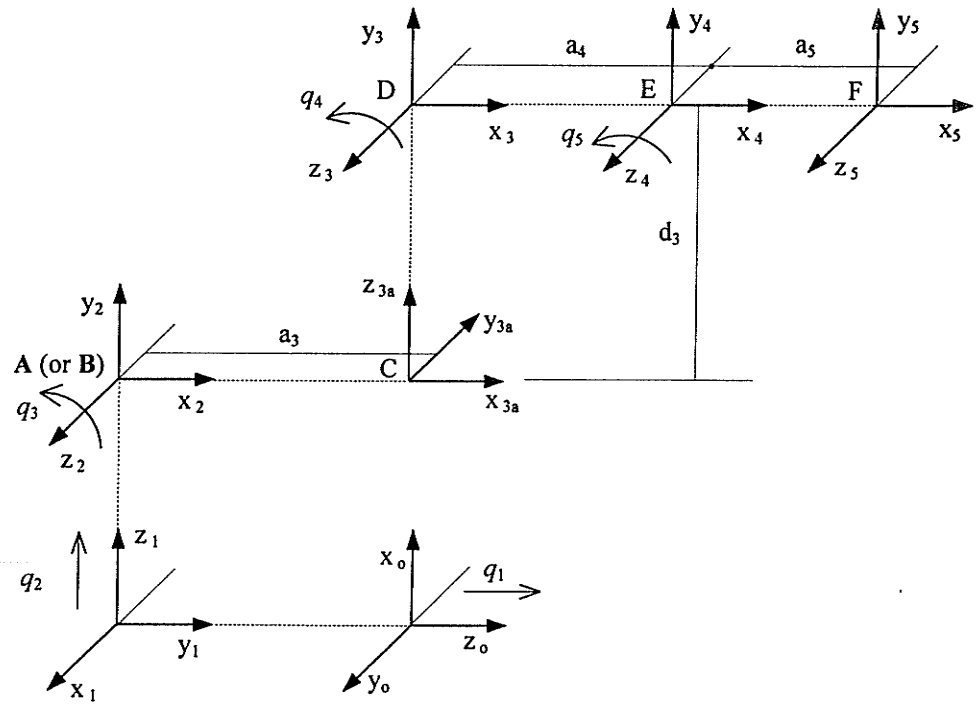

Figure 4.3. Link coordinate systems pertaining to Figure 4.2.

From the above relation, one can easily find the Jacobian, **J**:

$$\mathbf{J} = \begin{bmatrix} 1 & 0 & -l_1 \sin q_3 & 0 & 0 \\ 0 & 1 & l_1 \cos q_3 & 0 & 0 \end{bmatrix} \tag{4.4}$$

Assuming the impact is plastic, the velocity of point **B** becomes zero after impact. Thus, $\Delta \dot{\mathbf{x}}_b$, the change of the velocity of the point **B** due to the collision with the ground, will be $\Delta \dot{\mathbf{x}}_b = -\dot{\mathbf{x}}_{b\,before}$. $\dot{\mathbf{x}}_{b\,before}$ is the velocity of point **B** before the impact. Thus,

$\Delta \dot{\mathbf{q}} = \dot{\mathbf{q}}_{after} - \dot{\mathbf{q}}_{before}$ and

$$\dot{\mathbf{q}}_{after} = \dot{\mathbf{q}}_{before} + (\mathbf{M}(\mathbf{q}))^{-1}\,\mathbf{J}^T \left(\mathbf{J}\ (\mathbf{M}(\mathbf{q}))^{-1}\,\mathbf{J}^T\right)\left(-\dot{\mathbf{x}}_{b\,before}\right) \tag{4.5}$$

$\dot{\mathbf{q}}_{before}$ is the joint velocity vector before the impact and $\dot{\mathbf{q}}_{after}$ is the joint velocity vector after the impact.

Equation (4.5) describes the instantaneous change in the joint velocities immediately after the impact with the ground. The new joint velocities, $\dot{\mathbf{q}}_{after}$, along with the current joint positions, which remain unchanged during the short duration of collision, constitute the initial values of the system states for subsequent simulation times.

4.2 Computational Algorithm

During the simulation, it is important to identify different phases of the operations, i.e., whether the manipulator is going to tip over or not and if it is going to tip over, about which edge it will. This is done by calculating the net moment about the front and rear edges of the base. To calculate the net moment, the interaction forces/torques between the manipulator and the base should be continuously determined. These forces are calculated using any conventional method such as Newton-Euler. The virtual link method developed

in Chapter 2 is used again to calculate the coupling forces/torques between the base and the manipulating links. Once these forces/torques are calculated, the net moments about the front edge **B**, M_f, and rear edge **A**, M_r, are computed (see Figure 4.4):

$$M_f = \tau + w_{base}(a_f - x_{cg}) - F_x d_3 - F_y a_f \tag{4.6}$$

$$M_r = \tau - w_{base}(a_r + x_{cg}) - F_x d_3 + F_y a_r \tag{4.7}$$

According to the values of M_f and M_r, one can determine about which edge the mobile manipulator is going to tip over.

$$\begin{array}{lll} M_f > 0 \text{ and } M_r < 0 & \text{the base is stationary (Phase 1).} & \\ M_f > 0 \text{ and } M_r > 0 & \text{the base is tipping over the rear edge } \mathbf{A} \text{ (Phase 2A).} & (4.8) \\ M_f < 0 \text{ and } M_r < 0 & \text{the base is tipping over the front edge } \mathbf{B} \text{ (Phase 2B).} & \end{array}$$

With reference to the flow chart shown in Figure 4.5, the computational algorithm is stated as follows:

1- Input the initial values for the joint variables, $\mathbf{q}$, joint velocities, $\dot{\mathbf{q}}$, and the voltage signals applied to the hydraulic valves.

2- Calculate the net moments about the front and rear edges, M_f and M_r, using Equations (4.6) and (4.7).

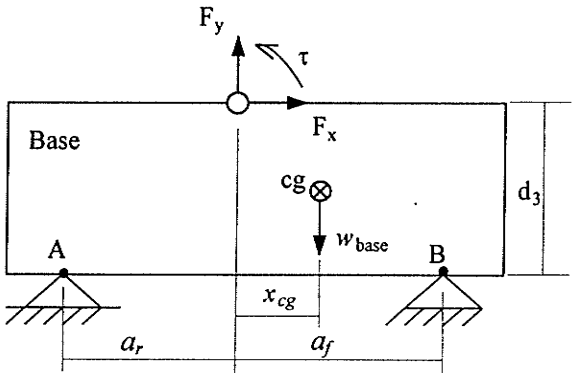

Figure 4.4. Coupling forces between the manipulator and the base.

3- Determine the status of the manipulator:

(i) Phase 1: use dynamic model 1, Equation (4.1) with $n = 2$, to calculate the joint variables, q_4 and q_5.

(ii) Phase 2A: use dynamic model 2a, Equation (4.1) with $n = 3$ and $a_3 = a_r$, to calculate the joint variables q_3, q_4, and q_5.

(iii) Phase 2B: use dynamic model 2b, Equation (4.1) with $n = 3$ and $a_3 = -a_f$, to calculate the joint variables q_3, q_4, and q_5.

4- For case (*ii*), when the base hits the ground at the front edge (numerically this is translated into $q_3 < \varepsilon$ and $\dot{q}_3 < -\varepsilon_v$, where ε and ε_v are small positive values), Equation (4.5) is used to calculate the new values of the joint velocities after the impact. The new values for the joint velocities after the impact with the rear edge are calculated in a similar way.

5- If the new rotational velocity of the base, $\dot{q}_3$, after the impact is in the same direction of the rotational velocity of the base before the impact, then the machine will turn over the other edge, i.e., if the base is rotating about the front edge, after the impact it will turn over the rear edge and vice versa. If the rotational velocity of the base after the impact is close to zero, then the machine is considered to be sitting on the ground and the first phase of the simulation is applied. If the rotational velocity of the base after the impact is in the opposite direction to the rotational velocity of the base before the impact, then the assumption of single impact used here is no longer valid and a double impact model should be used (not included in the model).

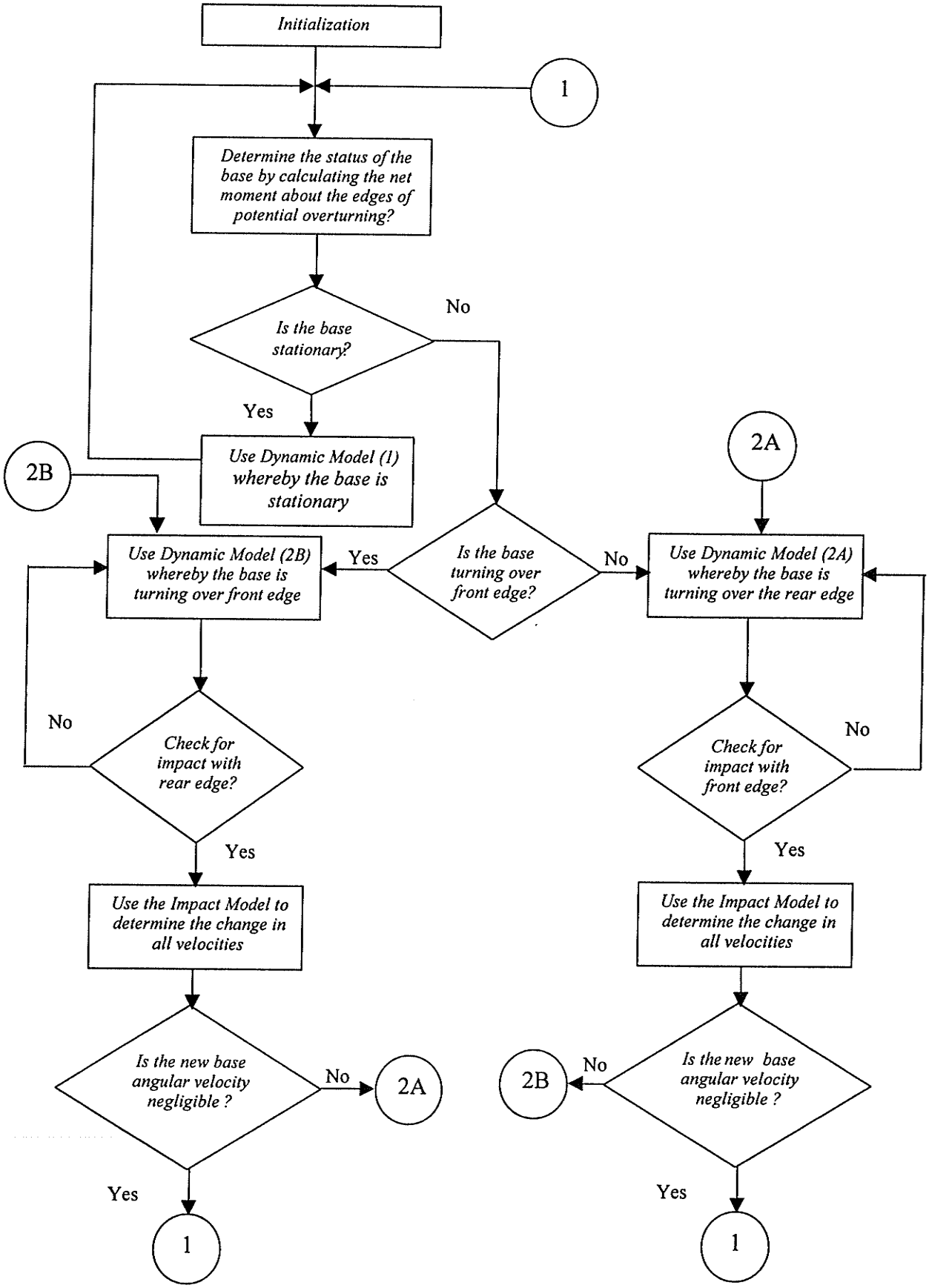

Figure 4.5. Flow chart of simulation model of mobile manipulator.

4.3 Simulation Results

The model developed is now exemplified with a typical mobile manipulator, similar to a Caterpillar M318 excavator-based log-loader. The dynamic parameters of the machine are listed in Table 4.2. The kinematic parameters are: a_f= -1 m, a_r= 4 m, a_4 = 5.2 m, a_5 = 1.8 m, and d_3 = 1.5 m.

Table 4.2. Dynamic Parameters

	mass (kg)	mass moment of inertia about the axis of rotation (kg m^2)	Center of gravity (x, y, z) m	Coordinate frame reference
base	12,000	90,523	(-2.0, -0.6, 0.0)	$\{x_3\ y_3\ z_3\}$
Boom	1,830	15,500	(-2.9, 0.2, 0.0)	$\{x_4\ y_4\ z_4\}$
Stick	688	610	(-0.9, 0.1, 0.0)	$\{x_5\ y_5\ z_5\}$

Two case studies are simulated. The first case simulates a typical operation of the log-loader staying on a horizontal ground. The task is to have the machine end-effector to perform a pick and place operation. The input voltages to the boom and stick servovalves are shown in Figure 4.6. In this task, the end-effector starts from a position close to the base carrying a 5000 kg load. The base is initially stable. The manipulator extends the end-effector to a possible 'dumping position' far from the base (see Figure 4.7). With reference to Figure 4.8, this move causes the machine to topple over. As the manipulator

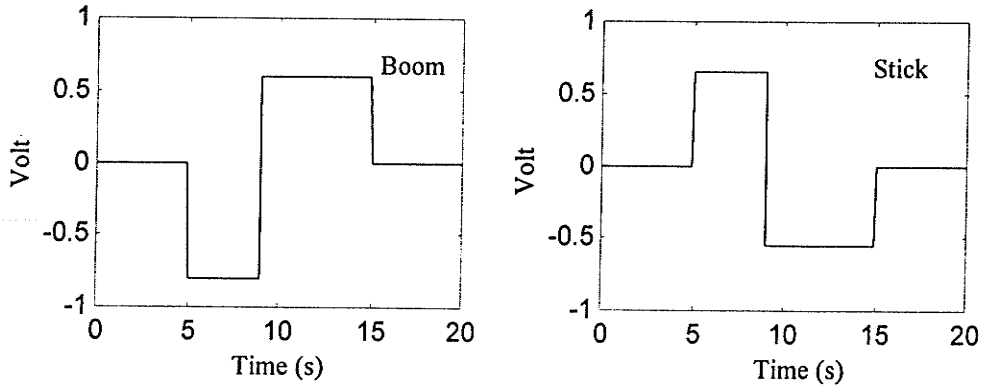

Figure 4.6. Input voltage to the servo-valves.

stops, the base starts to rotate over the front edge. Then, the end-effector retracts back to regain the stability. As is seen, the machine starts to roll back to a stable position.

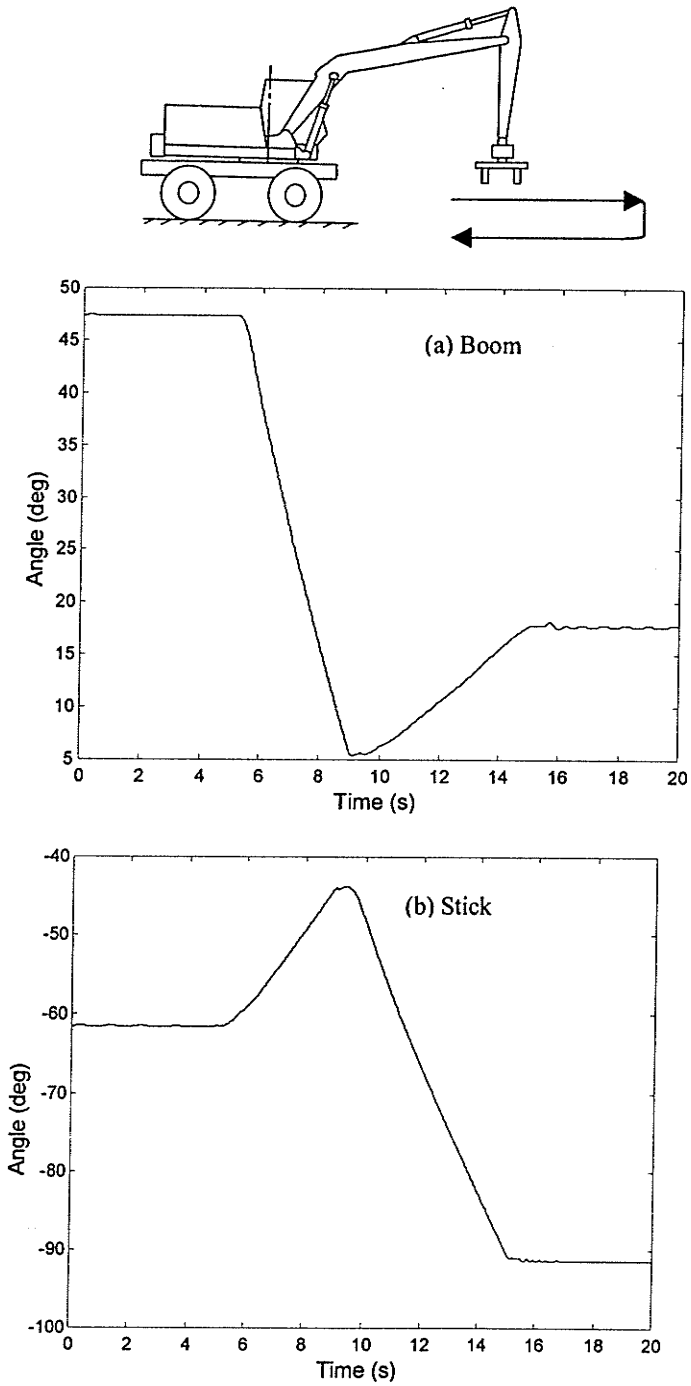

Figure 4.7. Manipulator movement during a pick and place operation.

The tip-over simulation model developed in this chapter is also compared with the energy stability measure developed by Ghasempoor and Sepehri (1998). Quantitatively, the two methods give similar indication about the stability of the mobile manipulator except for the stances where the base is tipping over. The energy stability method could not predict how the base responds to the movement of manipulator links, whereas, the present method does produce detailed behavior of the manipulator including the movement of the base. For example, the energy stability level of the manipulator has been calculated (see Section 2.2 for details about the method) and the result is shown in Figure 4.9. Comparing Figure 4.9 with Figure 4.8, the two methods give the same indication about the stability of the mobile manipulator before the tip-over (time period 0 to 9 seconds), and after the tip-over (time period 14.5 to 20 seconds). During the time period 9 to 14.5 seconds, when the tip-over occurs, the energy stability measure calculation is not valid whereas the present method gives information about the manipulator states. Figure 4.10 shows the input and output line pressures for both boom and stick hydraulic actuators.

The second case describes a task whereby the machine picks up a 4000 kg load while it is on an inclined plane (–20 degrees slope, see Figure 4.11). When the machine starts to lift the load, it starts to tip over. After the base rotates about 15 degrees over the front edge, the load is dropped. As shown in Figure 4.12, the machine regains the stability after dropping the load.

In summary, the results clearly showed the effect of the manipulator movement on overturning of such machines. Also, it was shown that by proper manipulation of the linkages, one could achieve stable conditions and prevent the machine tip-over.

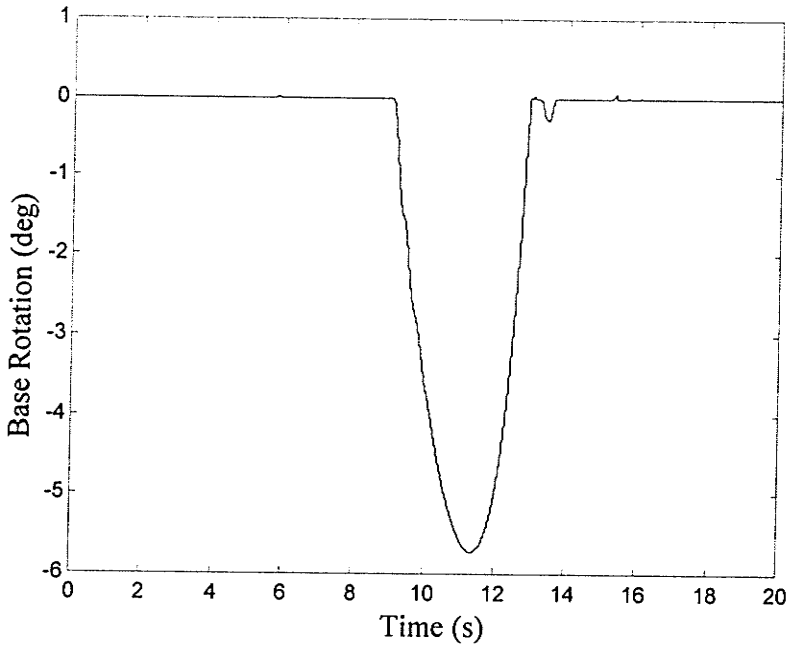

Figure 4.8. Base rotation over a horizontal plane (tip-over occurs at the front wheel).

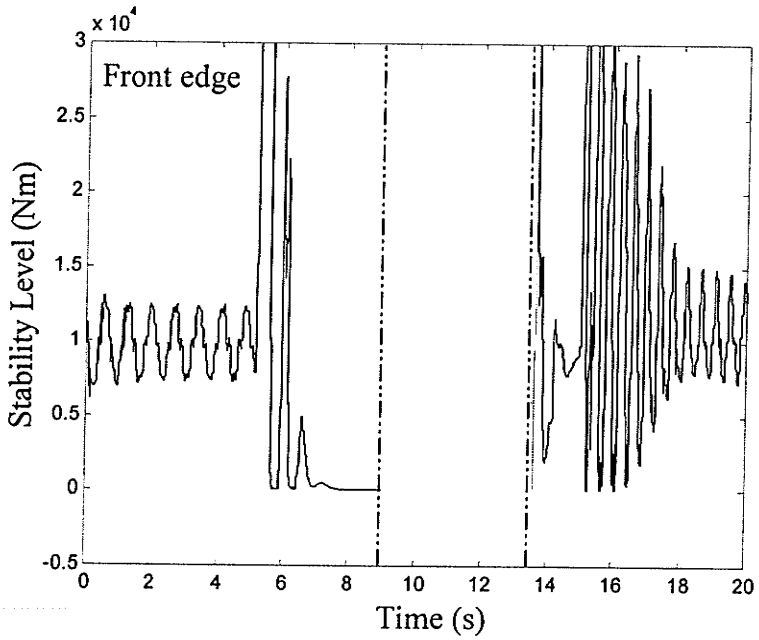

Figure 4.9. Energy stability level of front edge for the case shown in Figure 4.6.

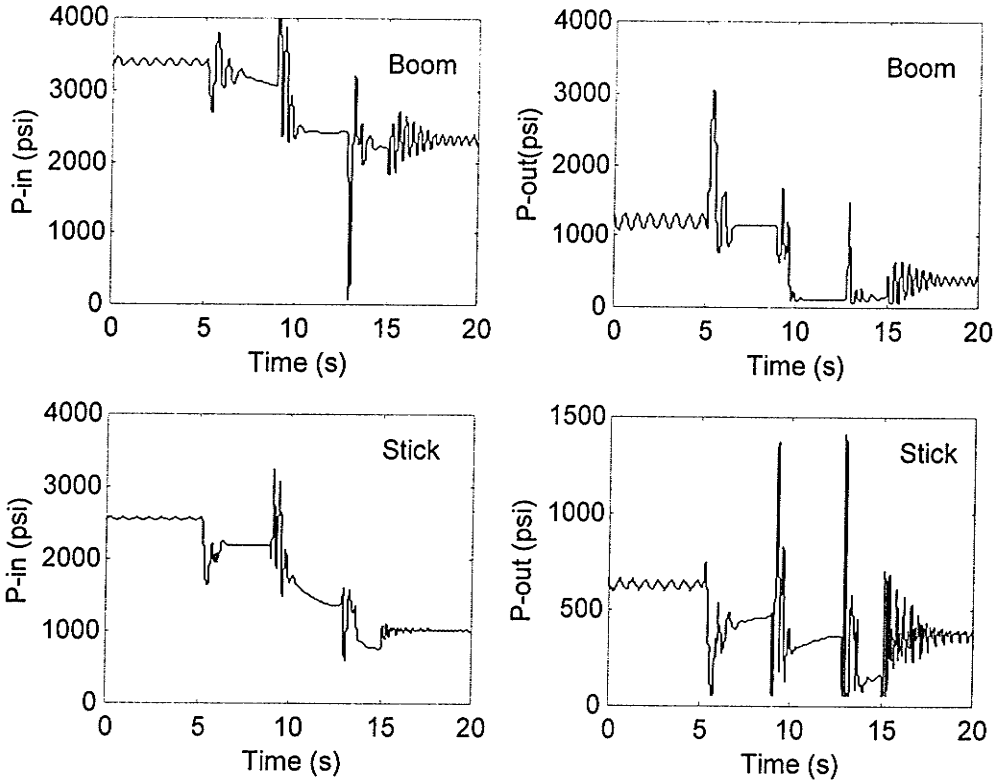

Figure 4.10. Input and output line pressures to and from the hydraulic actuators.

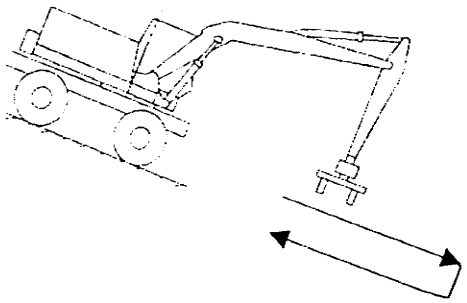

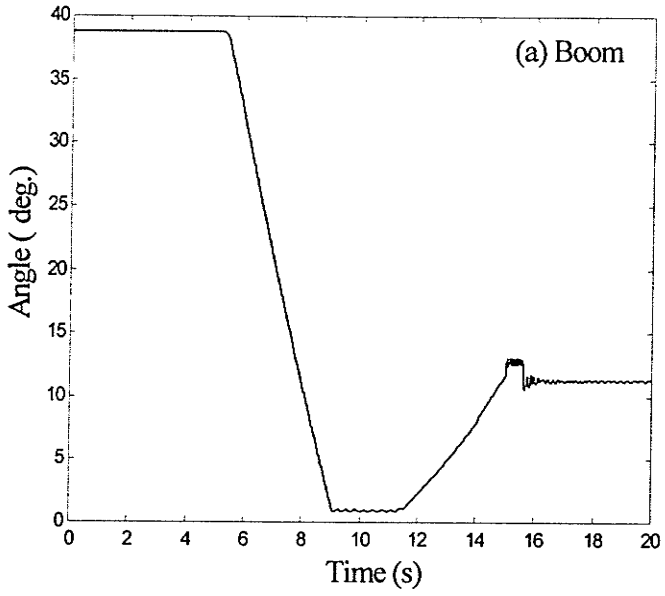

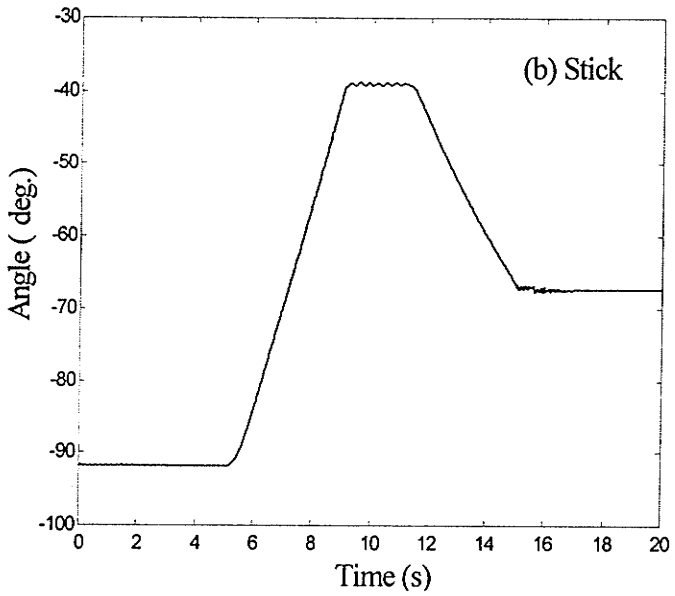

Figure 4.11. Manipulator movement, boom and stick, during a pick and place operation on an inclined plane.

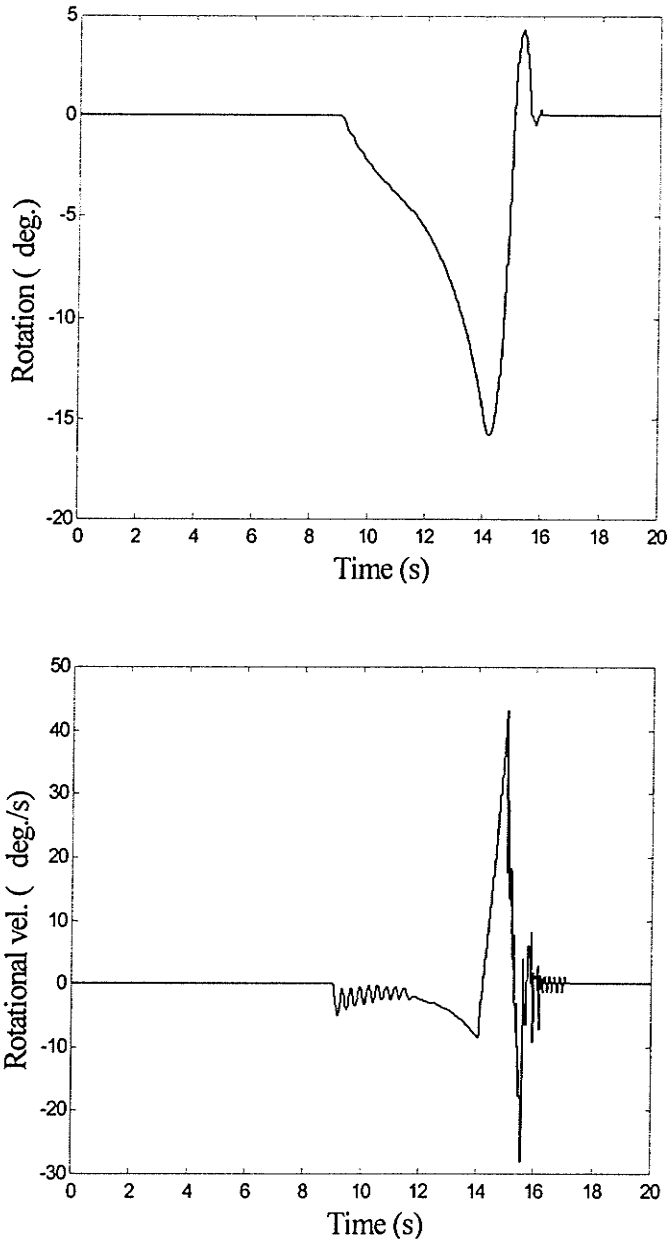

Figure 4.12. Rotational displacement and rotational velocity of the base due to manipulator motion shown in Figure 4.11.

Chapter 5

Stability Analysis Considering the Ground-Base Flexibility*

5.1 Introduction

The dynamic model developed in the previous chapter takes into account the dynamics of the base that can rock back and forth and the impact between the base and the ground. Although the model is capable of producing detailed response of the manipulator including the movement of the base, it relies on the assumption that the contact between the base and the ground is considered to be rigid. This assumption is not realistic and results in a non-smooth mathematical model. Dealing with equations of motion for non-smooth systems is more complicated than solving those of smooth systems, since the

* A version of this chapter has been published in *Robotica*, Vol. 20, pp. 607-613, 2002, "The Effect of Base Compliance on the Dynamic Stability of Mobile Manipulators," R.F. Abo-Shanab and N. Sepehri.

classical solution theories to ordinary differential equations require vector fields to be at least Lipschitz-continuous (Wu et al., 1998) and non-smooth systems fail this requirement. Thus, Filippov's solution theory (Filippov, 1960) must be used first, to ensure the existence, continuation, and uniqueness of the solution. This is not easy especially for systems with more than one discontinuity surface, which is the case in this model.

In this chapter, the model is improved to include the flexibility of the contact between the base and the ground. Inclusion of the flexibility, which is due to the suspension and the ground-tire compliance, results in a more realistic model of the entire system.

5.2 Development of the Model

The schematic diagram of the manipulator is shown in Figure 5.1 (c_r and c_f are the damping coefficients, k_r and k_f are the spring constants). The base is considered to be a rigid body, resting on two wheels that are longitudinally aligned and are modeled using the half car representation with Kelvin-Voigt spring damping system (Akpan and Kujath, 1998). The system damping is viscous, below the critical value and invariant with respect to changes of the kinematics configuration. In the present model, the base is considered to undergo a heave and a pitch motion. The friction between the base and the ground is assumed to be large enough to prevent the manipulator from skidding forward or backward. With reference to Figure 5.2, the manipulator is characterized to operate within two distinct phases:

Phase 1: The base is either resting on both edges $\overline{\mathbf{A}}$ and $\overline{\mathbf{B}}$ or turning over the rear edge $\overline{\mathbf{A}}$. In this phase, the base remains in contact with the ground on edge $\overline{\mathbf{A}}$, at all times.

Thus, in order to model the system, the connection between the point $\overline{\mathbf{A}}$ on the ground and point **A** located on the base, is modeled as a two-degree of freedom joint subject to force F_r^n (see Figure 5.2a) due to the flexibility between the base and the ground. One virtual link with prismatic joint is therefore added to represent the vertical motions, q_1, of point **A**. Similarly, point **B** is subject to force F_f^n originated from the flexibility between $\overline{\mathbf{B}}$ and **B**. The mobile robot is then considered as a 4-link serial manipulator subject to two external forces, F_r^n and F_f^n.

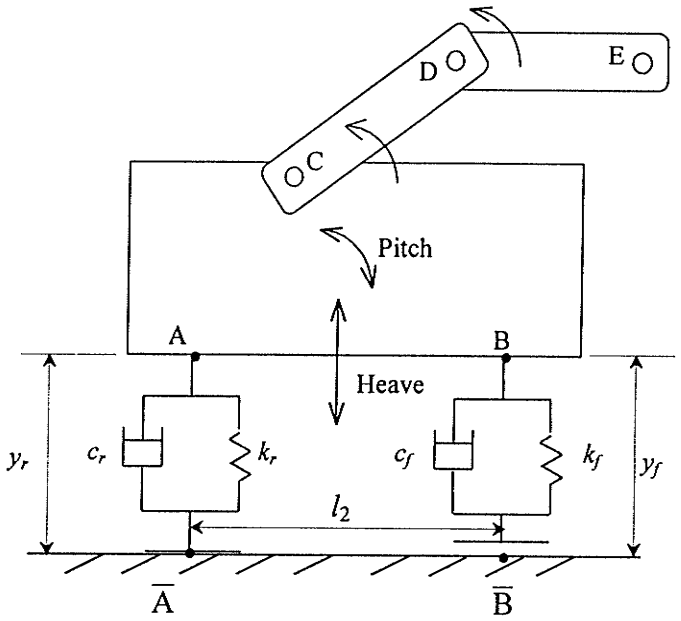

Figure 5.1. Schematic diagram of planar mobile manipulator.

Phase 2: The base is either resting on both edges $\overline{\mathbf{A}}$ and $\overline{\mathbf{B}}$ or turning over the front edge $\overline{\mathbf{B}}$. In this phase, the base remains in contact with the ground on edge $\overline{\mathbf{B}}$, at all times. As in the first phase, the connection between the point $\overline{\mathbf{B}}$ on the ground and point **B** located on the base is modelled as a two-degree of freedom joint subject to force F_f^n

(see Figure 5.2b). One virtual link with prismatic joint is therefore added to represent the vertical motion, q_1, at this point. Point **A** is subject to force F_r^n.

Switching between the two phases is based on calculating the height of the rear and front edges above the ground, i.e., y_r and y_f in Figure 5.1. As far as y_r is less than the

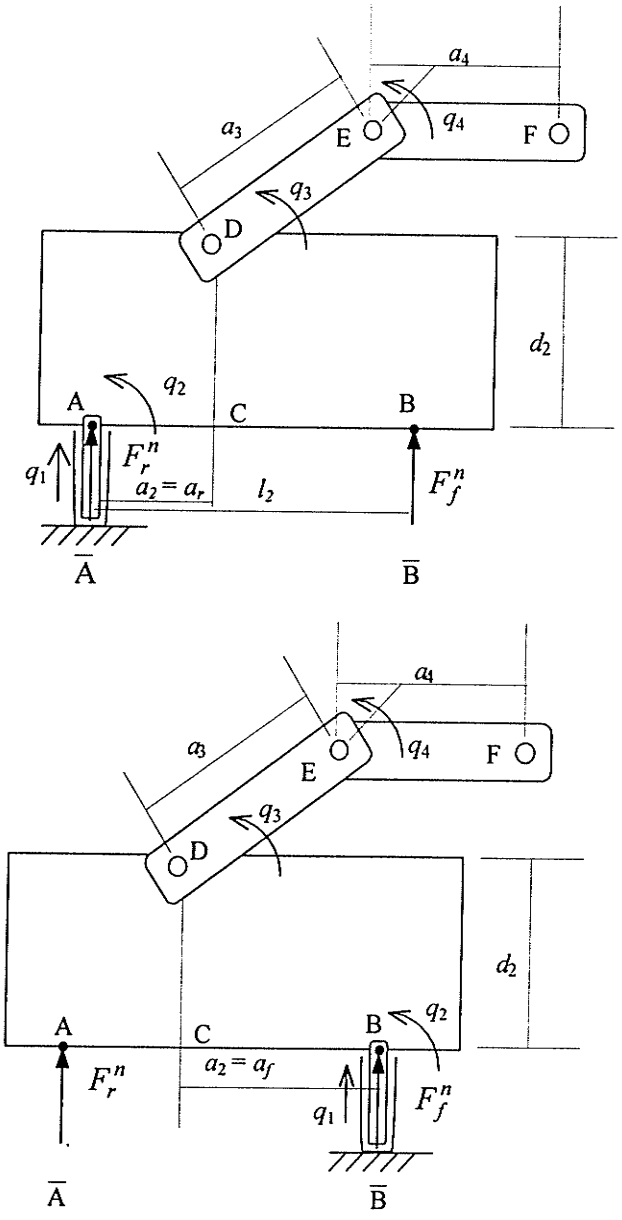

Figure 5.2. Schematic diagram of the mobile manipulator including the virtual links.

undeformed length of the spring, x_o, the first phase is considered. Once y_r becomes greater than x_o, the second phase is applied.

Figure 5.3 shows the Denavit-Hartenberg (DH) coordinate systems applied to the manipulator. Note that $a_2 = a_r$ for the first phase and $a_2 = a_f$ for the second phase. The dynamic equations describing the above two phases are simply derived based on Lagrange-Euler formulation as follows:

$$\tau = \mathbf{M}(\mathbf{q})\ \ddot{\mathbf{q}} + \mathbf{C}(\mathbf{q}, \dot{\mathbf{q}}) + \mathbf{G}(\mathbf{q}) + \tau_{susp} \tag{5.1}$$

where τ_{susp} is the vector of the generalized forces due to the suspension.

For phase 1, we have (refer to Figure 5.2a):

$$F_r^n = -k_r(q_1 - x_o) - c_r\dot{q}_1 \tag{5.2}$$

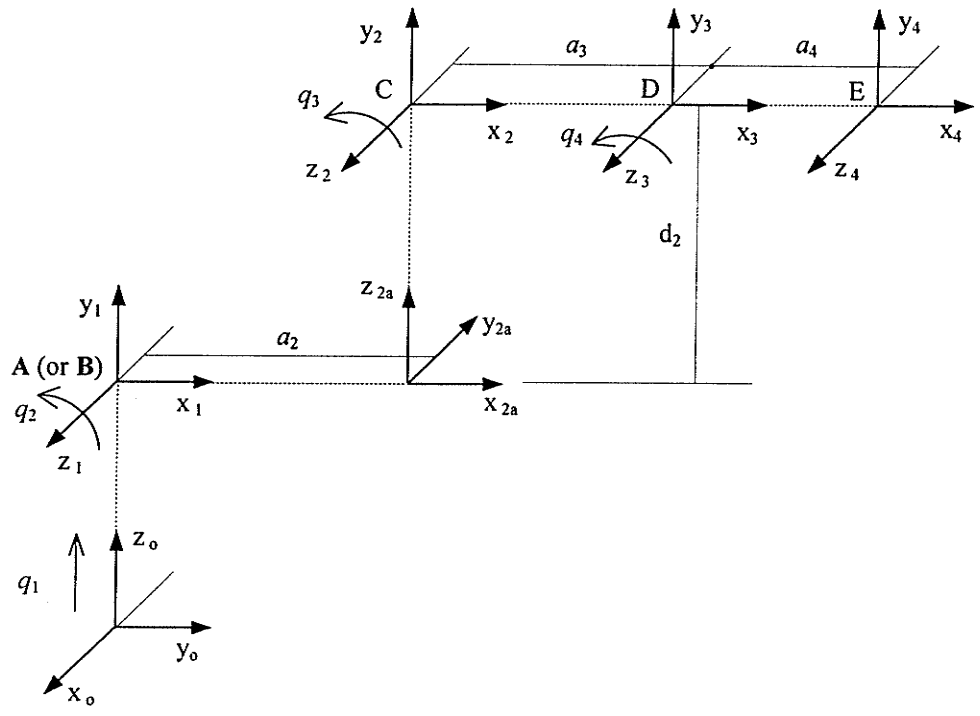

Figure 5.3. Link coordinates pertaining to Figure 5.2.

$$F_f^n = -k_f(q_1 + l_2 \sin q_2 - x_o) - c_f(\dot{q}_1 + l_2 \cos q_2 \dot{q}_2) \tag{5.3}$$

$$\tau_{susp} = \left\{ -F_r^n - F_f^n, -F_f^n l_2 \cos q_2, 0, 0 \right\}^T \tag{5.4}$$

For phase 2, we have (refer to Figure 5.2b):

$$F_r^n = -k_r(q_1 - l_2 \sin q_2 - x_o) - c_r(\dot{q}_1 - l_2 \cos q_2 \dot{q}_2) \tag{5.5}$$

$$F_f^n = -k_f(q_1 - x_o) - c_f \dot{q}_1 \tag{5.6}$$

$$\tau_{susp} = \left\{ -F_r^n - F_f^n, F_r^n l_2 \cos q_2, 0, 0 \right\}^T \tag{5.7}$$

In the above equations, c_r and c_f are the damping coefficients, k_r and k_f are the spring constants, l_2 is the distance between the front and rear edges, and x_o is the natural (undeformed) length of the springs.

5.3 Simulation Results

The movement of the implement is limited to a planar motion in this simulation. The kinematic parameters of the machine are listed in Table 5.1. The parameters pertaining to the flexibility between the base and the ground are chosen as $k_f = k_r = 35 \times 10^5$ N/m and $c_f = c_r = 15 \times 10^4$ Ns/m. These values provide a natural frequency of ≈ 3.5 Hz and a damping ratio of ≈ 0.47 in the vertical direction. Note that these values change with the manipulator configuration and payload. The dynamic parameters are listed in Table 5.2.

The simulated task is to have the machine end-effector perform a pick and place operation. The voltages applied to the servo-valves are the same as those shown in Figure 4.6. Due to the inclusion of base compliance, the boom and stick movements are slightly different from those for rigid base case. Figure 5.4 shows the manipulator movement

during the task for a compliant and rigid base. In this task, the end-effector starts from a position close to the base carrying 5000 kg load. The base is initially stable. The manipulator extends the end-effector to a possible 'dumping position' far from the base.

Table 5.1. Mobile Manipulator Link coordinate parameters

Link	θ_i	d_i	a_i	α_i	Variables
1	$\pi/2$	q_1	0	$\pi/2$	q_1
2	q_2	0	a_f or a_r	$-\pi/2$	q_2
2a	0	d_2	0	$\pi/2$	-
3	q_3	0	a_3	0	q_3
4	q_4	0	a_4	0	q_4

Table 5.2. Dynamic Parameters

	mass (kg)	mass moment of inertia (kg m^2)	Center of gravity (x, y, z) m	Coordinate frame
base	12,000	90,523	(-2.0, -0.6, 0.0)	$\{x_2\ y_2\ z_2\}$
Boom	1,830	15,500	(-2.9, 0.2, 0.0)	$\{x_3\ y_3\ z_3\}$
Stick	688	610	(-0.9, 0.1, 0.0)	$\{x_4\ y_4\ z_4\}$

With reference to Figure 5.5a, this move causes the machine to tip over when the end-effector extends its arm far enough from the base. Figure 5.5b shows the displacement of point **B** on the front of the base, during the task. Note that the front edge remains in contact with the ground as long as the vertical displacement of the point **B** is less than the undeformed length of the spring (x_o = 0.3 m). As the base starts to tip over about the front edge, the implement retracts back to regain the stability. As is seen, the machine starts to roll back to a stable position. Note that, at time $t \approx 5$ seconds, at which the implement starts moving, the base experiences a slight pitch motion. This is due to the coupled dynamics between the base and the other links.

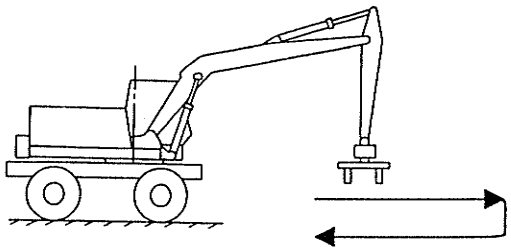

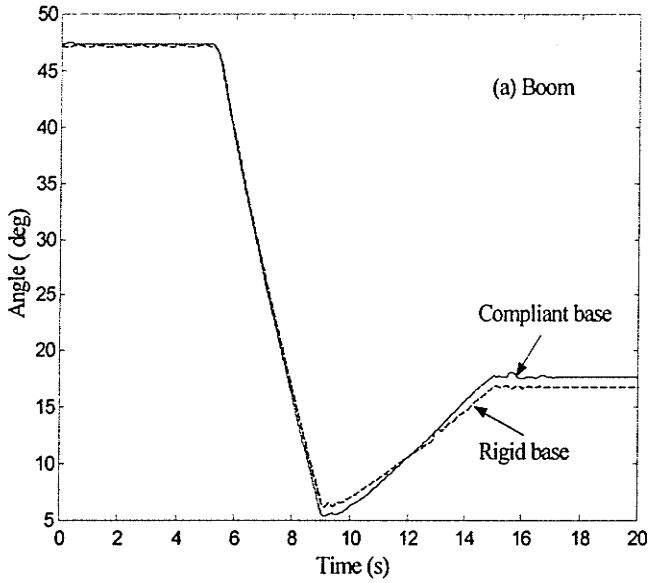

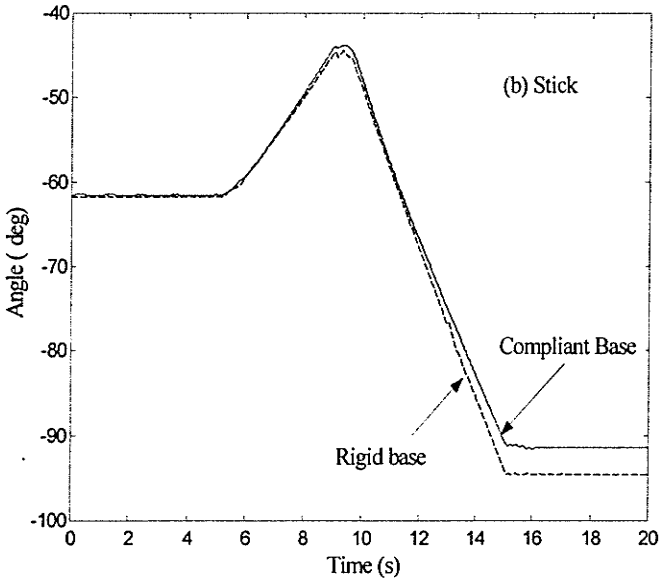

Figure 5.4. Manipulator movement during a pick and place operation for rigid and compliant bases.

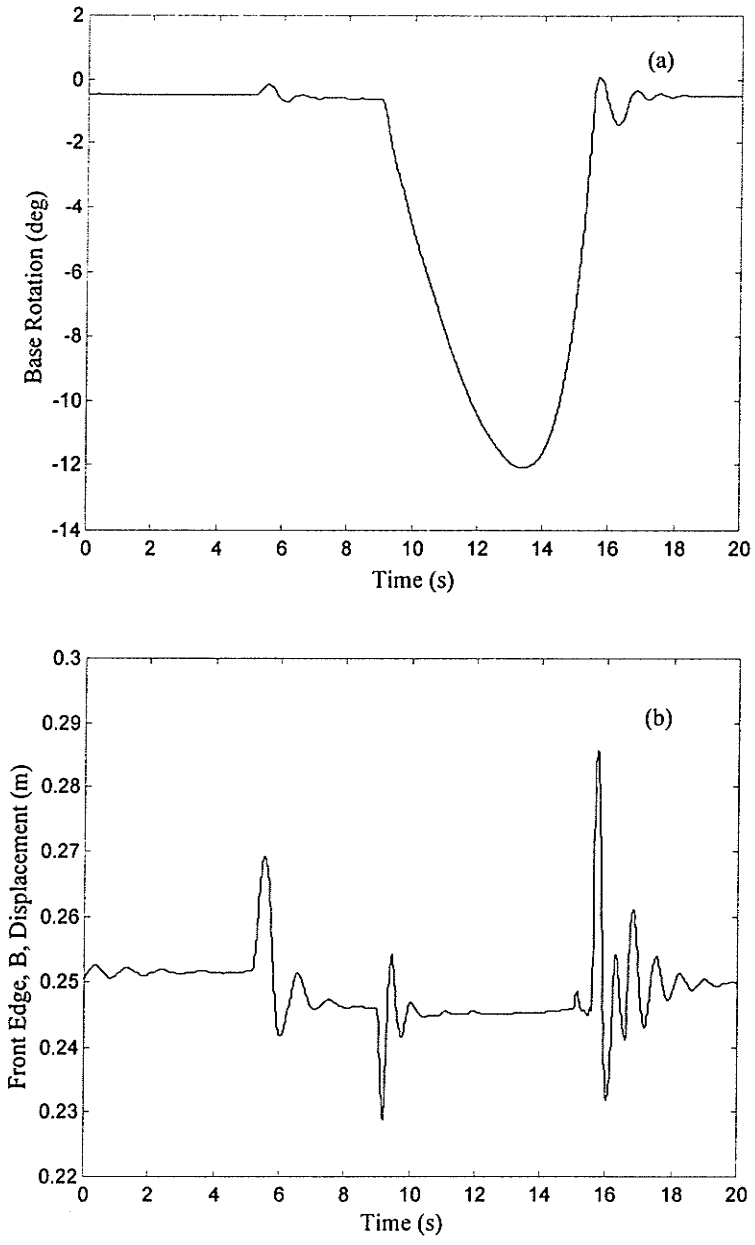

Figure 5.5. History of: (a) base rotation and (b) vertical movement of point **B** on the front of the base, during the task.

The effects of various stiffness and damping values pertaining to the flexibility between the base and the ground, on the magnitude of tip over rotation are also studied. The responses are compared with those obtained using the previous model in which no base compliance was included. Figures. 5.6 and 5.7 show the results of using different stiffness and damping coefficients, respectively. Figure 5.6 clearly shows that the stability of the system decreases (i.e., the magnitude of the tip over rotation increases) as the stiffness decreases. On the other hand, Figure 5.7 indicates that the stability of the machine decreases as the damping decreases. Overall, the angular movement of the base during the whole manipulator motion, in the case of flexible contact, is greater than the angular movement of the base for the rigid contact case. This indicates that the

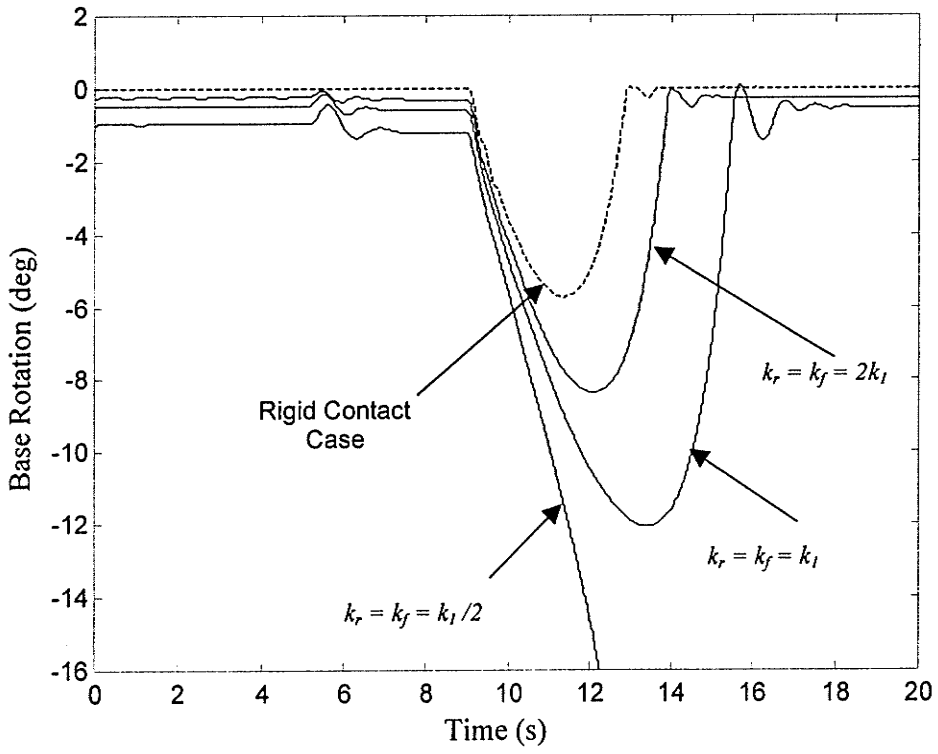

Figure 5.6. Effect of increasing the stiffness while the damping coefficient is kept constant, $k_1 = 35\times10^5$ N/m and $c_r = c_f = 15\times10^4$ Ns/m.

compliance between the base of the manipulator and the ground tends to reduce the machine stability.

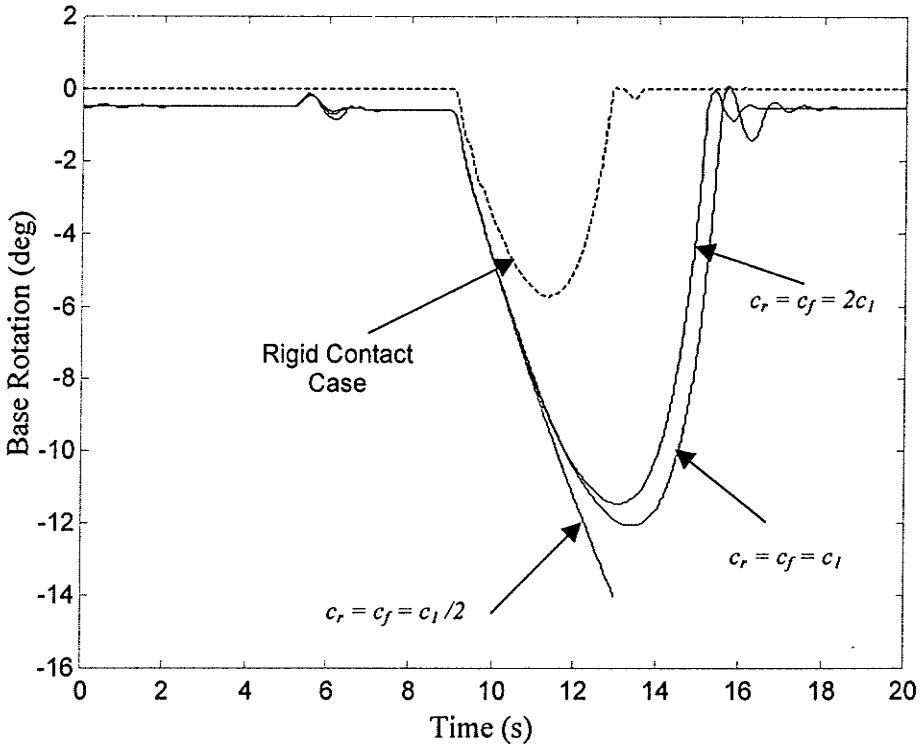

Figure 5.7. Effect of increasing the damping while the stiffness is kept constant, $k_r = k_f = 35 \times 10^5$ N/m and $c_1 = 15 \times 10^4$ Ns/m.

Chapter 6

Stability Analysis Considering the Friction Effects

6.1 Introduction

In this chapter, the model developed previously is extended to include the effect of the friction between the wheels and the ground. Here, it is assumed that the wheels of the mobile manipulator are locked in place. Thus, there is no rolling and the friction is due to only the stick-slip motion between the wheels and the ground. Two specific friction models, namely the Karnopp friction model and the LuGre dynamic tire friction model, are employed and evaluated. Karnopp friction model (Karnopp, 1985) is an example of a static friction model in which the friction force is described as a function of the velocity difference between the sliding surfaces (Gaul and Nitsche, 2001). LuGre* friction model (Canudas de Wit and Tsiotras, 1999) is a dynamic friction model, built upon Dahl friction

* This model was developed through a collaboration among researchers at the Lund Institute of Technology (Sweden) and in Grenoble, France (Laboratoire d'Automatique de Grenoble).

model (Dahl, 1976). LuGre friction model has been used to describe the friction forces between the tire and the road for vehicle control and simulation studies (Claeys et al., 2001).

The schematic diagram of a planar mobile manipulator including the flexibility of the contact between the base and the ground, and the ground reaction forces is shown in Figure 6.1. F_f^f and F_r^f are the friction forces and F_f^n and F_r^n are the normal forces. The base, which was previously considered to undergo only a heave and a pitch motion, is now allowed to skid forward or backward depending on the nature of forces applied to it as well as the friction between the wheels and the ground.

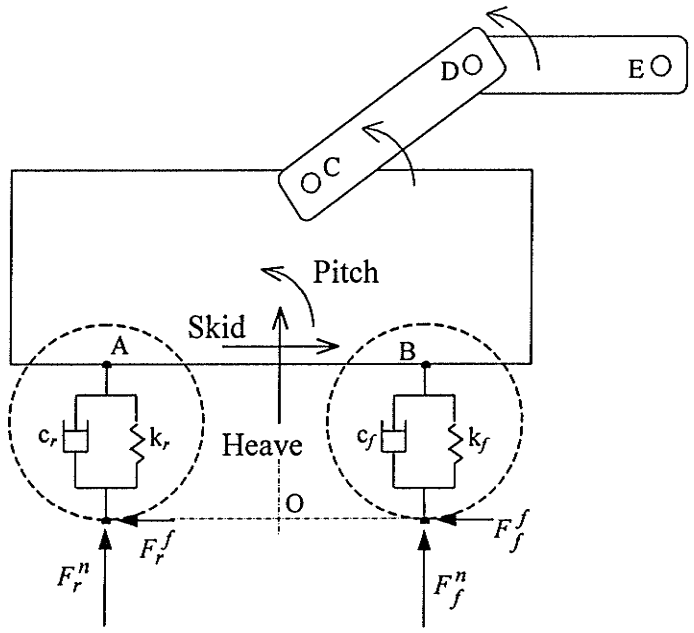

Figure 6.1. Schematic diagram of planar mobile manipulator including ground reaction forces.

6.2 Karnopp Friction Model

The friction model proposed by Karnopp (1985) requires only the knowledge of two values: stick friction and slip friction. With reference to Figure 6.2, the Karnopp model is expressed as follows:

$$F^f = \begin{cases} F^d \operatorname{sgn}(v) & |v| > D_v \\ F^i & |v| \le D_v \text{ and } |F^i| \le F^s \\ F^s \operatorname{sgn}(F^i) & |v| \le D_v \text{ and } |F^i| > F^s \end{cases} \tag{6.1}$$

where F^d is the slipping friction force, F^i is the reactive force at the contact due to the applied forces to the body, F^s is the maximum sticking friction force, and v is the relative velocity between the wheel and the ground. The switchover from stick friction to slip friction, however, causes some instability in the numerical simulation of the Karnopp model. Therefore the switchover is assumed to take place at certain velocity, D_v, which is small enough to be considered negligible but at the same time large enough to prevent excessive stiffness in the numerical integration (Sepehri et al., 1996).

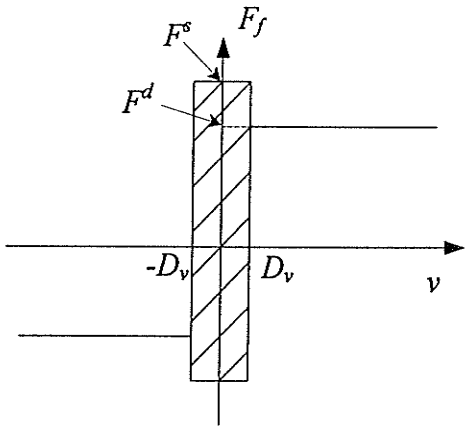

Figure 6.2. Karnopp friction model.

Note that in order to apply the Karnopp model, the reaction horizontal forces at the wheels, F_f^i and F_r^i, should be known. In order to accomplish this, it is assumed that there is a spring-damper system in the horizontal direction (see Figure 6.3). The reactive

forces (F_{fh}^{susp} and F_{rh}^{susp}) can now be determined as equal to the force originating from the virtual spring-damper systems.

To derive the dynamic equations, two virtual links with prismatic joints are added to represent the relative horizontal and vertical translational movements (q_1 and q_2) of point **G** on the base, with respect to the ground (see Figure 6.3). The second virtual link is connected to the base by a revolute joint characterizing the rotational (pitch) movement of the base, q_3. Denavit-Hartenberg (DH) coordinate systems are assigned to the manipulator's links as shown in Figure 6.4. The manipulator link coordinate parameters are listed in Table 6.1.

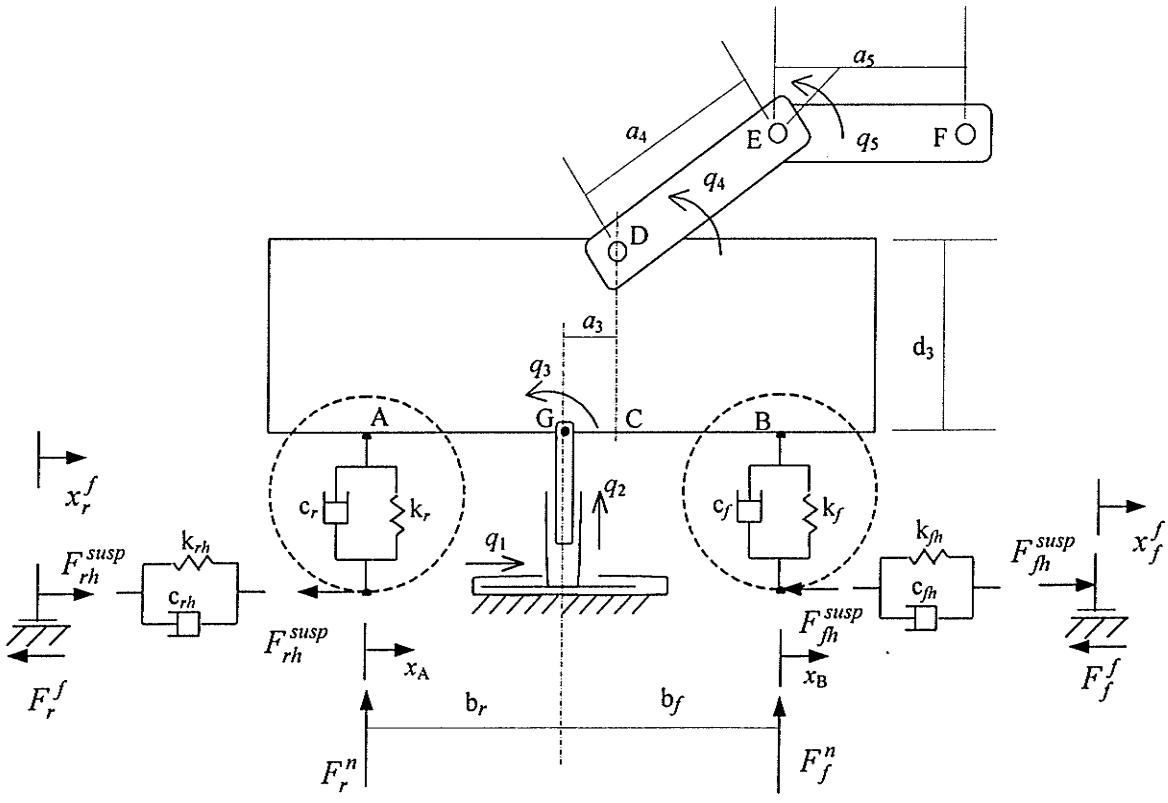

Figure 6.3. Schematic diagram of a planar mobile manipulator including virtual links, base compliance and friction forces.

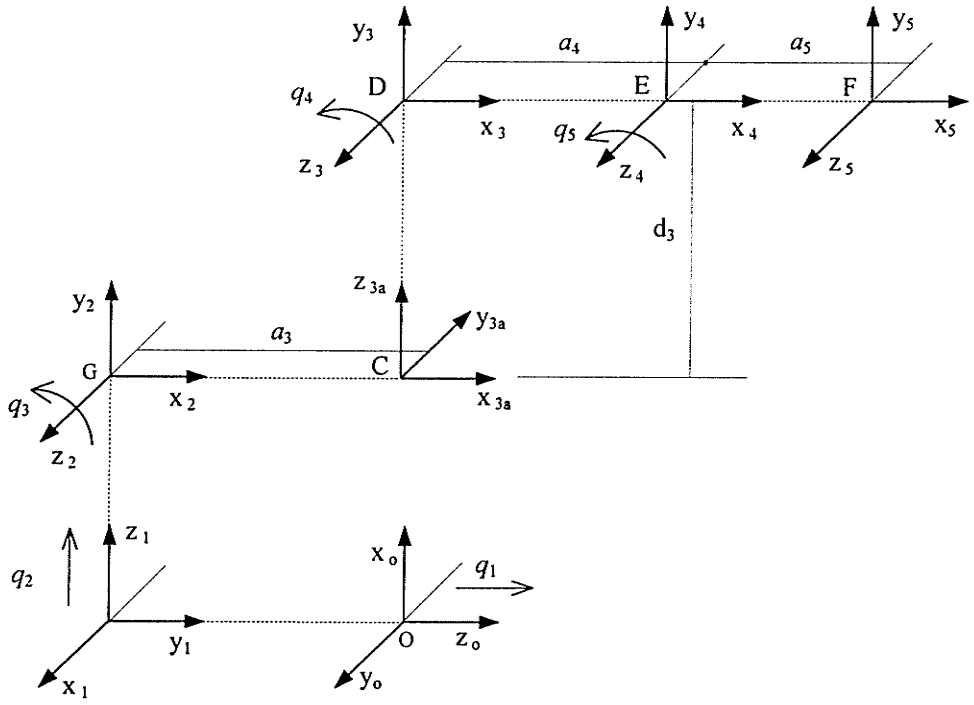

Figure 6.4. Link coordinate systems pertaining to Figure 6.3.

Table 6.1. Mobile Manipulator Link coordinate parameters

Link	θ_i	d_i	a_i	α_i	Variables
1	$\pi/2$	q_1	0	$\pi/2$	q_1
2	$\pi/2$	q_2	0	$\pi/2$	q_2
3	q_3	0	a_3	$-\pi/2$	q_3
3a	0	d_3	0	$\pi/2$	-
4	q_4	0	a_4	0	q_4
5	q_5	0	a_5	0	q_5

The dynamic equations are derived based on LE formulation:

$$\tau = \mathbf{M}(\mathbf{q})\ \ddot{\mathbf{q}} + \mathbf{C}(\mathbf{q},\dot{\mathbf{q}}) + \mathbf{G}(\mathbf{q}) + \tau_{susp} \tag{6.2}$$

where τ_{susp} is the vector of the generalized force at each joint due to the ground reaction forces. The ground reaction forces are determined as follows:

$$F_r^n = -k_r(q_2 - b_r \sin q_3 - x_o) - c_r(\dot{q}_2 - b_r \cos q_3 \dot{q}_3) \tag{6.3}$$

$$F_f^n = -k_f(q_2 + b_f \sin q_3 - x_o) - c_f(\dot{q}_2 + b_f \cos q_3 \dot{q}_3) \tag{6.4}$$

$$F_r^f = F_{rh}^{susp} = c_{rh}(\dot{x}_A - \dot{x}_r^f) + k_{rh}(x_A - x_r^f) \tag{6.5}$$

$$F_f^f = F_{fh}^{susp} = c_{fh}(\dot{x}_B - \dot{x}_f^f) + k_{fh}(x_B - x_f^f) \tag{6.6}$$

where

$$x_A = q_1 + b_r(1 - \cos q_3)$$

$$x_B = q_1 - b_f(1 - \cos q_3)$$

From Equations (6.5) and (6.6):

$$\dot{x}_r^f = \dot{x}_A - \frac{\left| F_r^f - k_{rh}(x_A - x_r^f) \right|}{c_{rh}} \tag{6.7}$$

$$\dot{x}_f^f = \dot{x}_B - \frac{\left| F_f^f - k_{fh}(x_B - x_f^f) \right|}{c_{fh}} \tag{6.8}$$

$$F_r^f = \begin{cases} F_r^d \operatorname{sgn}(\dot{x}_r^f) & \left|\dot{x}_r^f\right| > D_{v_r} \\ F_{rh}^{susp} & \left|\dot{x}_r^f\right| \le D_{v_r} \text{ and } \left|F_{rh}^{susp}\right| \le F_r^s \\ F_r^s \operatorname{sgn}(F_{rh}^{susp}) & \left|\dot{x}_r^f\right| \le D_{v_r} \text{ and } \left|F_{rh}^{susp}\right| > F_r^s \end{cases} \tag{6.9}$$

$$F_f^f = \begin{cases} F_f^d \operatorname{sgn}(\dot{x}_f^f) & \left|\dot{x}_f^f\right| > D_{v_f} \\ F_{fh}^{susp} & \left|\dot{x}_f^f\right| \le D_{v_f} \text{ and } \left|F_{fh}^{susp}\right| \le F_f^s \\ F_f^s \operatorname{sgn}(F_{fh}^{susp}) & \left|\dot{x}_f^f\right| \le D_{v_f} \text{ and } \left|F_{fh}^{susp}\right| > F_f^s \end{cases} \tag{6.10}$$

Note that $F_f^s = \mu_{s_f} F_f^n$, $F_f^d = \mu_{c_f} F_f^n$, $F_r^s = \mu_{s_r} F_r^n$, and $F_r^d = \mu_{c_r} F_r^n$. μ_c is the Coulomb friction coefficient and μ_s is the static friction coefficient.

Then, the vector of the generalized forces due to the ground reaction forces, τ_{susp}, is:

$$\tau_{susp} = \left\{F_{fh}^{susp} + F_{rh}^{susp},\ -F_r^n - F_f^n, \tau_3, 0, 0\right\}^T \tag{6.11}$$

where

$$\tau_3 = F_{rh}^{susp}(q_2 - b_r \sin q_3) + F_{fh}^{susp}(q_2 + b_f \sin q_3) + F_r^n b_r \cos q_3 - F_f^n b_f \cos q_3 \tag{6.12}$$

6.3 LuGre Friction Model

The LuGre tire dynamic friction model describes arbitrary steady-state friction characteristics, supports hysteresis behavior due to frictional lag, spring-like behavior in stiction, and gives a varying break-away force depending on the rate of change of the applied force (Canudas de Wit et al., 1995). The model is inspired by the bristle interpretation of friction (see Figure 6.5) as introduced by Haessig and Friedland (1991) and is characterized as the average deflection force of elastic springs.

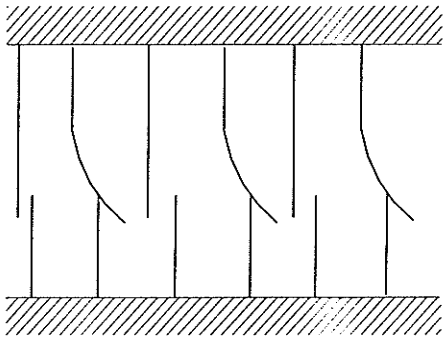

Figure 6.5. Friction interface between two surfaces is thought as a contact between bristles. For simplicity the bristles on the lower part are shown as being rigid (Canudas de Wit et al., 1995).

When a tangential force is applied, the bristles will deflect. If the deflection is sufficiently large, the bristles start to slip (Canudas de Wit and Tsiotras, 1999).

The friction force, F^f, generated from the bending of the bristles is described as:

$$F^f = (\sigma_o z + \sigma_1 \dot{z} + \sigma_2 v) F^n \tag{6.13}$$

where σ_o is the normalized lumped stiffness, σ_1 is the normalized lumped damping, σ_2 is the normalized viscous relative damping, F^n is the normal force, and v is the relative velocity between the two surfaces. The average deflection of the bristles is denoted by z and is modeled by the following relation:

$$\dot{z} = v - \frac{\sigma_o |v|}{\eta(v)} z \tag{6.14}$$

The function $\eta(v)$ contains information about the velocity dependence of friction. It is positive and depends on many factors such as material properties, lubrication, and temperature.

$$\eta(v) = \mu_c + (\mu_s - \mu_c) e^{-\left|v/v_s\right|^\alpha} \tag{6.15}$$

In (6.15), μ_c is the Coulomb friction coefficient, μ_s is the static friction coefficient, and v_s is the Stribeck velocity, which helps to define the velocity dependence of friction. α is an application-dependent exponent. Canudas de Wit and Tsiotras (1999) suggested $\alpha = 0.5$ for modeling the friction between tire and ground.

Similar to the Karnopp friction model, two virtual links with prismatic joints are added to the model of Figure 6.1 to represent the horizontal and vertical movements, q_1 and q_2, of the base (see Figure 6.6). Denavit-Hartenberg (DH) coordinate systems applied to the manipulator are the same as those shown in Figure 6.4 and the manipulator coordinate

parameters are listed in Table 6.1. Equation (6.2) is then used to describe the manipulator dynamics based on LE formulation. The friction forces at the rear and the front wheels, F_f^f and F_r^f, are calculated as follows:

$$F_r^f = \left(\sigma_{or} z_r + \sigma_{1r} \dot{z}_r + \sigma_{2r} \dot{x}_A\right) F_r^n \tag{6.16}$$

$$F_f^f = \left(\sigma_{of} z_f + \sigma_{1f} \dot{z}_f + \sigma_{2f} \dot{x}_B\right) F_f^n \tag{6.17}$$

The normal forces at the front and the rear wheels, F_f^n and F_r^n, are calculated using Equations (6.3) and (6.4), respectively. Further,

$$\dot{z}_r = \dot{x}_A - \frac{\sigma_{or} |\dot{x}_A|}{\eta_r(\dot{x}_A)} z_r \tag{6.18}$$

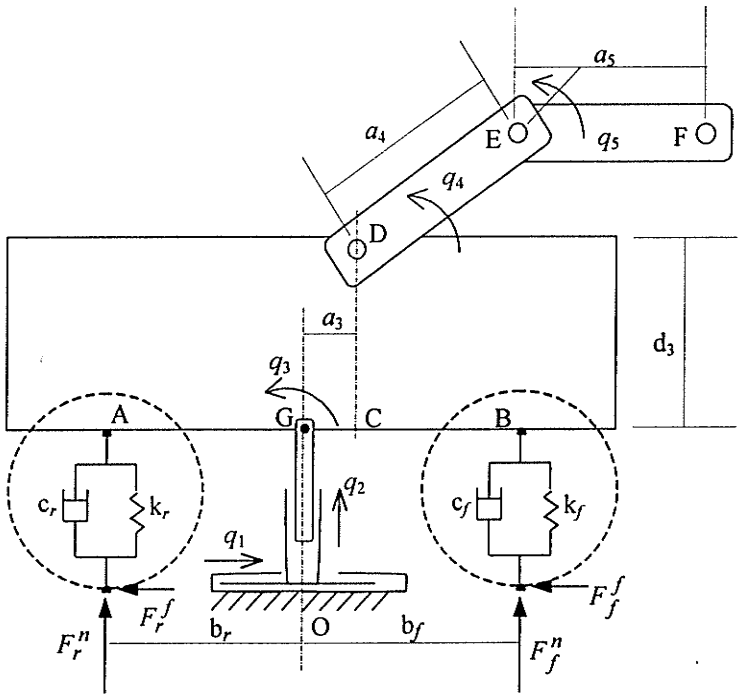

Figure 6.6. Schematic diagram of planar mobile manipulator including the virtual links, base compliance and LuGre friction forces.

and

$$\dot{z}_f = \dot{x}_B - \frac{\sigma_{of}|\dot{x}_B|}{\eta_f(\dot{x}_B)} z_f \tag{6.19}$$

where

$$\eta_r(\dot{x}_A) = \mu_{c_r} + (\mu_{s_r} - \mu_{c_r}) e^{-\left|\frac{\dot{x}_A}{v_{s_r}}\right|^{0.5}} \tag{6.20}$$

$$\eta_f(\dot{x}_B) = \mu_{c_f} + (\mu_{s_f} - \mu_{c_f}) e^{-\left|\frac{\dot{x}_B}{v_{s_f}}\right|^{0.5}} \tag{6.21}$$

Then

$$\tau_{susp} = \left\{F_f^f + F_r^f, -F_f^n - F_r^n, \tau_3, 0, 0\right\}^T \tag{6.22}$$

where

$$\tau_3 = F_r^f (q_2 - b_r \sin q_3) + F_f^f (q_2 + b_f \sin q_3) + F_r^n b_r \cos q_3 - F_f^n b_f \cos q_3 \tag{6.23}$$

6.4 Simulation Studies

Simulations are conducted to evaluate the inclusion of two friction models described in the previous sections into the simulation model. The benchmark test for the simulation is the same as the one described in Section 4.3. The kinematic parameters are $a_3 = 1.5\,\text{m}$, $a_4 = 5.2\,\text{m}$, $a_5 = 1.8\,\text{m}$, $b_f = 2.5\,\text{m}$, $b_r = 2.5\,\text{m}$, and $d_3 = 1.5\,\text{m}$ (see Figures 6.3 and 6.6). The dynamic parameters are the same as those listed in Table 4.2. The friction coefficients were chosen as $\mu_{s_f} = \mu_{s_r} = 0.05$ and $\mu_{c_f} = \mu_{c_r} = 0.03$. These friction coefficients are the only parameters required for the Karnopp model. The LuGre model,

however, uses other parameters, the values of which are $\sigma_{o_f} = \sigma_{o_r} = 40$ 1/m, $\sigma_{1_f} = \sigma_{1_r} = 4.9487$ s/m, $\sigma_{2_f} = \sigma_{2_r} = 0.0018$ s/m, and $v_{s_f} = v_{s_r} = 12.5$ m/s. These values were used by Canudas de Wit and Tsiotras (1999) for tire friction models and gave results that matched reasonably well with their experimental data.

Figures 6.7 to 6.9 show the base movements and the friction forces during the task using both Karnopp and LuGre models. The trends of the results of the two models are similar; however, there are some differences in the sliding and rotation motions of the base. These differences were expected due to the manner in which friction is formulated by each model. Figure 6.10 shows the total friction force originating from both the front and the rear wheels. The total friction force predicted by Karnopp model is less than that predicted by LuGre model during the sliding motion of the base. The reason is believed to be partly due to the fact that Karnopp model does not include Stribeck effect*. Therefore, Karnopp model predicts more sliding motion than that predicted by LuGre model.

The results of these two models are also compared with those obtained by the simplified model, which was developed in the previous chapter based on the assumption that the friction between the base and the ground is high enough to prevent the base from skidding forward or backward. Figure 6.11 shows the simulation results using different models. It is seen that the simplified model results in an estimation of the tip-over rotation, which is less than those obtained using LuGre or Karnopp model.

---

* Stribeck (1902) observed that for low velocities, the friction force decreases continuously with increasing velocities and increases for higher velocities. This phenomenon is named Stribeck effect (see Armstrong-Helouvry et al. (1994) for details).

Finally, LuGre model and Karnopp model are used to investigate the effect of the variation of the frictional properties between the base and the ground on the machine tip-over stability. Figures 6.12 and 6.13 show that, for the simulation reported here, reducing the friction between the base and the ground increases the machine stability. This is valid up to a certain limit, below which the machine starts to also skid during the tipping over, causing it to become less stable. This can be seen in Figures 6.12 and 6.13. With reference to these figures, at $t = 9\,\mathrm{s}$, the machine starts to slide for low friction. This motion negatively affects the machine stability. However, low friction should not be a choice to increase the machine stability since it allows the machine to slide, which is dangerous and should be avoided.

To summarize, LuGre model characterizes the ground-tire friction, since it is continuous and captures a variety of behaviors, such as pre-sliding displacement, hysteresis effect, stick-slip motion, and varying break-away force. The price paid for such a versatile model is that it is a six-parameter model. Karnopp model, on the other hand, is simpler than LuGre model as it uses two parameters only. The model, however, is discontinuous and does not take into account some of the friction phenomena such as Stribeck effect and varying break-away force. Note that although LuGre model uses more states than those used by Karnopp model, the virtual flexibility that has been added in the horizontal direction to allow the calculation of the reactive force at each wheel when using the Karnopp model increased the model states to a number similar to LuGre model. LuGre model has been chosen in the subsequent chapter to model the friction force.

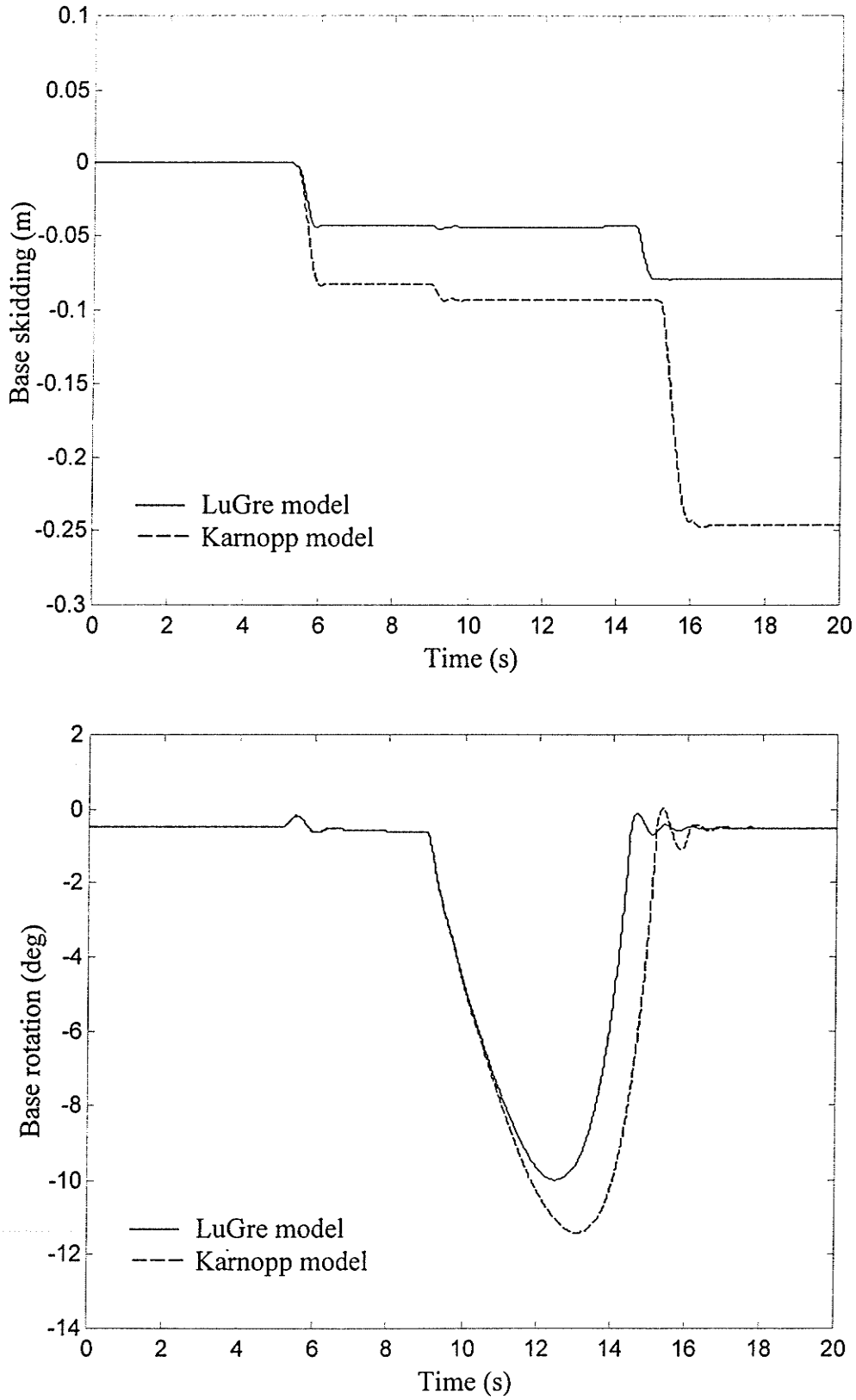

Figure 6.7. Base movement during the task

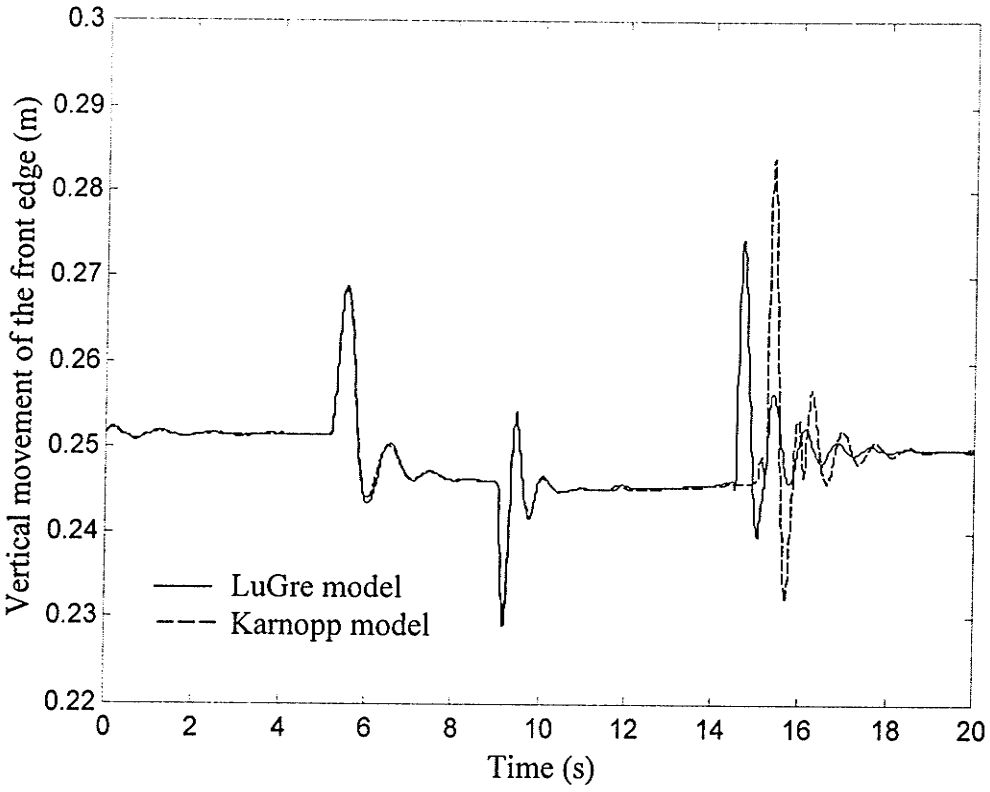

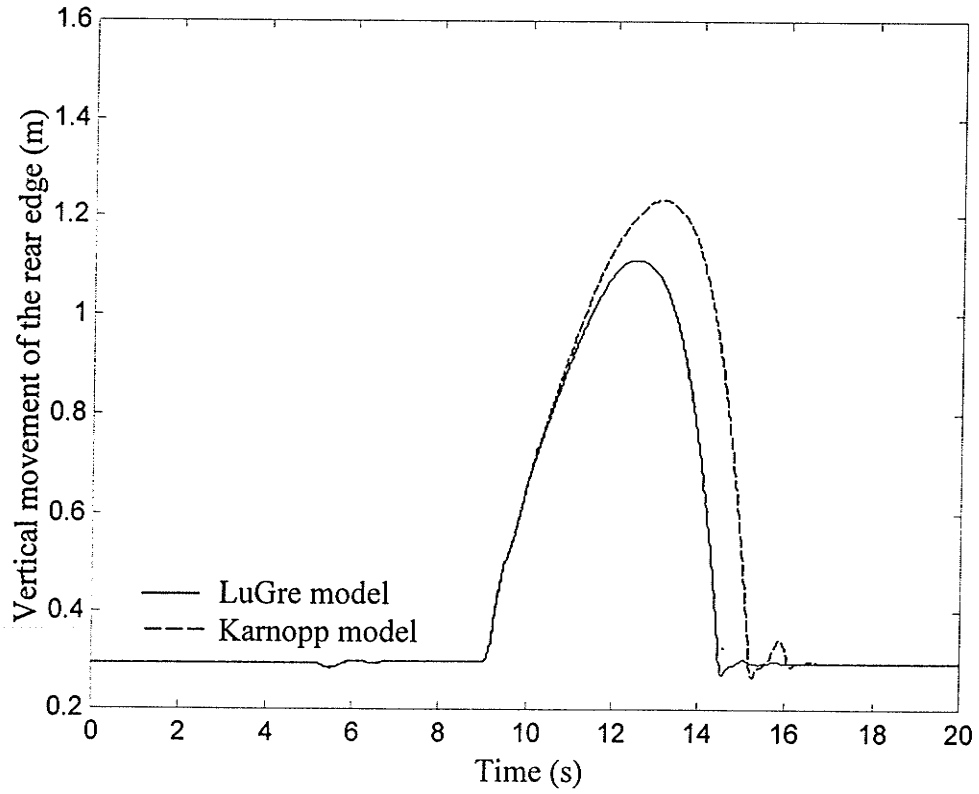

Figure 6.8. Vertical movement of the front and the rear edges.

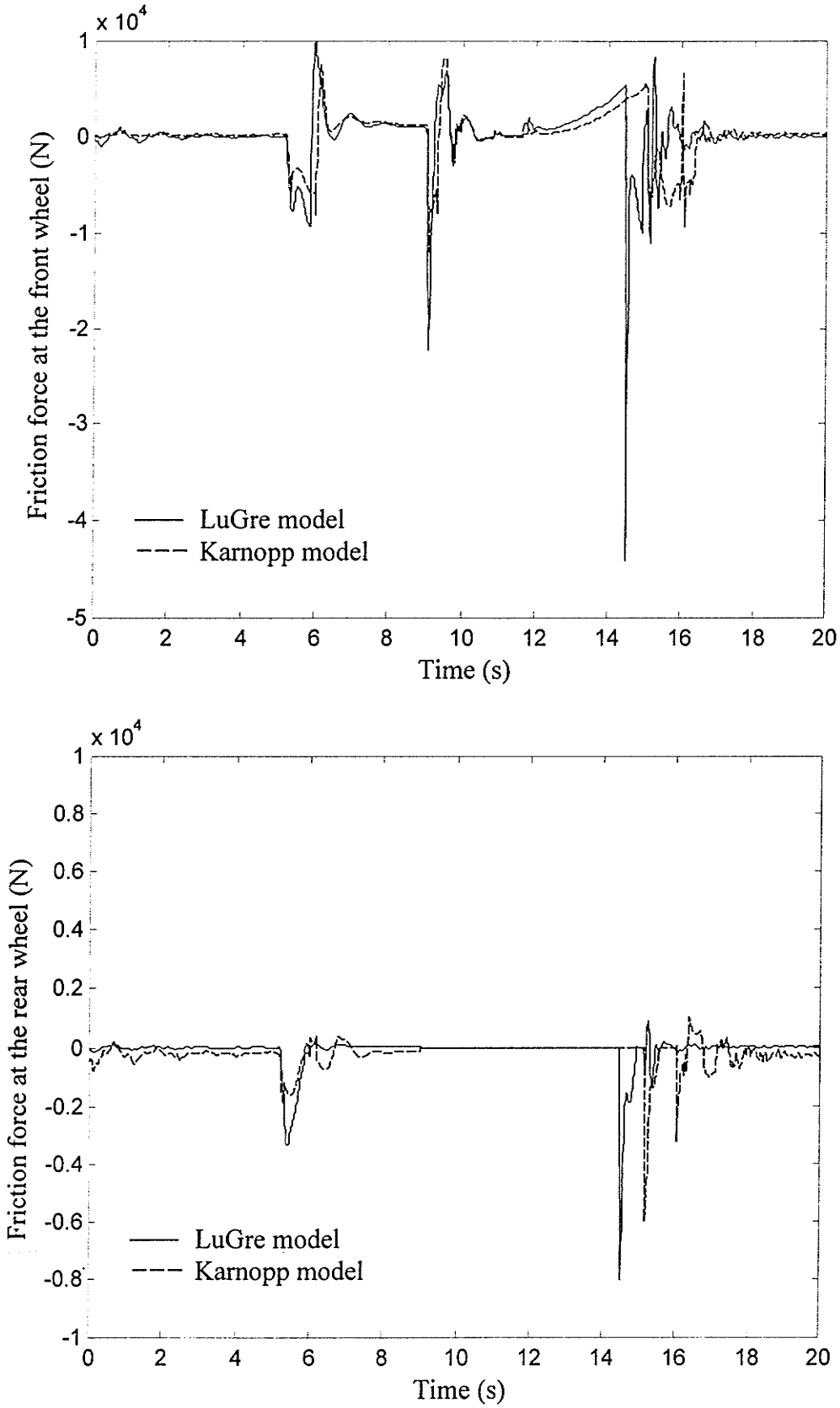

Figure 6.9. Friction forces at the front and rear wheels.

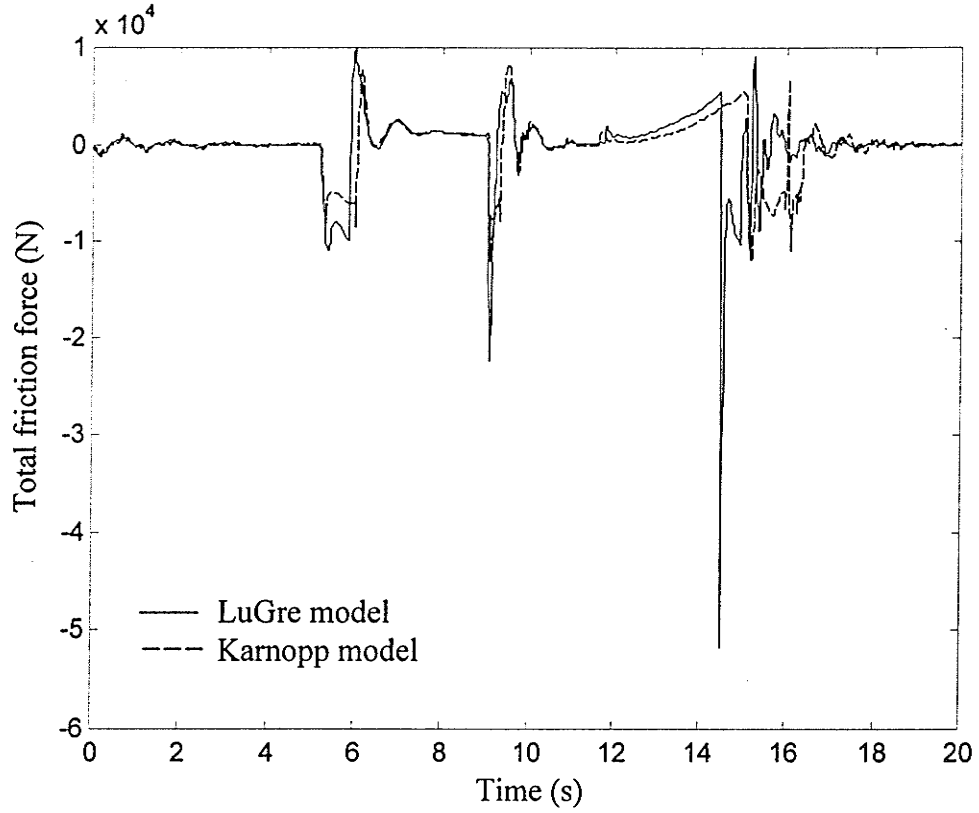

Figure 6.10. Total friction forces affecting the base during the task.

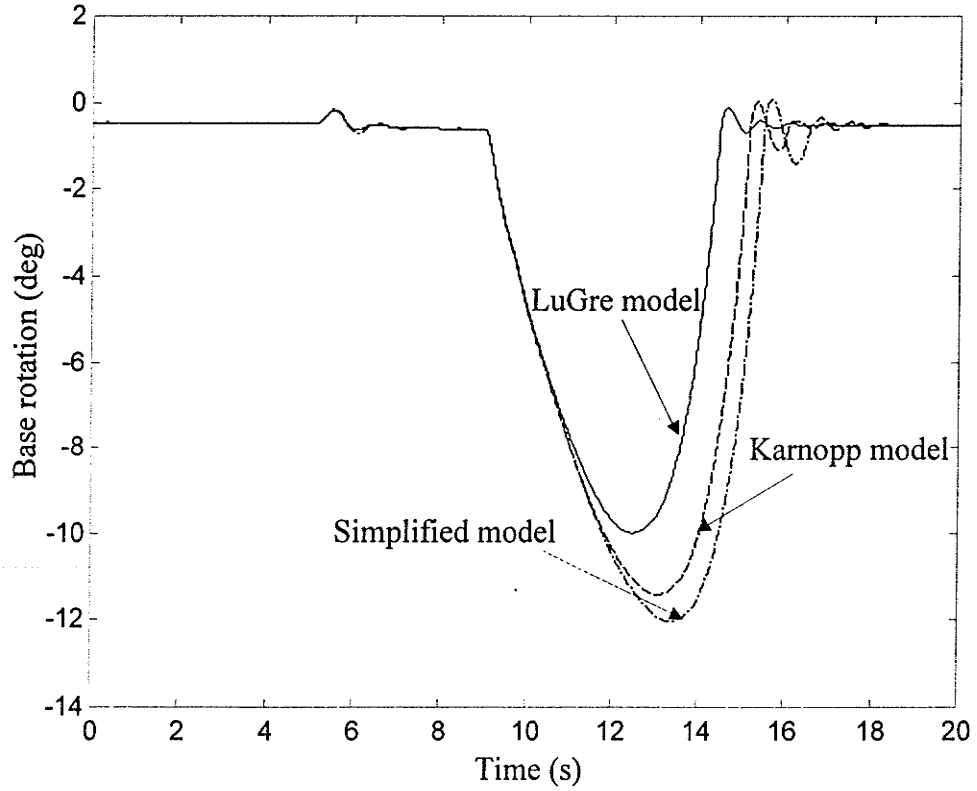

Figure 6.11. Base rotation using different friction models.

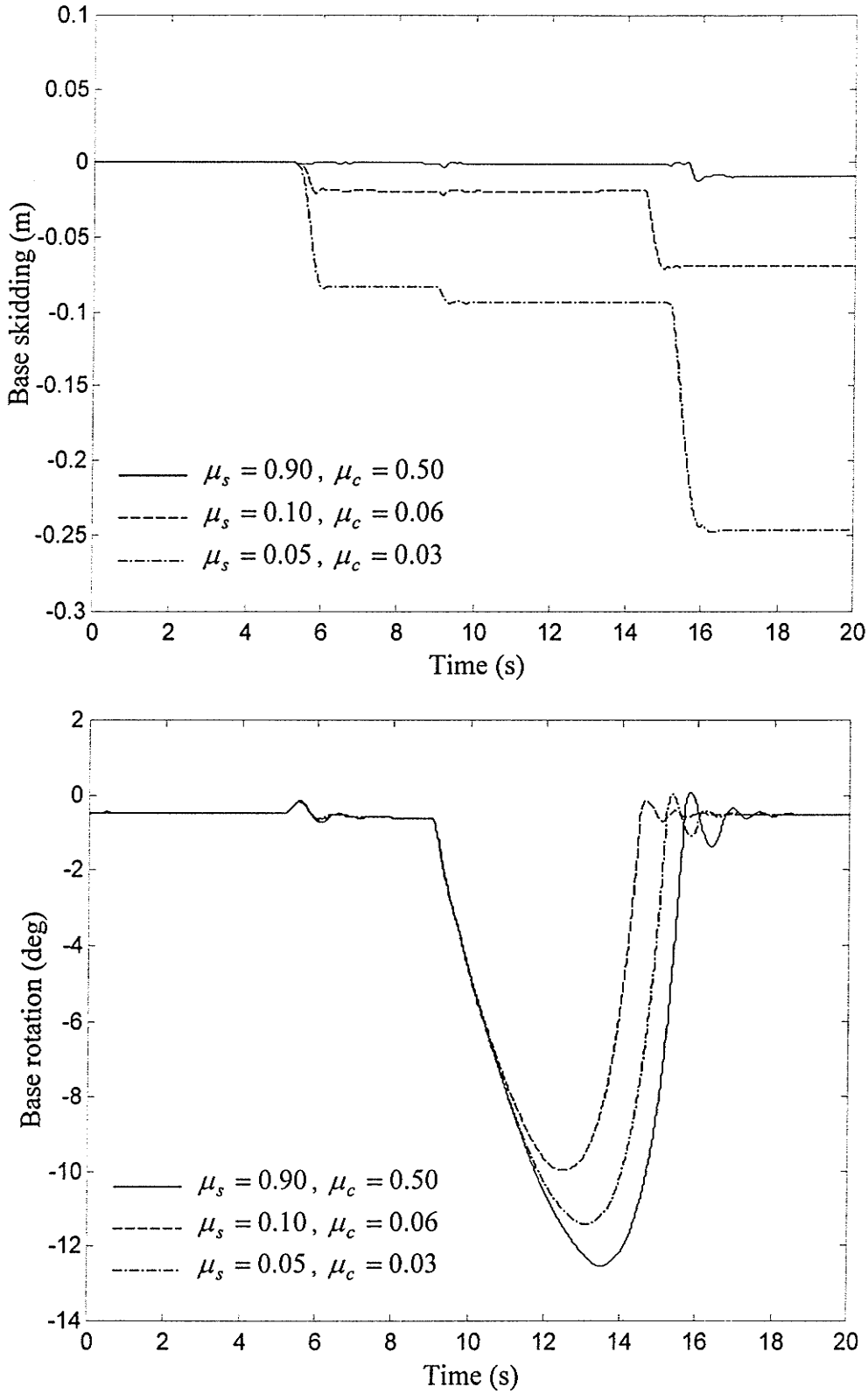

Figure 6.12. Base movement, skid and rotation, using Karnopp model with different friction coefficient values.

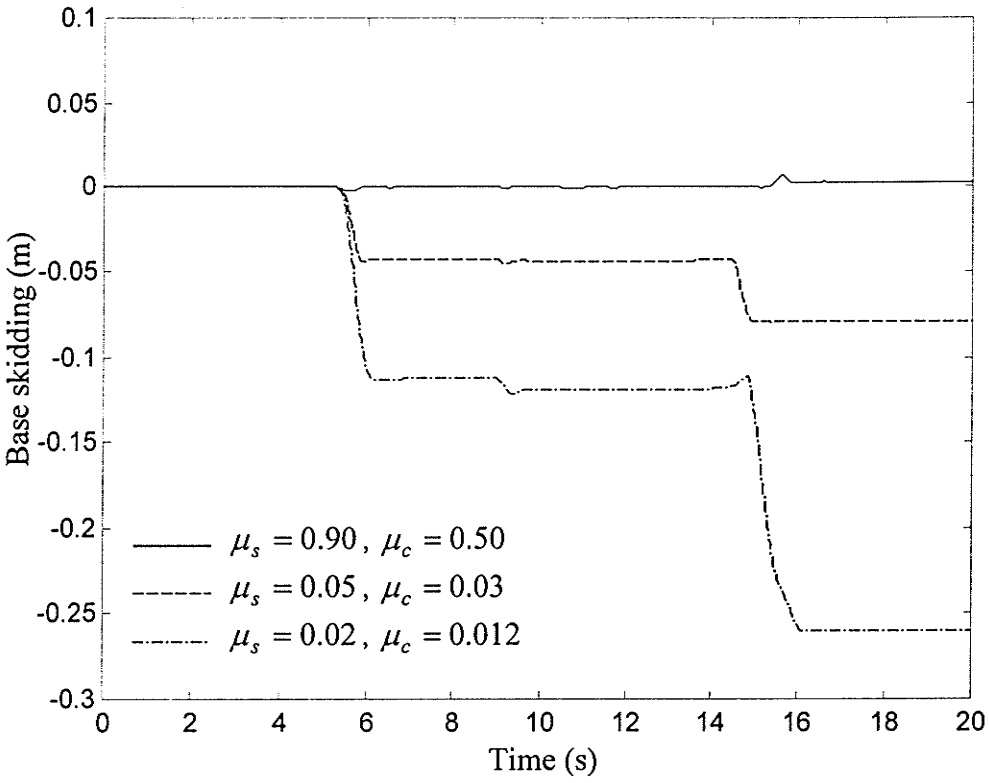

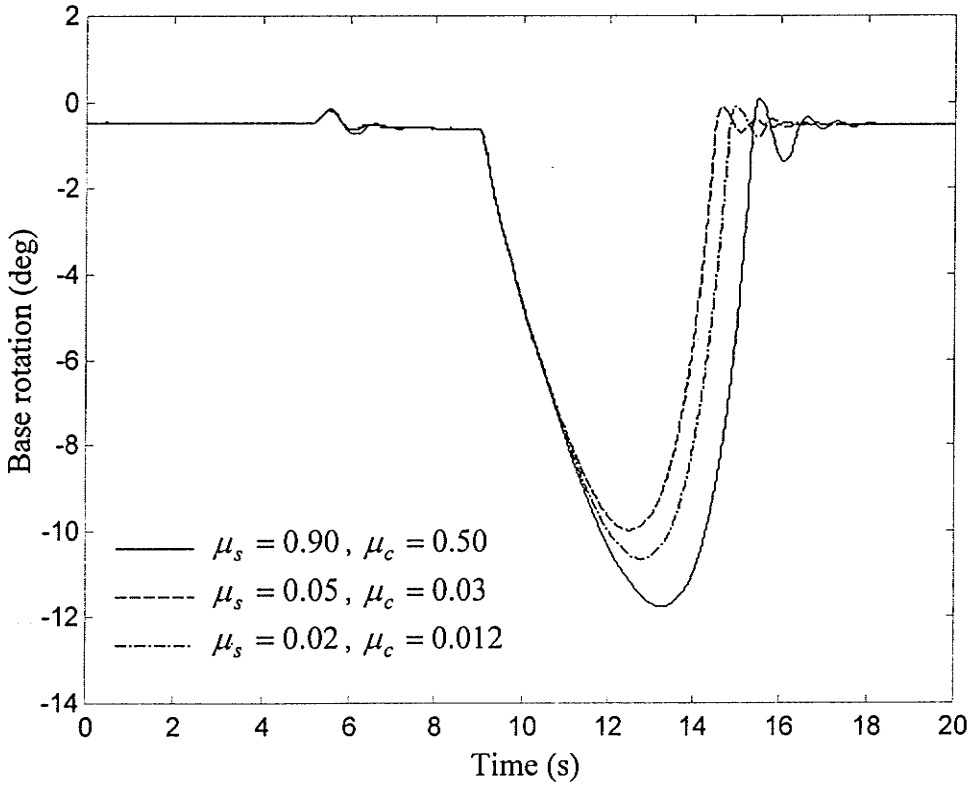

Figure 6.13. Base movement, skid and rotation, using LuGre model with different friction coefficient values.

Chapter 7

Stability Analysis during Spatial Motions

In this chapter, a complete simulation model of mobile manipulators that are subject to tip-over is developed. The model includes the dynamics of the base, the flexibility between the base and the ground, and the friction between the tires and the ground. This model is then applied to the study stability of a Caterpillar excavator-based log-loader machine. The effects of different factors that may play a role in the stability of the machine are also investigated.

7.1 Development of the Dynamic Model

Figure 2.8 shows a typical excavator-based log-loader. The machine can be considered as a three-degree of freedom manipulator mounted on mobile platform with an additional moveable implement. The base is considered as a rigid body, resting on four wheels. The combined vehicle suspension and ground-tire compliance is represented by Kelvin-Voigt spring damping system at each wheel (Akpan and Kujath 1998). The damping is viscous, below the critical value and invariant with respect to changes of the kinematic

configuration. Figure 7.1 shows a schematic diagram of the manipulator's base including the external forces whereas Figure 7.2 shows a top view of the manipulator mounted on the mobile platform.

To model the general three-dimensional motion of the base, five virtual links are added between the base and the ground to describe the position and the orientations of the base. Figure 7.3 shows the schematic diagram of the base and the virtual links. The first three virtual links are with prismatic joints to position a selected point on the base. The other two virtual links and the base itself have revolute joints to describe the orientations of the base in space. Thus, the machine can be modeled as a fixed base manipulator with $(5 + n)$ links, where n is the total number of the manipulator's links including the base ($n = 4$ for the machine under study).

The dynamic equations for the original system plus the virtual links are then derived

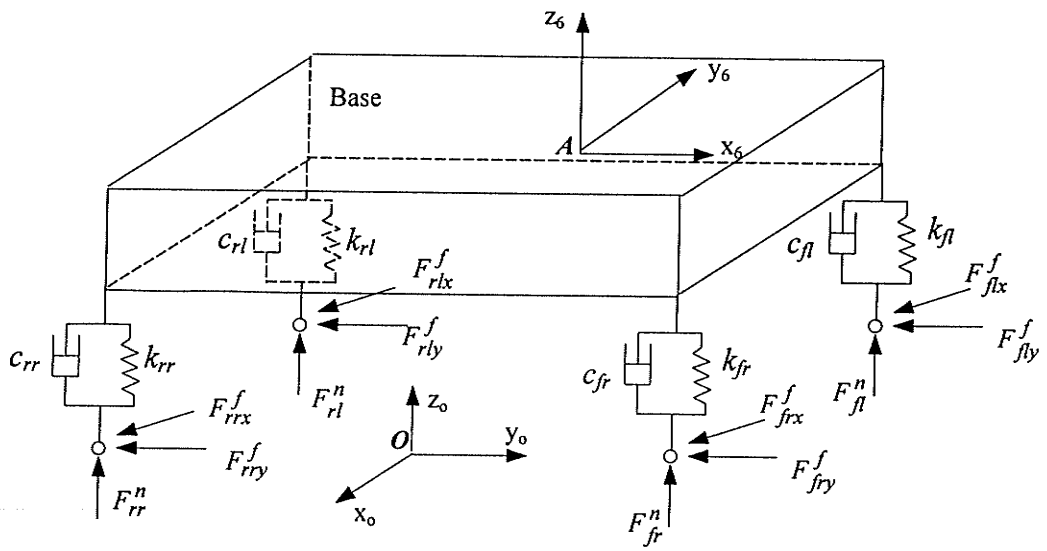

Figure 7.1. Schematic diagram of the manipulator base including the external forces.

using conventional Lagrange-Euler (LE) formulation for serial link fixed base manipulators, which is given in any robotics textbook. By setting the kinematic and dynamic parameters of the virtual links to zero, the final dynamic equations for the original system are obtained.

The Denavit-Hartenberg (DH) coordinate systems pertaining to the machine kinematics are shown in Figure 7.4. The kinematic parameters are given in Table 7.1. The dynamic equations are derived as follows:

$$\tau = \mathbf{M}(\mathbf{q})\ddot{\mathbf{q}} + \mathbf{C}(\mathbf{q},\dot{\mathbf{q}}) + \mathbf{G}(\mathbf{q}) + \mathbf{J}^{\mathrm{T}}\mathbf{F} \tag{7.1}$$

where $\mathbf{q} = \{q_1, q_2, ..., q_{5+n}\}^T$, $\dot{\mathbf{q}}$ and $\ddot{\mathbf{q}}$ are vectors of the joint variables, velocities and accelerations, $\tau(t) = \{\tau_1, \tau_2, .., \tau_{5+n}\}^T$ is the generalized force vector applied at joints $i = 1, 2, .., 5+n$. Term $\mathbf{J}^{\mathrm{T}}\mathbf{F}$ denotes the effect of the external forces $\mathbf{F}$ (due to flexibility and friction between the ground and the base) transferred to point A on the base, which is

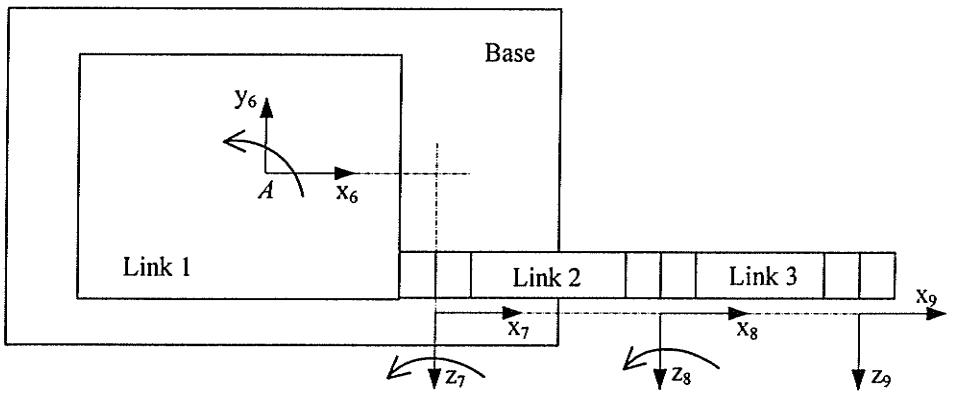

Figure 7.2. Top view of mobile manipulator.

the origin of the coordinate frame 6, as shown in Figures 7.3 and 7.4. **J** is the Jacobian used to calculate the effect of these forces and moments at each joint.

The elements of the $((5+n)\times(5+n))$ inertial acceleration-related symmetric matrix, $\mathbf{M(q)}$, are derived using the following relations:

$$\begin{aligned} M_{ij} &= Trace\left\{\Delta_i\left[\sum_{p=\max(6,j)}^{5+n}\mathbf{T}_p\mathbf{I}_p\mathbf{T}_p^T\right]\Delta_j^T\right\} && (j\geq i) \\ M_{ji} &= M_{ij} && (i<j) \end{aligned} \tag{7.2}$$

Note that the first five links are virtual links. Thus, the elements of their inertia matrices are zeros and therefore the summation shown in Equation (7.2) and subsequent Equations (7.4) and (7.5), starts from $p=\max(6,j)$ instead of $p=j$.

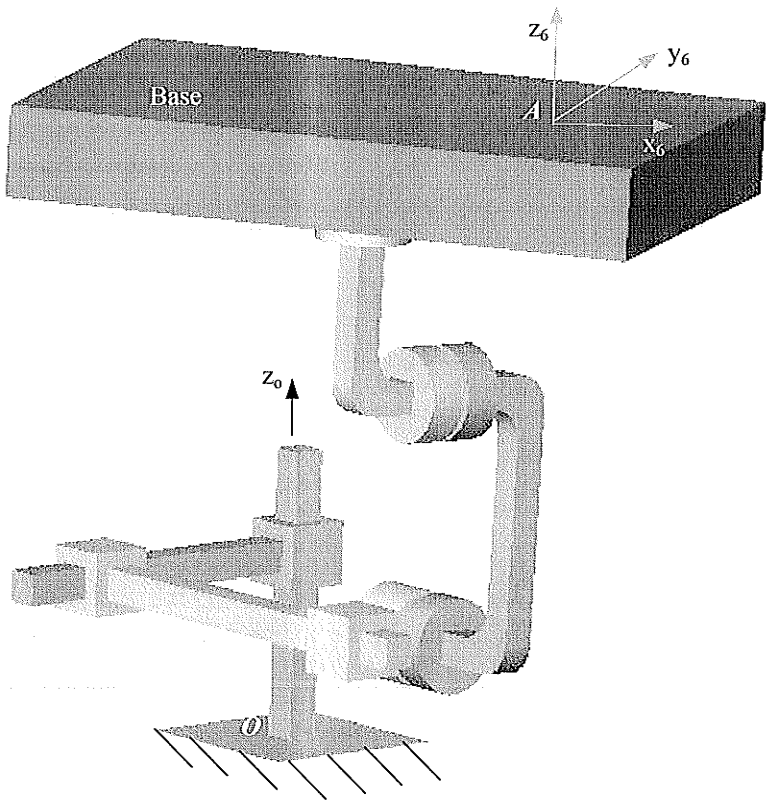

Figure 7.3. 3D presentation of mobile manipulator base with the virtual links.

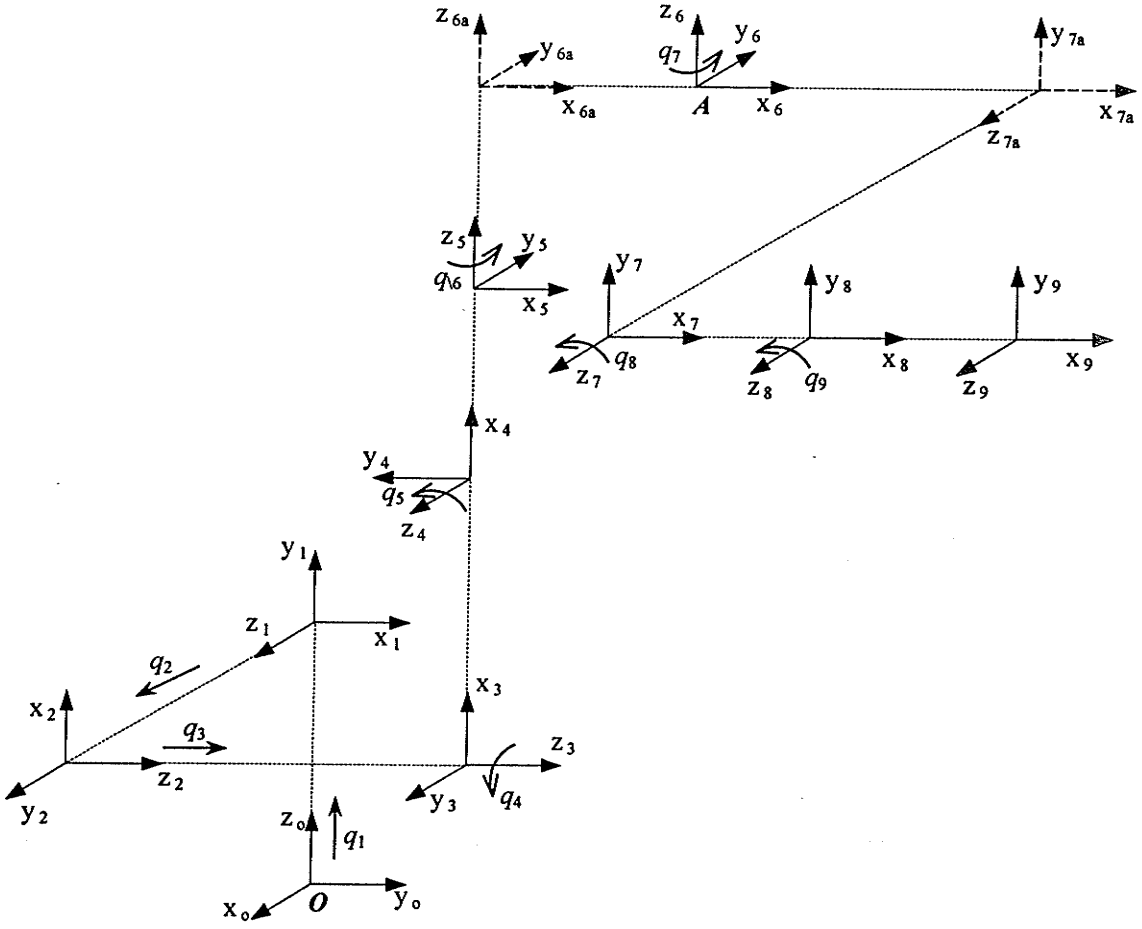

Figure 7.4. Denavit-Hartenberg Link coordinates for general 3D motions.

Table 7.1 Kinematic parameters.

Link	θ_i (rad)	d_i (m)	a_i (m)	α_i (rad)	Variables
1	$\pi/2$	q_1	0	$\pi/2$	q_1
2	$\pi/2$	q_2	0	$\pi/2$	q_2
3	0	q_3	0	0	q_3
4	q_4	0	$a_4 = 0$	$-\pi/2$	q_4
5	q_5	0	$a_5 = 0$	$-\pi/2$	q_5
6a	q_6	$d_6 = 0.23$	0	0	q_6
6	0	0	$a_6 = 0.2$	0	-
7a	q_7	0	$a_7 = 0.35$	$\pi/2$	q_7
7	0	$d_7 = 0.12$	0	0	-
8	q_8	0	$a_8 = 5.2$	0	q_8
9	q_9	0	$a_9 = 1.8$	0	q_9

The elements of the Coriolis and centrifugal force vector $\mathbf{C}(\mathbf{q}, \dot{\mathbf{q}}) = \{c_1, c_2, ..., c_{5+n}\}^T$ are determined as follows:

$$c_i = \sum_{j=1}^{5+n} \sum_{i=1}^{5+n} c_{ijk} \dot{q}_j \dot{q}_k \tag{7.3}$$

where

$$c_{ijk} = Trace\left\{ \Delta_i \left[\sum_{p=\max(6,j)}^{5+n} \mathbf{T}_p \mathbf{I}_p \mathbf{T}_p^T \right] \Delta_j^T \Delta_k^T \right\} \qquad (j \geq i,\ j \geq k)$$

$$c_{ikj} = c_{ijk} \tag{7.4}$$

$$c_{kji} = -c_{ijk} \qquad (j < i,\ j < k)$$

The elements of the gravitational force vector $\mathbf{G}(\mathbf{q}) = \{G_1, G_2, ..., G_{5+n}\}^T$ are:

$$G_i = -\left(\mathbf{g}^T;0\right)\Delta_i\left[\sum_{p=\max(6,i)}^{5+n} m_p \mathbf{T}_p\left(\mathbf{r}_p^p;1\right)\right] \tag{7.5}$$

where $\mathbf{g}$ is the gravitational acceleration vector in base coordinate frame, $\mathbf{r}_i^i$ is the position vector of mass center of link i in coordinate frame i. In Equations (7.2), (7.4), and (7.5), $\mathbf{T}_i$ is the homogeneous transformation matrix from coordinate frame i to the reference coordinate frame. $\mathbf{I}_i$ is defined as

$$\mathbf{I}_i = \begin{bmatrix} \mathbf{I}_i^i + m_i \mathbf{r}_i^i \mathbf{r}_i^{i^T} & m_i \mathbf{r}_i^i \\ m_i \mathbf{r}_i^{i^T} & m_i \end{bmatrix} \tag{7.6}$$

where $\mathbf{I}_i^i$ is a 3×3 inertial matrix of link i about its mass center in coordinate frame i and m_i is the mass of link i. Δ_i is a differential operator and is defined as (Sallam et al. 1998):

$$\Delta_i = \begin{bmatrix} \lambda_i \hat{\mathbf{z}}_{i-1} & \left[\lambda_i \hat{\mathbf{p}}_{i-1} + (1-\lambda_i)\mathbf{E}\right]\mathbf{z}_{i-1} \\ \mathbf{0} & 0 \end{bmatrix} \tag{7.7}$$

where $\mathbf{z}_i$ is z-axis of coordinate frame i, and $\mathbf{p}_i$ is the position vector of the origin of coordinate frame i with respect to the reference coordinate system. $\lambda_i = 1$ for revolute joints and $\lambda_i = 0$ for prismatic joints. $\mathbf{E}$ is the identity matrix. The symbol '^' in (7.7) denotes a skew symmetric matrix with zero diagonal values. For example, given a vector $\mathbf{u} = \{u_x, u_y, u_z\}^T$, $\hat{\mathbf{u}}$ is defined as:

$$\hat{\mathbf{u}} = \begin{bmatrix} 0 & -u_z & u_y \\ u_z & 0 & -u_x \\ -u_y & u_x & 0 \end{bmatrix}$$

The normal forces at each wheel (F_{fr}^n, F_{fl}^n, F_{rr}^n, and F_{rl}^n) are calculated based on the deflection of the spring damper system. For example, the normal force at the front right wheel, F_{fr}^n, is calculated as follows:

$$F_{fr}^n = \frac{\partial R_{fr}}{\partial \dot{q}_1} + \frac{\partial V_{fr}}{\partial q_1} \tag{7.8}$$

where R is the Rayleigh's dissipation function and V is the potential energy function due to the spring.

$$V_{fr} = \frac{1}{2} k_{fr} \left[\left\{ \mathbf{T}_6 \mathbf{r}_{fr}^6 \right\}_z - l_o \right]^2 \tag{7.9}$$

$$R_{fr} = \frac{1}{2} c_{fr} \left[\frac{d}{dt} \left\{ \mathbf{T}_6 \mathbf{r}_{fr}^6 \right\}_z \right]^2 \tag{7.10}$$

then

$$F_{fr}^n = \left(c_{fr} \left\{ \left[\sum_{i=1}^{6} \frac{\partial \mathbf{T}_6}{\partial q_i} \dot{q}_i \right] \mathbf{r}_{fr}^6 \right\}_z + k_{fr} \left[\left\{ \mathbf{T}_6 \mathbf{r}_{fr}^6 \right\}_z - l_o \right] \right) \left\{ \frac{\partial \mathbf{T}_6}{\partial q_1} \mathbf{r}_{fr}^6 \right\}_z \tag{7.11}$$

where , $\mathbf{r}_{fr}^6$ is the position vector of front right edge defined in coordinate frame 6 (see Figure 7.4). l_o is the natural length of the spring. c and k are the damping and stiffness coefficients, respectively, and the subscript z means the z component of the vector.

The normal forces at other wheels (F_{fl}^n, F_{rr}^n, and F_{rl}^n) are calculated in a similar manner.

LuGre tire friction model is used to calculate the friction forces between the wheels and the ground. The components of the friction force at the front right wheel, F_{fry}^f and F_{frx}^f, are defined as:

$$F_{fry}^{f} = \left(\sigma_{o\,fry} z_{fry} + \sigma_{1\,fry} \dot{z}_{fry} + \sigma_{2\,fry} v_{fry}\right) F_{fr}^{n} \tag{7.12}$$

$$F_{frx}^{f} = \left(\sigma_{o\,frx} z_{frx} + \sigma_{1\,frx} \dot{z}_{frx} + \sigma_{2\,frx} v_{frx}\right) F_{fr}^{n} \tag{7.13}$$

where σ_o is the normalized lumped stiffness, σ_1 the normalized lumped damping, σ_2 is the normalized viscous relative damping, F^n is the normal force. The average deflection of the bristles at the front right wheel in y and x directions are modeled as follows:

$$\dot{z}_{fry} = v_{fry} - \frac{\sigma_{o\,fry} |v_{fry}|}{\eta_y(v_{fry})} z_{fry} \tag{7.14}$$

$$\dot{z}_{frx} = v_{frx} - \frac{\sigma_{o\,frx} |v_{frx}|}{\eta_x(v_{frx})} z_{frx} \tag{7.15}$$

where v is the relative velocity between the wheel and the ground. The function $\eta(v)$ contains information about the velocity dependence of friction. It is positive and depends on many factors such as material properties, lubrication, and temperature.

$$\eta_y(v_{fry}) = \mu_{c\,fry} + (\mu_{s\,fry} - \mu_{c\,fry}) e^{-\left|\frac{v_{fry}}{v_{s\,fry}}\right|^{0.5}} \tag{7.16}$$

$$\eta_x(v_{frx}) = \mu_{c\,frx} + (\mu_{s\,frx} - \mu_{c\,frx}) e^{-\left|\frac{v_{frx}}{v_{s\,frx}}\right|^{0.5}} \tag{7.17}$$

where μ_c is the Coulomb friction coefficient and μ_s is the static friction coefficient. v_s is the Stribeck velocity (helps to define the velocity dependence of friction).

The friction forces at other wheels (F_{fly}^{f}, F_{flx}^{f}, F_{rry}^{f}, F_{rrx}^{f}, F_{rly}^{f}, and F_{rlx}^{f}) are calculated using the same method.

The normal and the friction forces at each wheel are transferred as forces and moments to point *A* (the origin of the coordinate frame 6, as shown in Figures 7.3 and 7.4). Then, the Jacobian is used to calculate the effect of these forces and moments at each joint.

Considering *A* as end-effector, one can calculate the Jacobian **J** as follows:

$$\mathbf{J}_i = \begin{bmatrix} \mathbf{z}_{i-1} \\ \mathbf{0} \end{bmatrix} \qquad \text{for prismatic joints } (i=1,2,3) \tag{7.18}$$

$$\mathbf{J}_i = \begin{bmatrix} \mathbf{z}_{i-1} \times \mathbf{r}_A^{i-1} \\ \mathbf{z}_{i-1} \end{bmatrix} \qquad \text{for revolute joints } (i=4,5,6) \tag{7.19}$$

where $\mathbf{z}_i$ is the vector of the z axis of the coordinate system i defined in the reference frame. $\mathbf{r}_A^{i-1}$ is the position vector of the point *A* defined in the (i-1) coordinate system.

7.2 Simulation Studies

Dynamic parameters of the machine under investigation are listed in Tables 7.2 and 7.3. The suspension parameters are $k_{fr} = k_{fl} = k_{rr} = k_{rl} = 17.5 \times 10^5$ N/m and $c_{fr} = c_{fl} = c_{rr} = c_{rl} = 7.5 \times 10^4$ Ns/m. These values are chosen to provide a natural frequency of ≈ 3 Hz and damping ratio ≈ 0.4 in the vertical direction. Note that the natural frequencies and damping ratios change with the manipulator configuration and payload. The friction model parameters are chosen as follows:

$\sigma_{o_{frx}} = \sigma_{o_{flx}} = \sigma_{o_{rrx}} = \sigma_{o_{rlx}} = 40$ 1/m, $\sigma_{o_{fry}} = \sigma_{o_{fly}} = \sigma_{o_{rry}} = \sigma_{o_{rly}} = 40$ 1/m,

$\sigma_{1_{frx}} = \sigma_{1_{flx}} = \sigma_{1_{rrx}} = \sigma_{1_{rlx}} = 4.9487$ s/m, $\sigma_{1_{fry}} = \sigma_{1_{fly}} = \sigma_{1_{rry}} = \sigma_{1_{rly}} = 4.9487$ s/m,

$\sigma_{2_{frx}} = \sigma_{2_{flx}} = \sigma_{2_{rrx}} = \sigma_{2_{rlx}} = 0.0018$ s/m, $\sigma_{2_{fry}} = \sigma_{2_{fly}} = \sigma_{2_{rry}} = \sigma_{2_{rly}} = 0.0018$ s/m.

These values were used by Canudas de Wit et al. (1999) for tire friction models and gave results matched reasonably well their experimental data. The static and dynamic friction coefficients were chosen as follows:

$$\mu_{c_{frx}} = \mu_{c_{flx}} = \mu_{c_{rrx}} = \mu_{c_{rlx}} = 0.5,\ \mu_{s_{frx}} = \mu_{s_{flx}} = \mu_{s_{rrx}} = \mu_{s_{rlx}} = 0.9.$$

The swing is actuated by a hydraulic motor whereas the boom and the stick are actuated by hydraulic cylinders. The cylinders and the swing motor are powered by means of pressure and flow through the main valves. The equations governing the hydraulic actuation system are given in detail in Chapter 2. The following case studies are conducted to observe the effects of different manipulator motions and combined vehicle suspension and ground-tire compliance on the machine stability.

Table 7.2. Mass and center of gravity of each link with respect to its coordinate frame.

	mass (kg)	x_c (m)	y_c (m)	z_c (m)
Base	6932	-0.056	0.0	-0.23
Cabin	8031	-1.4	0.0	-0.16
Boom	1830	-2.9	0.2	0
Stick	688	-0.9	0.1	0

Example 1: effect of the swing motion

Figure 7.5 shows the rotation of the cabin over the base when handling a 2000 kg load with different speeds. The cabin rotates a full revolution before it is brought to a stop. Due to the rotation of the swing, the centrifugal forces produce moments about x_6 and y_6 axes. These moments depend on the angular speed of the swing. Figure 7.6 shows the

effect of different swing motions on the vehicle stability. It is shown that moving the swing with high speeds significantly decreases the machine stability and can even cause a complete tip-over.

Table 7.3. Inertia tensor data

	I_{xx} (kg m^2)	I_{yy} (kg m^2)	I_{zz} (kg m^2)	I_{xy} (kg m^2)	I_{xz} (kg m^2)	I_{yz} (kg m^2)
Base	3340	6683	9778	0	0	0
Cabin	15700	0	200	0	0	0
Boom	15400	100	0	-1100	0	0
Stick	600	0	0	0	-70	0

Example 2: effect of boom and stick movements

In this example, we study the effect of the boom and stick movements on the vehicle stability. The manipulator is to perform a planar pick and place operation. The end-effector moves from a position close to the base carrying a 5100 kg load. The machine extends the arm to a possible 'dumping position' far from the base (see Figure 7.7). This move causes the manipulator to tip over and if there is no action taken to retract the manipulator, it turns over completely. Figure 7.8 shows the same manipulator movement with a recovery motion. As soon as the base starts to tip over, the arm retracts back to its original position. The machine rolls back to a stable position. This shows that by proper manipulation of the links of the manipulator, some of tip-over situations can be recovered.

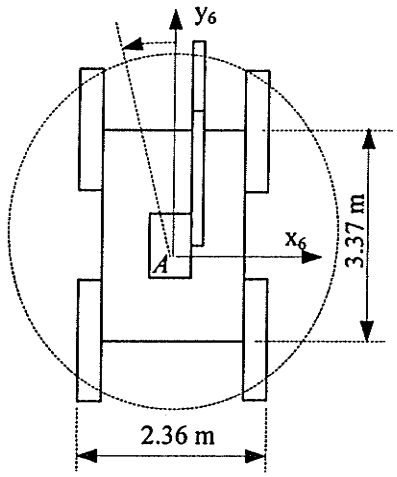

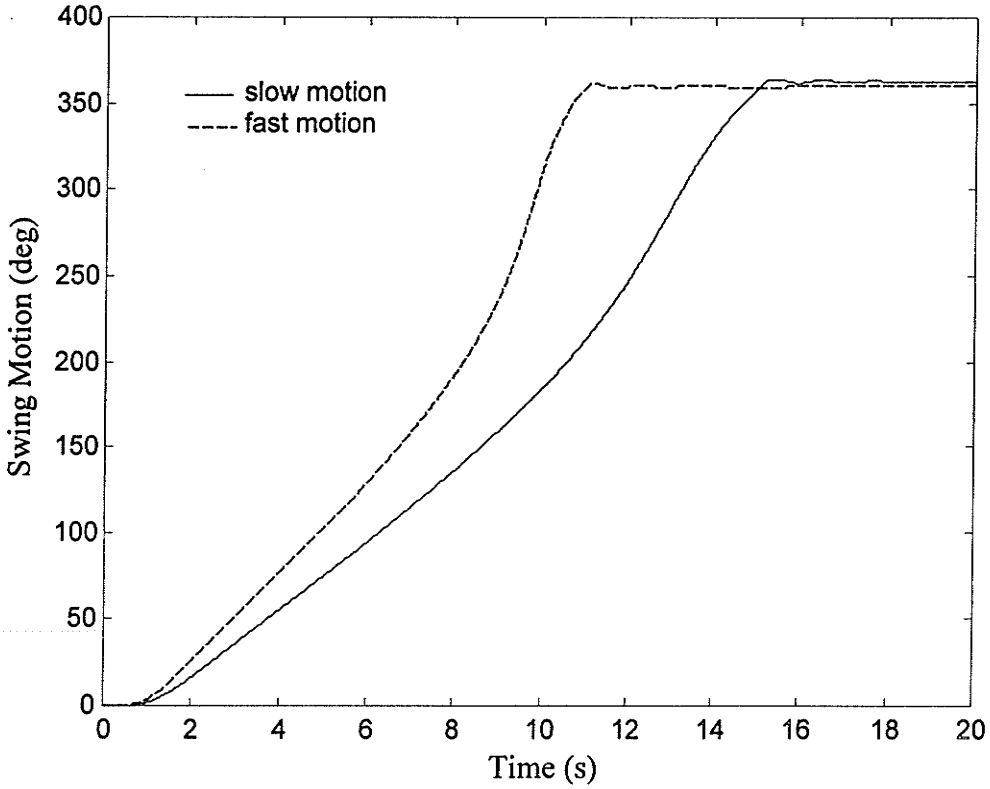

Figure 7.5. Swivel of manipulator.

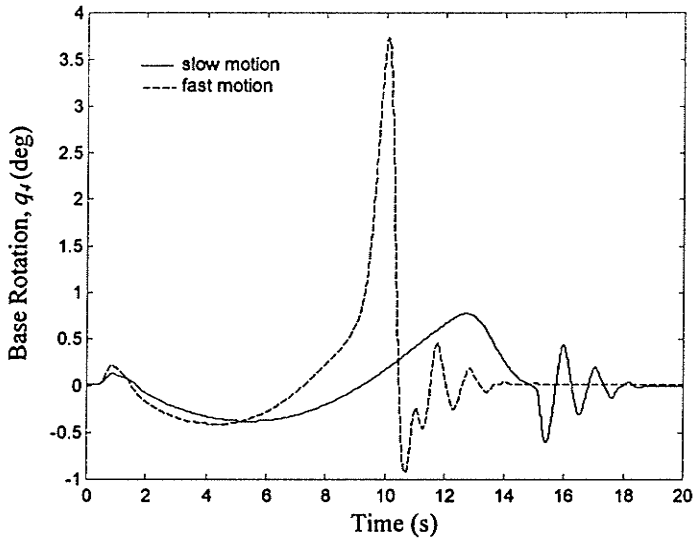

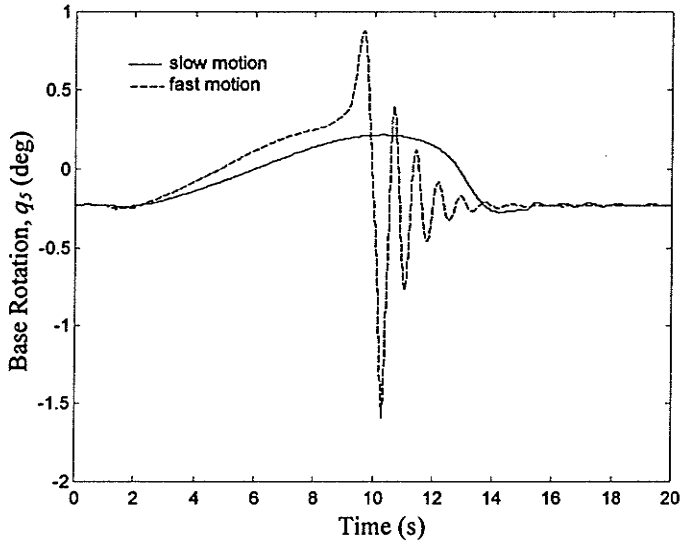

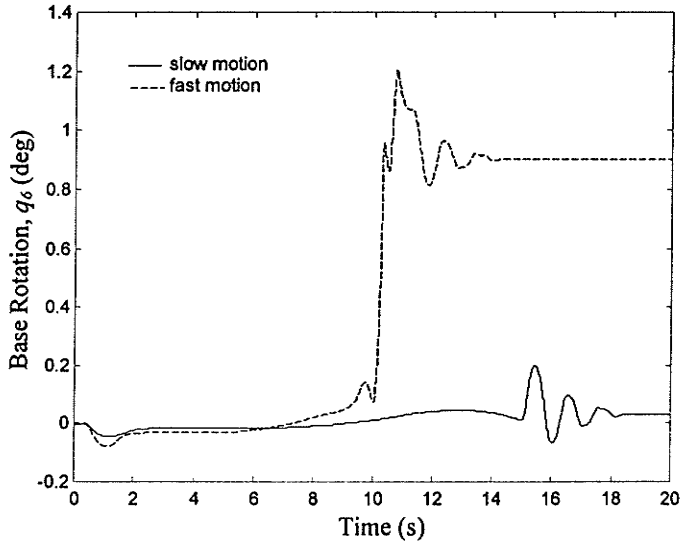

Figure 7.6. Rotation of the base with various speeds of swing

Example 3: effect of flexibility between the base and the ground

In this case study, the sensitivity of the machine stability to the variation of the stiffness and the damping of the flexibility between the base and the ground is investigated. Consistent with the setup in Example 2, we simulated the same manipulator movement as shown in Figure 7.8 but with various stiffness and damping coefficients.

Figure 7.9 shows the effect of changing the stiffness while the damping coefficients are kept constant. It is seen that increasing the stiffness of the contact between the base and the ground improves the stability. Figure 7.10 shows that increasing the damping, while the stiffness is kept constant, increases the machine stability. However, it is seen that changing the system stiffness has greater influence on the machine stability than that of the system damping.

Example 4: effect of hydraulic compliance

Hydraulic parameters such as the bulk modulus of the hydraulic fluid exhibit large variations during actual operations (Merrit 1967 and Yao et al. 1998). Also, different types of hydraulic fluids have different values of bulk modulus. Here, we investigate the effect of the hydraulic compliance variation, due to changes of the effective bulk modulus, on the stability of mobile manipulators. Figure 7.11 shows that using lower effective bulk modulus increases the machine stability. However, optimization should be made to select the optimal value of the bulk modulus since high bulk modulus is recommended for control purposes of these machines (Merrit 1967).

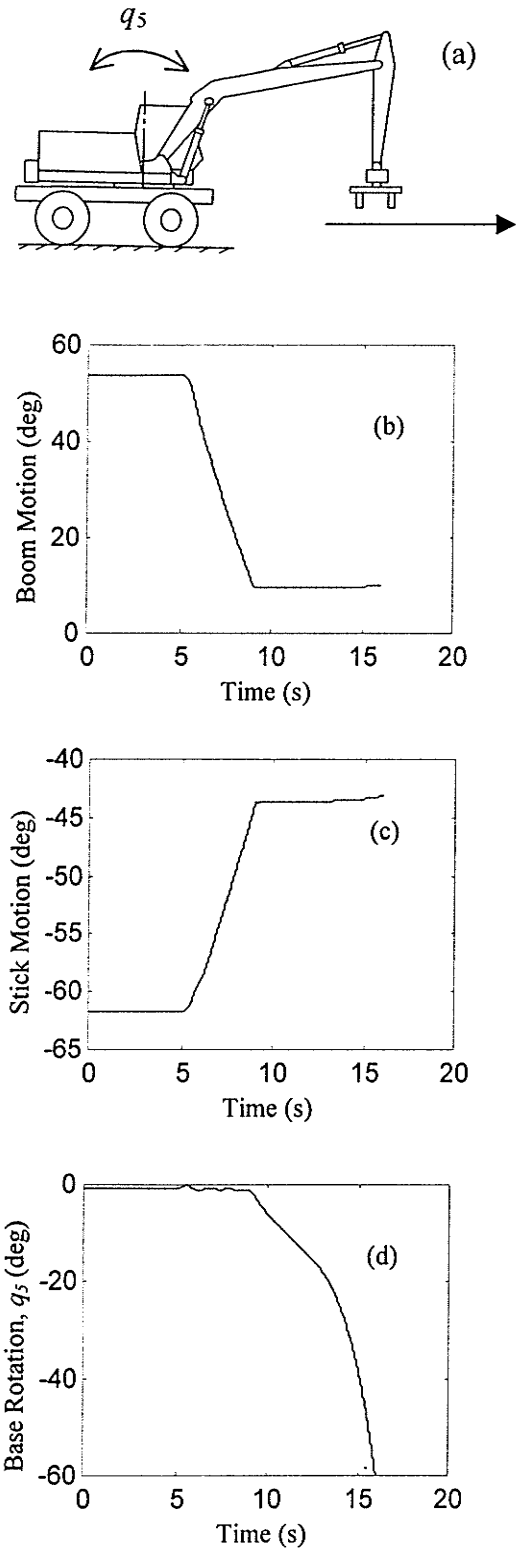

Figure 7.7. Base rotation during the manipulator motion.

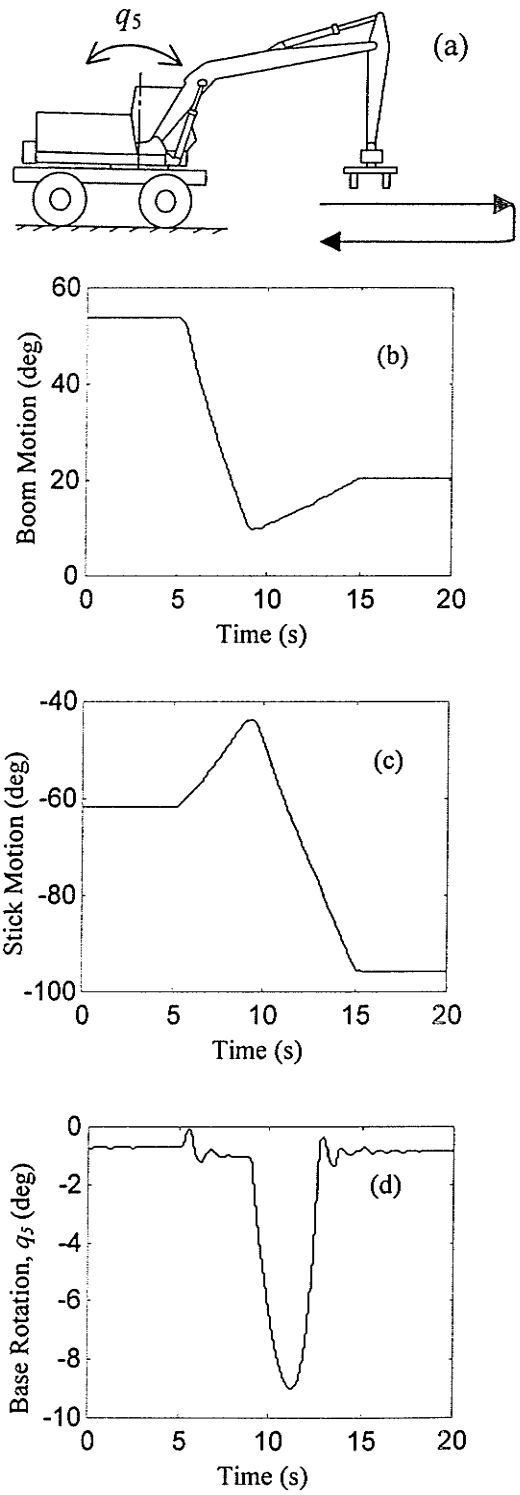

Figure 7.8. Base rotation during the manipulator recovery motion.

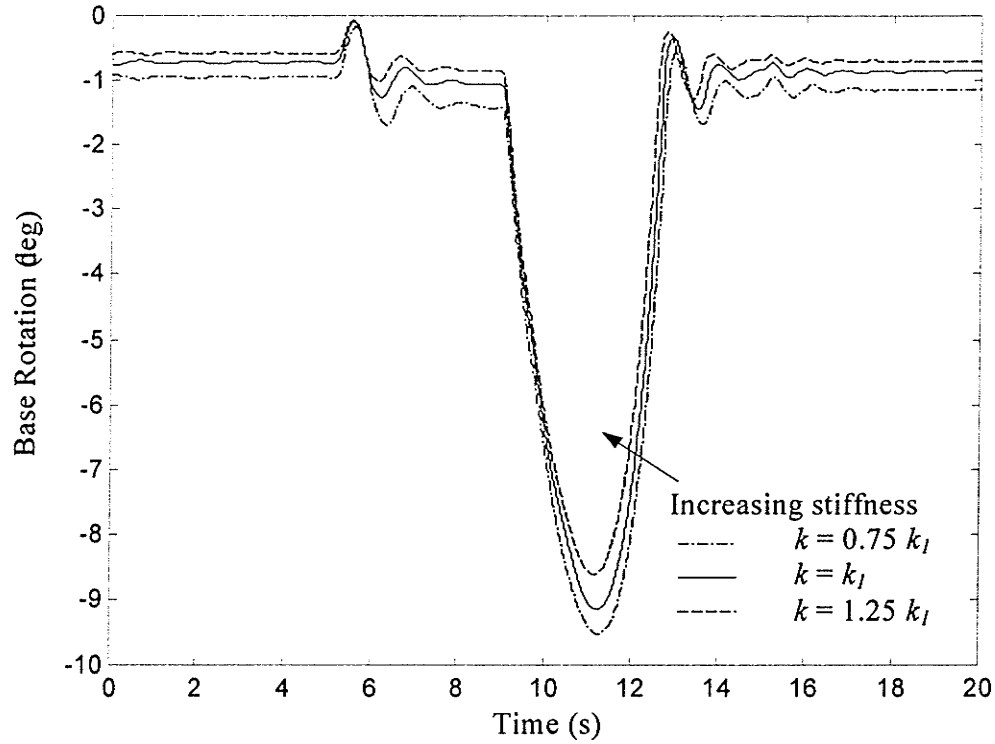

Figure 7.9. Effect of increasing ground-base stiffness on machine stability, $k_l = 17.5 \times 10^5$ N/m.

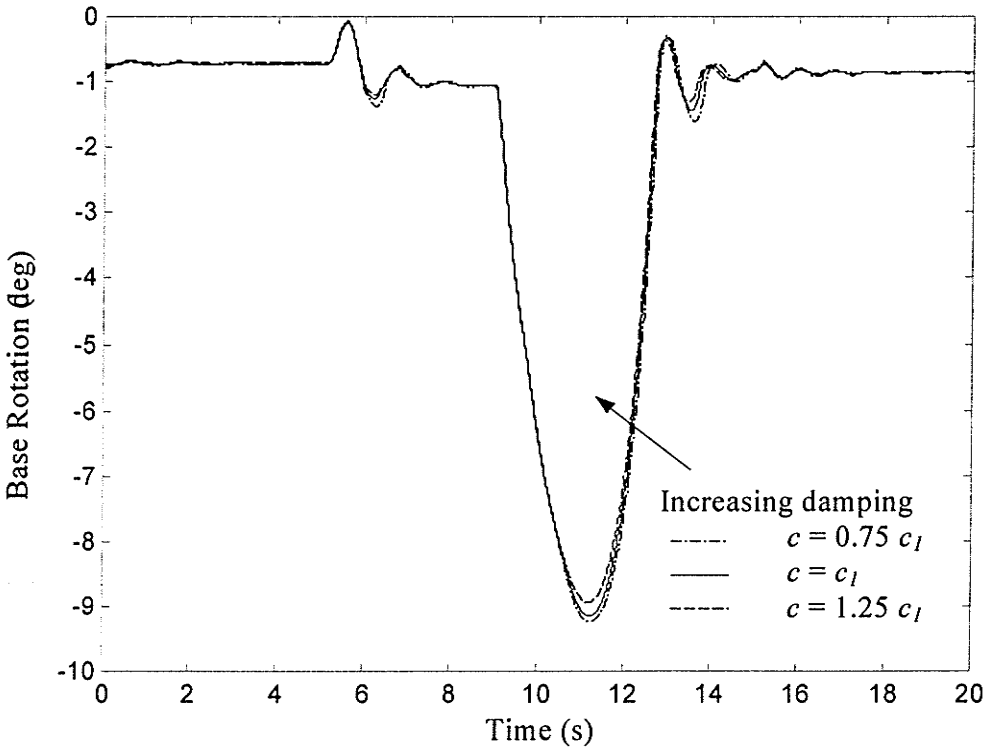

Figure 7.10. Effect of increasing ground-base damping on machine stability, $c_l = 7 \times 10^4$ Ns/m.

Example 5: comparison between the effects of simultaneous and sequential motions of manipulator links on the machine stability

This example illustrates the advantage of applying a coordinated-motion over sequential motion, in performing the manipulator's tasks. Two different trajectories are adopted to do the same pick and place operation, similar to that in Example 2 (see Figure 7.8). Using the first trajectory, the boom and stick move simultaneously, whereas in the second, they move in consecutive order (see Figure 7.12). During simultaneous movement, the manipulator links have more time to reach their final rotational positions and therefore they move slower than in the case of sequential motion. The results shown in Figure 7.12 indicate that the machine is stable during simultaneous motion, whereas it tips over during sequential motion. This is due to the effect of the inertial forces and moments, which are larger in the sequential motion case.

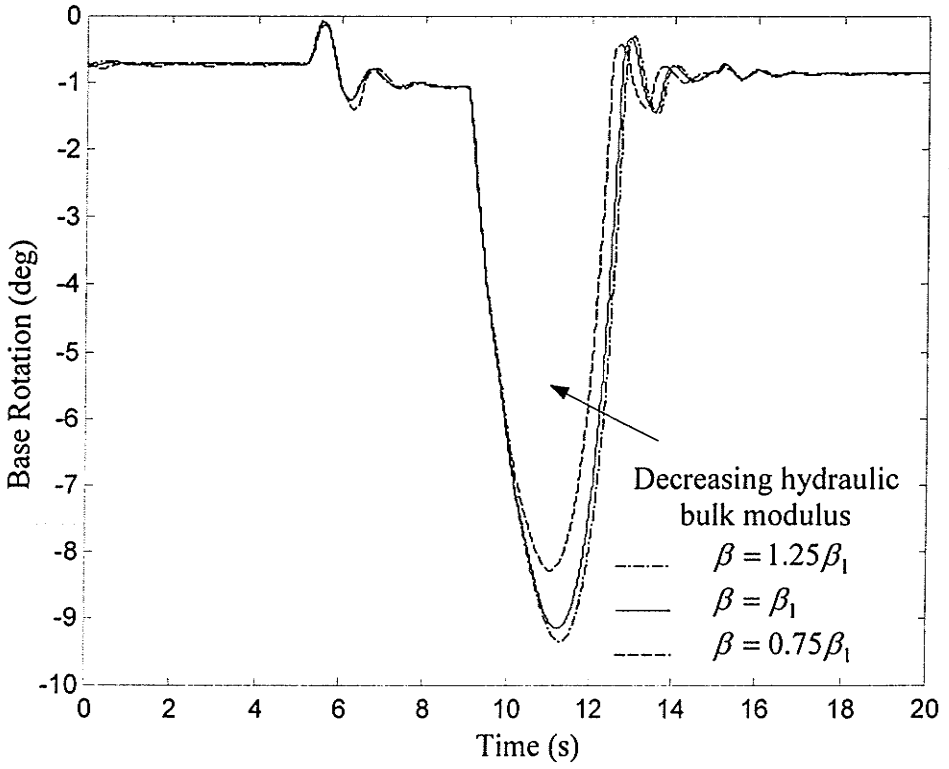

Figure 7.11. Effect of hydraulic compliance on machine stability; $\beta_1 = 120 \times 10^3$ psi.

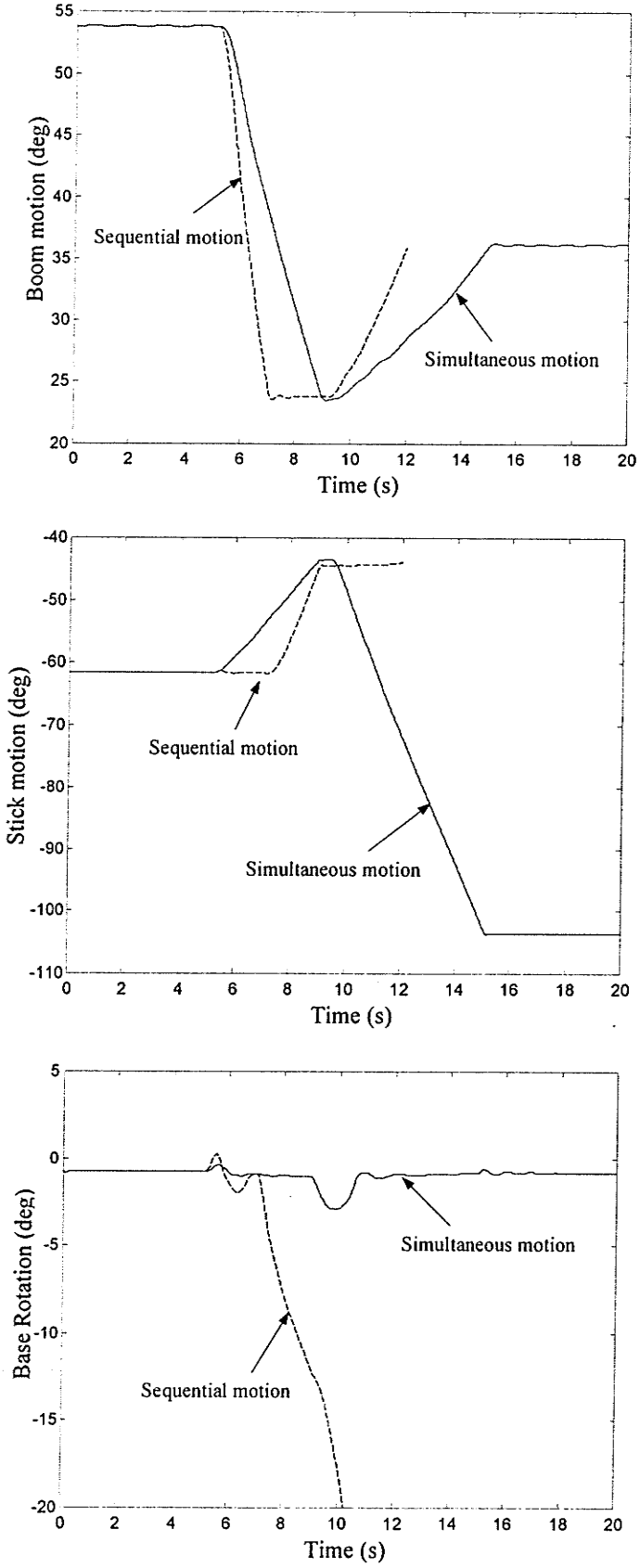

Figure 7.12. Machine stability during simultaneous and sequential motions of boom and stick.

Chapter 8

Summary and Concluding Remarks

Mobile manipulators play important roles in unstructured environments. These manipulators are, however, susceptible to tip-over instability. This thesis presents a step-by-step development of a complete dynamic model to study and analyze the tip-over motion and stability of mobile manipulators due to the movement of their arms. The challenge was to build a simulation model capable of producing detailed information about the effect of the flexibility between the base and the ground, the effect of the friction between the tires and the ground, and the interaction between the vehicle and the manipulator including the payload. Towards this goal, the contact between the base and the ground was considered as a multi-degree of freedom joint, and the novel method of virtual links was developed to formulate the problem into a fixed base serial-link manipulator with single degree of freedom at each joint. This process allowed the derivation of differential equations that describe the dynamics of the entire system to be

conducted in a more systematic and easier manner. A Caterpillar excavator-based hydraulic machine was chosen to demonstrate the development presented in this thesis. This machine incorporates many aspects of typical robotic systems and is similar to many heavy-duty hydraulic equipment units. Thus, the analysis, development, and results reported in this thesis can be applied to other similar mobile robotic systems or to heavy-duty mobile manipulators.

The contributions of this thesis are as follows:

1. The method of virtual links (VL) was developed. This method is useful for modeling non-fixed base robots or manipulators with multi-degree of freedom joints. It also allows calculation of the reaction forces/torques at any chosen manipulator joint directly without solving a system of differential algebraic equations. Two examples were presented to substantiate the method. The first example was to model a link having a spherical joint. The second example was to calculate the reaction forces at a chosen manipulator joint. The application of the VL method to model non-fixed base manipulators was also demonstrated throughout different chapters of this thesis. The novelty of this method is that using virtual links, all the dynamic models and simplifications made to develop the equations of motion for manipulators with fixed bases and single degree of freedom at each joint, can be applied for manipulators with non-fixed bases and/or multi-degree of freedom at some joints.

2. The complete model of the dynamics of general 3D motions of mobile manipulators was developed. Built upon the method of virtual links, the model takes into account the detailed dynamics of the base that can rock back and forth during the movement of the manipulator. This phenomenon, to the best of the author's knowledge, has not been

considered in pervious work. The developed model also takes into account the flexibility and friction of the contact between the base and the ground.

In arriving at this complete model, first, a dynamic model for a planar mobile robot, which considers both the base and the ground to be rigid, was developed. Both aspects of the impact, i.e., changes in the generalized states of the system and creation of impulsive forces, were included. Towards a more realistic model, the combined vehicle suspension and ground-tire compliance was incorporated next. It was shown that the flexibility of the contact reduces the manipulator's stability. Therefore, the flexibility between the base and the ground should be considered in the dynamic model to accurately investigate the stability of mobile manipulators. This model, however, assumed that the friction between the base and the ground at the points of contact is enough to prevent the manipulator from skidding. To remove this assumption, two friction models namely "Karnopp model" and "LuGre tire friction model" were employed to calculate the friction forces between the wheels and the ground and predict the skidding phenomenon. It was shown that the changes of the frictional properties between the wheels and the ground affect the machine stability. Based on the simulation results reported here, the machine tends to be more stable with less friction values up to a certain limit below which, the machine starts to also skid during the tipping over, causing it to become less stable. Karnopp model was found to be simple and required only the knowledge of two values: stick and slip friction. On the other hand, LuGre model is continuous and captures most of the friction phenomena, such as the hysteric behavior, the variations in the break-away forces, and the pre-sliding displacements.

Simulation of the Caterpillar excavator-based log-loader indicated that the flexibility of the contact between the base and the ground reduces the machine stability whereas the flexibility at the manipulator joints due to the hydraulic compliance improves the stability. The effects of the speed of the swing and the simultaneous or sequential movements of boom and stick links on the machine stability were also investigated. It was shown that by proper manipulation of the links, some tip-over situations could be recovered. To the best of the author's knowledge, these results are not found in the previous literature.

The results presented in this thesis, which is believed to be a further contribution to the stability analysis of mobile manipulators, in general, and heavy-duty hydraulic machines in particular, can be extended in the future, to work in various areas. First, the results of this study will lay the groundwork to design a method for on-line previewing of tip-over stability levels and identifying imminent upsets. The knowledge acquired from the simulation studies will be combined with previously developed extended method of energy stability (Ghasempoor and Sepehri, 1998) and the available sensory information on new machines, to develop an embedded system capable of displaying the proximity to instability and, upon sensing the imminent upset, producing preventive measures. Second, the model developed in this work can be used to evaluate various stability measures since they are not accompanied with simulation results of the base movements to validate them. Finally, the results of this work can be used to generate data for training an Artificial Neural Network (ANN) to learn the relationship between the machine's states and its stability. The idea of using ANN is promising. The practicality of this approach, however, requires more research.

References

Abo-Shanab, R.F. and N. Sepehri, 2003, "Dynamic stability Analysis of Mobile Manipulators During Spatial Motions," *ASME Journal of Dynamic systems, Measurements, and Control*, under review.

Abo-Shanab, R.F. and N. Sepehri, 2002a, "The Effect of Base Compliance on the Dynamic Stability of Mobile Manipulators," *Robotica; Journal of the International Federation of Robotics*, Vol. 20, pp. 607-613.

Abo-Shanab, R.F. and N. Sepehri, 2002b, "Dynamic Stability of Mobile Manipulators Considering Suspension Characteristics," *Proceedings of ASME Design Engineering Technical Conferences*, Montreal, Canada, Sept. 29-Oct. 2, paper number DETC2002/MECH-34227.

Abo-Shanab, R.F., N. Sepehri, and Q. Wu, 2002c, "On Dynamic Modelling of Robot Manipulators: the Method of Virtual Links," *Proceedings of ASME Design Engineering Technical Conference*, Montreal, Canada, Sept. 29-Oct. 2, paper number DETC2002/MECH-34225.

Abo-Shanab, R.F. and N. Sepehri, 2001a, "On Dynamic Stability of Manipulators Mounted on Mobile Platforms," *Robotica, Journal of the International Federation of Robotics*, Vol. 19, pp. 439-449.

Abo-Shanab, R.F., Q. Wu, and N. Sepehri, 2001b, "On Derivation of Constrained Multiple Rigid Body Dynamic Equations," *Proceedings of the American Control Conference*, Arlington, VA, USA, pp. 3565-3569.

Abo-Shanab, R.F. and N. Sepehri, 2001c, "On Dynamic Stability of Manipulators Mounted on Moveable Platforms," *Proceedings of the IEEE International Symposium on Computational Intelligence in Robotics and Automation*, Banff, Alberta, Canada, pp. 479-485.

Akpan, U. O. and M. R. Kujath, 1998, "Sensitivity of a Mobile Manipulator Response to System Parameters," *ASME Journal of Vibration and Acoustics*, Vol. 120, pp. 156-163.

Armestrong-Helouvery, B., P. Dupont, and C. Canudas de Wit, 1994, "A Survey of Models, Analysis Tools and Compensation Methods for the Control of Machines with Friction," *Automatica*, Vol. 30, pp. 1083-1138.

Baumgarte, J.W., 1972, "Stabilization of constraints and integrals of motion in dynamical systems," *Computer Methods in Applied Mechanics and Engineering*, Vol. 1, pp.1-16.

Baumgarte, J.W., 1983, "A new method of stabilization for holonomic constraints," *ASME Journal of Applied Mechanics*, Vol. 50, pp. 869-870.

Bayo, E., Garcia de Jalon, J. and Serna, M.A., 1988, "A Modified Lagrangian Formulation for the Dynamic Analysis of Constrained Mechanical Systems," *Computer Methods in Applied Mechanics and Engineering*, Vol. 17, pp. 183-195.

Blajer, W., 1992, "Index of Differential-Algebraic Equations Governing the Dynamics of Constrained Mechanical Systems," *Applied Mathematical Modelling*, Vol. 16, pp.70-77.

Canudas de Wit, C. and P. Tsiotras, 1999, "Dynamic Tire Friction Models for Vehicle Traction Control," *Proceedings of the* 38th *Conference on Decision and Control*, Phoenix, AZ, pp. 3746-3751.

Canudas de Wit, C., H. Olsson, K. Astrom, and P. Lischinsky, 1995, " A New Model for Control of Systems with Friction," *IEEE Transactions on Automatic Control*, Vol. 40, pp. 419-425.

Carter, F.M. and Cherchas, D.B., 1999, "Motion Control of Non Fixed Base Robotic Manipulators," *Robotica, Journal of the International Federation of Robotics*, Vol. 17, pp. 143-157.

Claeys, X., J. Yi, R. Horowitz, L. Alvarez, and C. Canudas de Wit, 2001, "A Dynamic Tire/Road Friction Model for 3D Vehicle Control and Simulation," *Proceedings of the IEEE Intelligent Transportation Systems Conference*, Oakland, CA, pp. 483-488.

Dahl, P.R., 1976, "Solid Friction Damping of Mechanical Vibrations," *AIAA Journal*, Vol. 14, pp. 1675-1682.

Dubowsky, S. and E.E. Vance, 1989, "Planning Mobile Manipulator Motions Considering Vehicle Dynamic Stability Constraints," *Proceedings IEEE International Conference on Robotics and Automation*, Scottsdale, AZ, Vol. 3, pp. 1271-1276.

Dubowsky, S. and E. Papadopoulos, 1993, "The Kinematics, Dynamics, and Control of Free-Flying and Free-Floating Space Robotic Systems," *IEEE Transactions on Robotics and Automation*, Vol. 9, No. 5, pp. 531-543.

Dubowsky, S. and A.B. Tanner, 1987, "A Study of the Dynamics and Control of Mobile Manipulators Subjected to Vehicle Disturbances," *Proceedings of the Fourth International Symposium of Robotics Research*, Santa Cruz, CA, pp. 111-117.

Dubowsky, S., P.Y. Gu, and J.F. Deck, 1991, "The Dynamic Analysis of Flexibility in Mobile Robotic Manipulator Systems," *Proceedings of the VIII World Congress on the Theory of Machines and Mechanisms,* Prague, Czechoslovakia.

Filippov, A.F., 1960, "Differential Equations with Discontinuous Right-Hand Side," Math. Sbornik, vol. 51, pp. 99-128. (English translation: American Mathematical Society Translations, vol. 42, pp. 199-231, 1964).

Fu, K.S., R.C. Gonzalez, and C.S.G. Lee, 1987, *Robotics: Control, Sensing, Vision, and Intelligence*, McGraw-Hill, Singapore.

Garcia, E., J. Estremera, and P. Gonzalez de Santos, 2002, "A Comparative Study of Stability Margin for Walking Machines," *Robotica*, Vol. 20, pp. 595-606.

Gaul, L. and R. Nitsche, 2001, "The Role of Friction in Mechanical Joints," Applied Mechanics Review, Vol. 54, pp. 93-105.

Gear, C.W., 1971, "Simultaneous Numerical Solution of Differential-Algebraic Equations," *IEEE Transactions on Circuit Theory*, Vol. CT-18, No. 1, P89-95.

Ghasempoor, A. and N. Sepehri, 1998, "A Measure of Stability for Mobile Manipulators With Application to Heavy Duty Hydraulic Machines," *ASME Journal of Dynamic Systems, Measurement, and Control*, Vol. 120, pp. 360-370.

Haessig, D.A. and B. Friedland, 1991, "On the Modeling and Simulation of Friction," *ASME Journal of Dynamic Systems, Measurement, and Control*, Vol. 113, pp. 354-362.

Hemami, H., 1982, "A State Space Model for Interconnected Rigid Bodies," *IEEE Transactions on Automatic Control*, Vol. AC-27, No. 2, pp.376-382.

Hollerbach, J.M., 1980, "A Recursive Lagrangian Formulation of Manipulator Dynamics and a Comparative Study of Dynamic Formulation Complexity," *IEEE Transactions on Systems, Man, and Cybernetics*, Vol. 10, pp. 730-736.

Hootsmans, N.A.M., 1992, "The Control of Manipulators on Mobile Vehicles," Ph.D. Thesis, Dept. of Mechanical Engineering, MIT, Cambridge, MA.

Huang, Q., S. Sugano, 1995, "Manipulator Motion Planning for Stabilizing a Mobile-Manipulator," *Proceedings IEEE International conference on Intelligent Robots and Systems*, Pittsburgh, USA, pp. 467-472.

Huang, Q., S. Sugano, and K. Tanie, 1997, "Stability Compensation of a Mobile Manipulator by Manipulator Motion: Feasibility and Planning," *Proceedings IEEE/RSJ International conference on Intelligent Robots and Systems*, pp.1285-1292.

Huang, Q., S. Sugano, and K. Tanie, 1998, "Motion Planning for a Mobile Manipulator Considering Stability and Task Constraints," *Proceedings IEEE International conference on Robotics and Automation*, Leuvan, Belgium, Vol. 3, pp.2192-2198.

Iagnemma K., Rzepniewski A., Dubowsky S., Pirjanian P., Huntsberger T., Schenker P., 2000, "Mobile Robot Kinematic Reconfigurability for Rough-Terrain," *Proceedings SPIE's International Symposium on Intelligent Systems and Advanced Manufacturing*, Boston, MA, paper number 4196-47.

Karnopp, D., 1985, "Computer Simulation of Slip-Stick Friction in Mechanical Dynamic Systems," *ASME Journal of Dynamic systems, Measurements, and Control*, Vol. 107, pp. 100-103.

Li, Y. and A.A. Frank, 1986, "A Moving Base Robot," *Proceedings of the American Control Conference*, Seattle, WA, pp. 1927-1932.

Mahalingham, S., W. Whittaker, and M. Gaithersburg, 1989, "Terrain Adaptive Gaits for Walkers with Completely Overlapping Workspace," *Robots*, vol. 13, pp. 1-14.

Mani, N.K., Haug, E.J. and Atkinson, K.E., 1985, "Application of Singular Value Decomposition for Analysis of Mechanical System Dynamics," *ASME Journal of Mechanisms, Transmissions, and Automation Design*, Vol. 107, pp. 82-87.

McGhee, R.B. and A.A. Frank, 1968, "On the Stability Properties of Quadruped Creeping Gait," *Mathematical Biosciences*, Vol. 3, pp. 331-351.

McGhee, R.B. and G.I. Iswandhi, 1979, "Adaptive Locomotion of a Multilegged Robot over Rough Terrain," *IEEE Transactions on Systems, Man, and Cybernetics,* Vol. 9, pp. 176-182.

Meirovitch, L., 1970, *Methods of Analytical Dynamics*, McGraw-Hill Book Company, USA.

Messuri, D. and C. Klein, 1985, "Automatic Body Regulation for Maintaining Stability of a Legged Vehicle During Rough-Terrain Locomotion," *IEEE Journal of Robotics and Automation*, RA-1, No. 3, pp. 132-141.

Merritt, H.E., (1967), *Hydraulic Control Systems*, John Wiley and Sons, NY.

Nagy, P. V., s. Desa, and W.L. Whittaker, 1994, "Energy-Based Stability Measure for Reliable Locomotion of Statically Stable Walkers: Theory and Application," *International Journal of Robotics Research*, Vol. 13, No. 9, pp.272-287.

Papadopoulos, E. G., and D.A. Rey, 1996, "A New Measure of tip over Stability Margin for Mobile Manipulators," *Proceedings of the IEEE International conference on Robotics and Automation*, Minneapolis, Minnesota, pp. 3111-3116.

Papadopoulos, E. G., and D.A. Rey, 2000, "The Force-Angle Measure of Tip over Stability Margin for Mobile Manipulators," *Journal of Vehicle Systems Dynamics*, Vol. 33, pp. 29-48.

Park, K.C. and Chiou, J.C., 1988, "Stabilization of Computational Procedures for Constrained Dynamical Systems," *Journal of Guidance, Control, and Dynamics*, Vol. 11, pp. 365-370.

Rey, D. A., and E.G. Papadopoulos, 1997, "On-Line Automatic Tipover Prevention For Mobile Manipulators," *Proceedings of the IEEE International Conference on Intelligent Robots and Systems*, Piscataway, Vol. 3, pp. 1273-1278.

Rosen, A. and Edelstein, E., 1997, "Investigation of a New Formulation of the Lagrange Method for Constrained Dynamic Systems," *ASME Journal of Applied Mechanics*, Vol. 64, pp.116-122.

Sallam, M. M., R.F. Abo-Shanab, and A.A. Nasser, 1998, "Modified Methods for Dynamic Modeling of Robot Manipulators," *Proceedings of the ASME Design Engineering Technical Conference*, Atlanta, GA, Paper Number DETC98/MECH5860.

Seo, Y.I. and Y.S. Yoon, 1994, "Design of a Robust DynamicGait of the Biped Using the Concept of Dynamic Stability Margin," *Robotica*, Vol. 13, pp. 461-468.

Sepehri, N., P.D. Lawrence, F. Sassani, and R. Frenette, 1994, "Resolved Mode Teleoperated Control of Heavy Duty Hydraulic Machines," *ASME Journal of Dynamic Systems, Measurement, and Control*, Vol. 116, pp. 232-240.

Sepehri, N., F. Sassani, P. D. Lawrence, and A. Ghasempoor, 1996, "Simulation and Experimental Studies of Gear Backlash and Stick-Slip Friction in Hydraulic Excavator Swing Motion," *ASME Journal of Dynamic Systems, Measurement, and Control*, Vol. 118, pp. 463-467.

Sepehri, N. and P.D. Lawrence, 2000, "Mechatronic System Techniques in Teleoperated Control of Heavy-Duty Hydraulic Machines," *Mechatronic Systems Techniques and Applications* (editor: C.T. Leondes), Vol. 3, Gorden and Breach Science Publishers, Amsterdam, The Netherlands, pp. 309-373.

Shampine, L.F., Reichel, M.W. and Kierzenka, J.A., 1999, "Solving Index 1 DAEs in Matlab and Simulink," Society for Industrial and Applied Mathematics, Vol. 41, pp. 538-552.

Stribeck, R., 1902, "Die Wesrntlichen Eigenschaften der Glleit- und Rollentager - the key qualities of sliding and roller bearing," Zeitschrift des Vereines Seutscher Ingenieure, Vol. 46 (38,39), pp. 1442-1448, pp. 1432-1437.

Sugano, S., Q. Huang, and I. Kato, 1993, "Stability Criteria in Controlling Mobile Robotic Systems," *Proceedings of the IEEE/RSJ International Conference on Intelligent Robots and Systems*, Yokohama, Japan, Vol. 3, pp. 832-838.

Vafa, Z. and Dubowsky, S., 1987, "On the Dynamic of Manipulators in Space Using the Virtual Manipulator Approach," *Proceedings of the IEEE International Conference on Robotics and Automation*, Raleigh, North Carolina, pp.579-585.

Vaha, P.K. and M.J. Skibniewski, 1993, "Dynamic Model of Excavator," *Journal of Aerospace Engineering*, Vol. 6, pp. 148-158.

Wehage, R.A. and Haug, E.J., 1982, "Generalized Coordinate Partitioning for Dimension Reduction in Analysis of Constrained Dynamic Systems," *ASME Journal of Mechanical Design*, Vol. 104, pp.247-255.

Wu, Q., S. Onyshko, N. Sepehri, and A.B. Thronton-Trump, "On Construction of Smooth Lyapunov Functions for Non-Smooth Systems," *International Journal of Control*, vol. 69, pp. 443-457, 1998.

Yao, B., J. Zhang, D. Koehler, and J. Litherland, 1998, "High Performance Swing Velocity Tracking Control of Hydraulic Excavator," *Proceedings of the American Control Conference*, Philadelphia, pp. 818-822.

Yu, Q. and I. Chen, 2002, "A General Approach to the Dynamics of Nonholonomic Mobile Manipulator Systems," *ASME Journal of Dynamic Systems, Measurements, and Control*, Vol. 124, pp. 512-521.

Zheng, Y. and H. Hemami, 1985, "Mathematical Modeling of a Robot Collision with its Environment," *Journal of Robotic Systems*, Vol. 2, pp. 289-307.

Zomaya, A.Y., 1992, *Modelling and Simulation of Robot Manipulators: A Parallel Processing Approach*, World Scientific Publishing, Singapore, 1992.

Appendix

Derivation of velocity change due to collision with the ground

When a manipulator comes in contact with the environment, a geometric constraint is enforced to the system motion. The result will be an impact with a sharp change of the joint velocities (Zheng and Hemami, 1985). It is therefore required to compute at each time the new joint velocities just after each collision. The equations of motion of an *n*-link manipulator are given as:

$$\boldsymbol{\tau} = \mathbf{M}(\mathbf{q})\ddot{\mathbf{q}} + \mathbf{C}(\mathbf{q},\dot{\mathbf{q}}) + \mathbf{G}(\mathbf{q}) \tag{A1}$$

Suppose that the end-effector of one part of the manipulator collides with the ground. The position of the contact point on this manipulator is denoted by $\mathbf{x}_b$ in the base coordinate system. $\mathbf{x}_b$ can be expressed in terms of the generalized coordinates, $\mathbf{q}$, as

$$\mathbf{x}_b = \mathbf{f}(\mathbf{q}) \tag{A2}$$

Let the contact point of the environment be $\mathbf{x}_s$. The collision occurs when $\mathbf{x}_b = \mathbf{x}_s = \mathbf{f}(\mathbf{q})$. In association with each constraint, a generalized force Γ acts on the system equations:

$$\Gamma = \left[\frac{\partial \mathbf{f}(\mathbf{q})}{\partial \mathbf{q}}\right]^T \zeta = \mathbf{J}^T\zeta \tag{A3}$$

where $\mathbf{J}$ is the Jacobian and ζ is a suitable column vector of Lagrange multipliers.

Then, the equations of motion for the constraint system are:

$$\boldsymbol{\tau} + \mathbf{J}^T\zeta = \mathbf{M}(\mathbf{q})\ddot{q} + \mathbf{C}(\mathbf{q},\dot{\mathbf{q}}) + \mathbf{G}(\mathbf{q}) \tag{A4}$$

In the case of collision, the constraint is brought about at the moment of impact. The constraint force is subject to an abrupt change immediately before and after the collision.

As the time of collision is infinitesimally short, the constraint force can be modeled as an impulse at the moment of collision. Let the generalized constraint force be denoted as

$$\Gamma_\delta = \left[\frac{\partial \mathbf{f}}{\partial \mathbf{q}}\right]^T \zeta = \mathbf{J}^T \zeta$$

In the case of collision, Equation (A4) becomes

$$\tau + \Gamma_\delta = \mathbf{M}(\mathbf{q})\ddot{q} + \mathbf{C}(\mathbf{q},\dot{\mathbf{q}}) + \mathbf{G}(\mathbf{q}) \tag{A5}$$

During the infinitesimally short time interval of collisions, the joint positions of the system remain unchanged, since joint angular velocities are finite whose integrals over an infinitesimally short time interval are zero. According to this basic assumption, one may integrate both sides of Equation (A5) in an infinitesimally short time interval and have

$$\lim_{\Delta t \to 0} \int_{t_o}^{t_o+\Delta t} \Gamma_\delta \, dt = \lim_{\Delta t \to 0} \int_{t_o}^{t_o+\Delta t} \mathbf{M}(\mathbf{q})\ddot{\mathbf{q}} \, dt + \lim_{\Delta t \to 0} \int_{t_o}^{t_o+\Delta t} [\mathbf{C}(\mathbf{q},\dot{\mathbf{q}}) + \mathbf{G}(\mathbf{q}) - \tau] dt \tag{A6}$$

The second term of the left side vanishes as $\Delta t \to 0$. Equation (A6) thus becomes

$$\int_{t_o}^{t_o+\Delta t} \Gamma_\delta \, dt = \mathbf{M}(\mathbf{q})[\dot{\mathbf{q}}(t_o + \Delta t) - \dot{\mathbf{q}}(t_o)] \tag{A7}$$

Since the magnitude of an impulse tends towards infinite as $\Delta t \to 0$, the right side of Equation (A7) converges to finite quantity. We may further denote

$$\mathbf{T}_\delta = \int_{t_o}^{t_o+\Delta t} \Gamma_\delta \, dt$$

$$\text{Then } \mathbf{T}_\delta = \mathbf{J}^T \int_{t_o}^{t_o+\Delta t} \zeta \, dt \tag{A8}$$

and call $\mathbf{T}_\delta$ the generalized impulsive force. From Equation (A7) one may have

$$\dot{\mathbf{q}}(t_o + \Delta t) - \dot{\mathbf{q}}(t_o) = \mathbf{M}^{-1}(\mathbf{q})\,\mathbf{T}_\delta \tag{A9}$$

where $\dot{\mathbf{q}}(t_o + \Delta t)$ and $\dot{\mathbf{q}}(t_o)$ represents the joint angular velocities immediately before and after the collision. Thus, the mathematical relation between the instantaneous change of the joint angular velocities and the generalized impulsive force is established. The relation between the change of the velocity of the point of contact on the robot and the change of the generalized angular velocities is:

$$\mathbf{J}[\dot{\mathbf{q}}(t_o + \Delta t) - \dot{\mathbf{q}}(t_o)] = \dot{\mathbf{x}}_b(t_o + \Delta t) - \dot{\mathbf{x}}_b(t_o) \tag{A10}$$

Using Equations (A8), (A9) and (A10), we have

$$\Delta\dot{\mathbf{x}}_b = \mathbf{J}\,\mathbf{M}^{-1}(\mathbf{q})\mathbf{J}^T \int_{t_o}^{t_o+\Delta t} \zeta \, dt$$

Then

$$\left(\mathbf{J}\,\mathbf{M}^{-1}(\mathbf{q})\mathbf{J}^T\right)^{-1} \Delta\dot{\mathbf{x}}_b = \int_{t_o}^{t_o+\Delta t} \zeta dt \tag{A11}$$

Multiplying both sides of Equation (A11) by $\mathbf{J}^T$

$$\mathbf{J}^T\left(\mathbf{J}\,\mathbf{M}^{-1}(\mathbf{q})\mathbf{J}^T\right)^{-1} \Delta\dot{\mathbf{x}}_b = \mathbf{J}^T \int_{t_o}^{t_o+\Delta t} \zeta \, dt \tag{A12}$$

From (A8) and (A12)

$$\mathbf{T}_\delta = \mathbf{J}^T\left(\mathbf{J}\,\mathbf{M}^{-1}(\mathbf{q})\mathbf{J}^T\right)^{-1} \Delta\dot{\mathbf{x}}_b$$

Equation (A9) will be

$$\Delta\dot{\mathbf{q}} = \mathbf{M}^{-1}(\mathbf{q})\mathbf{J}^T\left(\mathbf{J}\,\mathbf{M}^{-1}(\mathbf{q})\mathbf{J}^T\right)^{-1} \Delta\dot{\mathbf{x}}_b \tag{A13}$$

Equation (A13) determines the velocity change due to collision with the ground.